

Optical Spectroscopy of Novel Quantum Dot Structures

Romain Toro



Department of Physics and astronomy
University of Sheffield

Thesis submitted for the degree of Doctor of Philosophy
November 2013

Supervisor Dr A. Tartakovskii

Optical Spectroscopy of Novel Quantum Dot Structures

Romain Toro

Abstract

This thesis comprises works on novel quantum dot structures. New ways of growing III-V semiconductor quantum dots by integrating a ternary element or by growing on top of a silicon wafer are optically characterized, opening the way to more specific work on those new structures, while furthering our understanding of the epitaxy mechanisms behind them.

We study InGaAs/GaAs quantum dot structures monolithically grown on a silicon substrate, without use of germanium virtual substrate nor wafer bonding technique. Optical characterization of the sample with micro photoluminescence is performed and shows very good single quantum dot emission lines. Single photon emission from the InGaAs dots is demonstrated with photon correlation experiment showing clear anti-bunching. Photonic crystal cavities are fabricated for the first time with InGaAs dots monolithically grown on silicon and exhibit very high quality factor up to 13000 with a large percentage of cavities having Q-factors over 9000. This allows observation of Purcell effect for single photon emitting QDs and strong light-matter coupling between InGaAs QDs and cavities.

We also investigate unexpected emission lines on the same sample. The lines are identified as interface fluctuations in a GaAs/AlGaAs short period superlattice, making them the first Interface fluctuation quantum dots grown directly on silicon. Further optical characterization confirms the quantum dot nature of the emissions. Polarization measurements allow study of the fine structure splitting of exciton/bi-exciton pairs and the single photon emission of the dots is demonstrated.

Finally in a subsequent chapter we investigate InP/GaInP quantum dots with arsenic deposited during the growth process. Magneto-optic PL of samples with different concentrations of As allows to determine how the As changes the characteristics of the dots. Schottky diodes are fabricated and tested to show good characteristics, and electric field experiments demonstrate charge control over this new kind of dots.

Acknowledgements

I'd like to thank all the people who supported me during this thesis, first of all my family, my mom and dad and my sister Elsa, but also all my precious friends Adeline, Alexandre aka Thaithai, Anne-Emmanuelle, Ariane, Aurélien, Damien, Elodie, Gaëtan, Matthieu, Mike, Thomas.

I'd like to thank my good friends from Sheffield, who made my stay all the more pleasant: Youmna, François, Lore, Magda, Marin, Argyrios, Yue "Coco", Wenzhou. Of course, I want to acknowledge the support provided by the academic and technical staff here at University of Sheffield, particularly Pr. Mark Fox, Pr. Maurice Skolnick, Pr. David Mowbray, Chris Vickers, Peter Robinson, Richard Nicholson, Richard Webb, Steve Collins.

A particular regard is sent to my tutor Tim Richardson, who left us too soon. May he rest in peace, and the charity he gave so much to, prosper.

I thank all my fellow PhD students and post-doc who provided help and made me feel at home here, Osvaldo, Jorge, Daniel, Odilon, Claire, John Q, Rikki, Stefan, Andreas, Robert B, Tim, Lloyd, Ehsaneh, Kenny, Scott, Andrew R, John B, Deivis, Andrew F, Maksym, Maxim, Nikola, Ben, Jasmin, James, Robert S, plus all I forgot.

Additionally, I'd like to thank all the people from the European network Spinoptronics and Clermont4, who were my second family during this thesis. Thank you Feng, Petr, Fabio, Mladen, Elena, Jonas, Guillaume, Alexey, Maria, Jorge, Andrei N, Andrei B, Dima and the other I forgot.

Finally I want to thank my examiners Pr. Richard Hogg and Pr. Raymond Murray for their time, and particularly Pr. Hogg for the enlightened advices he gave me about my thesis.

I also thank my supervisor Dr. Alexander Tartakovskii as is customary.

List of Publications

I. J. Luxmoore, **R. Toro**, O. Del Pozo-Zamudio, N. A. Wasley, E. A. Chekhovich, A. M. Sanchez, R. Beanland, A. M. Fox, M. S. Skolnick, H. Y. Liu, A. I. Tartakovskii “III-V quantum light source and cavity-QED on Silicon”, *Scientific Reports* 3, 1239, February 2013.

R. Toro, O. Del Pozo-Zamudio, M. N. Makhonin, A. M. Sanchez, R. Beanland, H. Y. Liu, M. S. Skolnick, A. I. Tartakovskii “Visible light single photon emitters monolithically grown on silicon”, soon to be submitted to *Applied Physics Letters*

O. Del Pozo-Zamudio, J. Puebla, E. A. Chekhovich, **R. Toro**, A. Krysa, R. Beanland, A. M. Sanchez, M. S. Skolnick, A. I. Tartakovskii, “Growth and magneto-optical characterization of InPAs/GaInP Quantum Dots”, soon to be submitted to *Physical Review B*

R. Toro, I. J. Luxmoore, O. Del Pozo Zamudio, N. A. Wasley, H. Y. Liu, M. S. Skolnick, A. I. Tartakovskii “Single-photon III-V quantum dot emitters and photonic crystal cavities monolithically grown on a Si substrate”, oral presentation at *UK Semiconductors 2012*, Sheffield June 2012

R. Toro, I. J. Luxmoore, O. Del Pozo-Zamudio, N. A. Wasley, E. A. Chekhovich, A. M. Sanchez, R. Beanland, A. M. Fox, M. S. Skolnick, H. Y. Liu, A. I. Tartakovskii “III-V quantum light source and cavity-QED on Silicon”, oral presentation at *QD Day 2013 Nottingham*, Nottingham January 2013

Contents

1	Introduction	7
1.1	Low dimensional semiconductors	7
1.1.1	Semiconductors and how they define our technology	7
1.1.2	Low-dimensionality in semiconductors	8
1.1.3	Quantum dots	10
1.1.4	Basic optical process in quantum dots: photoluminescence	12
1.2	Motivations: why are quantum dots desirable?	14
1.2.1	Quantum dot lasers	14
1.2.2	Entangled photon emitters	14
1.2.3	Quantum bit: a possible candidate?	15
1.3	Quantum dot fabrication	15
1.3.1	Epitaxial techniques	16
1.3.2	Self-assembled quantum dots	16
1.3.3	Interface fluctuations from quantum wells	18
1.3.4	Other types of quantum dots	19
1.4	Experimental work on quantum dots	20
1.4.1	Micro-photoluminescence	20
1.4.2	Measurement of fine structure splitting	23
1.4.3	Charge control using electric field	24
1.5	Organization of the thesis	26
2	Optical characterization and cavity coupling of InAs/GaAs quantum dots monolithically grown on silicon substrate	34
2.1	Introduction	34
2.2	Structural study	35
2.2.1	Previous attempts at growing III-V on IV	35
2.2.2	Structure description	36
2.2.3	Structure discussion	38
2.3	Spectral landscape and optical properties	42

2.3.1	Micro-photoluminescence experimental setup	42
2.3.2	Micro-PL spectra of QD ensembles	43
2.4	Photonic crystal cavities	48
2.4.1	Principle	49
2.4.2	Fabrication	50
2.4.3	Characterization of the performances	52
2.5	Single photon emission	54
2.5.1	Experimental setup	54
2.5.2	Results	56
2.6	Light-matter coupling	58
2.6.1	Principle	58
2.6.2	Weak coupling	59
2.6.3	Strong coupling	62
2.7	Conclusion	66
3	GaAs/AlGaAs single photon emitters from interface fluctuations of short period superlattice monolithically grown on silicon sub- strate	72
3.1	Introduction	72
3.2	Sample structure and experimental setup	73
3.2.1	Sample structure	73
3.2.2	Experimental setup	74
3.3	Optical identification of the internal layers	75
3.3.1	Principle	75
3.3.2	Variable etching technique	77
3.3.3	Interpretation of the results	78
3.3.4	Further confirmation with temperature dependence	80
3.4	Polarization study and fine structure of the dots	81
3.4.1	Principle of light polarization	81
3.4.2	Observation of fine structure splitting	83
3.4.3	Power dependence of exciton/bi-exciton pairs	85
3.5	Photon emission and lifetime properties	86
3.5.1	Experimental setup	86
3.5.2	Lifetime of interface quantum dots	87
3.5.3	Single photon emission	88
3.6	Conclusion	90

4	Effects of arsenic concentration in InPAs/GaInP self-assembled quantum dots	95
4.1	Introduction	95
4.2	Sample description	96
4.3	Spectral distribution of quantum dot emissions	98
4.4	Study of excitonic complexes through charge-controlled PL	100
4.4.1	Schottky diode fabrication	101
4.4.2	Principle of charge control by electric field	102
4.4.3	Results	103
4.5	Study of the effect of As concentration on magneto-optical properties	106
4.5.1	Experimental setup	106
4.5.2	Results	107
4.6	Conclusion	110
5	Conclusions	116

Chapter 1

Introduction

1.1 Low dimensional semiconductors

1.1.1 Semiconductors and how they define our technology

Materials can be classified in 3 categories, according to their electrical properties. Metals have their Fermi level in the middle of an allowed energy band (the conduction band), which allows charge carriers to be generated easily at room temperature. In the two other types of material, the Fermi level is in a forbidden band (band gap) situated between two permitted energy bands, the conduction band and the valence band. Due to the intermediate position of the Fermi level, without external energy contribution (basically at a temperature of 0 K) the conduction band is empty, and the valence band is completely filled, which means no bound electron from the valence band can attain a higher level of energy within the band. It would have to gain from an external excitation enough energy to “jump” from the valence band to the upper empty states situated in the conduction band. In insulators, the distance between the two bands, the band gap, is so big that it requires a lot of energy for the electrons to be excited. Therefore insulators do not conduct electricity easily. The third type of material is the semiconductor. Its band gap is of the order of 0.5 to 5 eV (Ge 0.63 eV, GaP 2.26 eV, diamond 5.5 eV). The possibility to engineer its energy diagram by doping it with different types of charge carriers has made semiconductors a widely researched topic since the 1950s. The association of two differently doped semiconductors (PN junction) is the basic building block of transistor structures, which are the basics of modern computation; therefore semiconductors are at the very heart of our society and our science.

Many engineers prophesied the predominance of semiconductors in human tech-

makes it possible to confine electrons and holes (virtual particles created by the absence of electrons in the valence band of the material), thus yielding interesting quantum properties. Figure 1.2 shows the form of the density of states functions for different structures, respectively bulk (3 dimensions), quantum well (2 dimensions), quantum wire (1 dimension) and quantum dot (0 dimension).

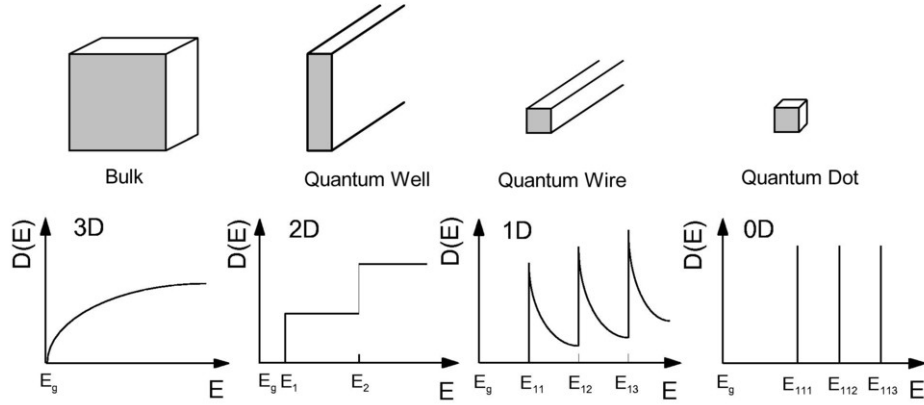


Figure 1.2: Form of the density of energy states for an electron in a semiconductor, represented for 3D (bulk), 2D (slab), 1D (wire) and 0D (dot) systems. Taken from [5].

As we can see on the lower part of the figure the density of states is asymptotic of $E^{1/2}$ for a bulk system, constant Heaviside function for a 2D system, proportional to $E^{-1/2}$ for 1D system and for a zero-dimensional system (namely a quantum dot) is a Dirac function. The density of states is continuous for a bulk semiconductor but starts to be quantized when the dimensionality is reduced in a quantum well. We can see energy thresholds E_1 and E_2 corresponding to the discrete energy levels that can be taken by electrons and holes in the direction of the quantization (the growth direction in epitaxially made quantum wells). Those energy levels are of the form $E_n = \hbar^2 \pi^2 n^2 / 2m^* L$ where L is the width of the well and m^* is the effective mass of the particle. They are illustrated on figure 1.3.

In the case of the quantum wire and quantum dot, the discrete energy levels are noted respectively with two and three indices (E_{ab} and E_{abc}) corresponding to the direction of quantization. If we take the example of a zero-dimensional cube as represented on the far right of figure 1.2, an energy level labelled E_{121} would correspond to the first level in the x direction, the second level in the y direction and the first level again in z direction.

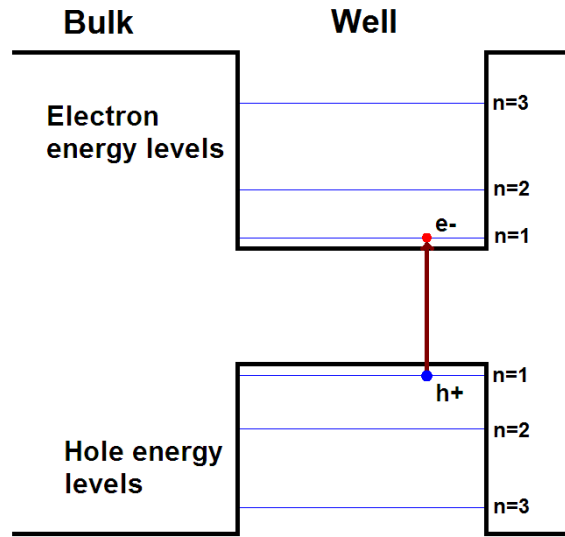


Figure 1.3: Diagram of the quantized energy levels in a quantum structure, for example a quantum well.

It is interesting to note the effects produced by an electric field applied to the direction of quantization. In a bulk semiconductor, an electric field would displace the electrons and holes to opposite sides of the material. In a quantum well (or any other quantum structure) the electron hole pair remains unseparated up to large electric fields due to the potential barriers of the well. Nevertheless the electric field decreases the energy of the electron and raises that of the hole, effectively redshifting the emission energy of the structure. This is called the quantum-confined Stark effect (QCSE) [6]. This ability to drag oppositely charged particles apart will be of particular interest for the charge control experiments described in chapter 4. Also, the total discretization of energy levels at 0D is a very interesting property that opens the way to manipulation of quantum effects in solid state matter. It is on this last structure, the zero-dimensional quantum dot, that the present thesis is based.

1.1.3 Quantum dots

Basically what is a quantum dot? It is a nanostructure which size is comparable to the electron wave-function. Its shape can be of a small ball, a square, a section of cylinder, a lens, in any case none of its characteristic lengths is significantly larger than the other (unlike wires or planes, which have ratios between their characteristic lengths of more than 10^2). Quantum dots can be made from solid state

clusters of atoms obtained using epitaxial growth, from electric fields applied to a two-dimensional electron gas (lateral QD or gated) or synthesized from chemical compounds dissolved in solution (colloidal) (see section 1.3). One of the most studied quantum dots are epitaxially grown using the properties of strain caused by lattice mismatch, phenomenon described in more details in the next section. Figure 1.4 gives a tunnelling electron microscope image of a lens shaped self-assembled quantum dot.

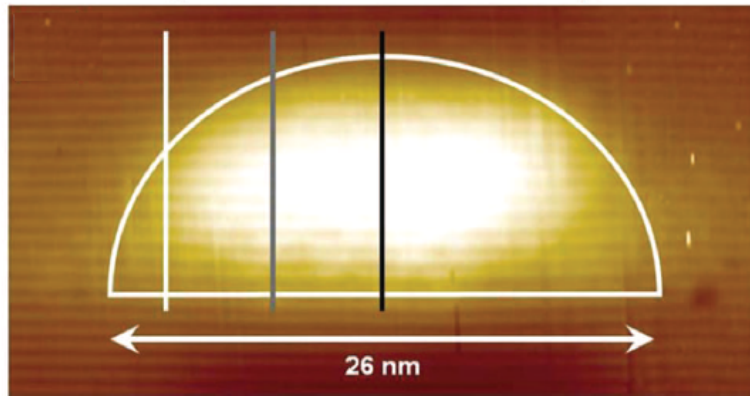


Figure 1.4: Cross-sectional tunnelling electron microscopy of a self-assembled quantum dot. Figure taken from [7].

One of the fundamental properties of quantum dots, and which is one of the main interests in working with those nanostructures, is their ability to confine charges in all three directions, exhibiting a discrete spectrum of energy levels. It is this discretized energy scale, similar to that of pure atoms, that earned quantum dots the name of “artificial atoms”. Quantum dots have a size comparable to that of the electron and hole wave-function, which allows effective spatial confinement of these. The size is usually of the order of a few to a few tens of nanometres. The materials used to grow them can be either elemental, comprised only of atoms from group IV (silicon, germanium) or compound III-V (group III gallium, indium, group V arsenic, phosphorus...) and II-VI (group II zinc, cadmium, group VI tellurium, selenium...). For more general literature about quantum dot early growth and study, see the following references [3, 8–14].

1.1.4 Basic optical process in quantum dots: photoluminescence

Excitation by a photon of the bulk semiconductor surrounding the dots will create an electron-hole pair. This pair can undergo radiative or non-radiative relaxation. Non-radiative relaxation includes dissipation of the energy in the form of heat by emitting a phonon, or transmission of its energy to defects. In direct bandgap semiconductors, the non-radiative process rates are much smaller than radiative ones, meaning materials such as GaAs are good light emitters. The radiative process in semiconductors can be described by a four-step or four-regime process [15]. The excitation pulse creates a coherent population of carriers having the same energy and phase as the excitation photons. The coherence is destroyed through carrier-carrier scattering, in a process occurring in a fast timescale of the order of 200 fs. The carriers also thermalize to lower levels of energy by emitting longitudinal optical phonons (LO phonon scattering) until they reach the lowest possible energy level. The timescale of this regime being very fast, the probability that a recombination happens before the carriers reach the lowest energy is negligible [6]. This leads to the formation of a non-thermal carrier population at the bottom of the conduction band (electrons) and the top of the valence band (holes). The thermalization of the carrier population happens during the non-thermal regime where carrier-carrier scattering redistributes the energies between carriers, and creates a population of carriers characterized by a temperature higher than that of the lattice (this process takes a few picoseconds). This is the hot-carrier regime. The population is by that point said to be in quasi-equilibrium, that is to say there is more charge carriers than would be only with the thermal excitation. More interactions between hot carriers and phonons allow the population to reach the unified temperature of the lattice (isothermal regime). It takes various times to reach thermal equilibrium, depending on the population and on the density of carriers. Between 1 and 100 ps are necessary to reach the isothermal regime. Finally, to reach the thermodynamic equilibrium the system was in before the excitation the carrier population must be reduced either by phonon scattering or by recombining and emitting photons having the bandgap energy [6, 15]. It takes more than 100 ps to reach this state.

During the thermalization regimes an exciton can be trapped into a neighbouring material with lower bandgap, namely one of the quantum dots (see figure 1.5). This process takes place on a time scale of around ten picoseconds [7].

This “trapping” is made possible by the difference between the bandgap of

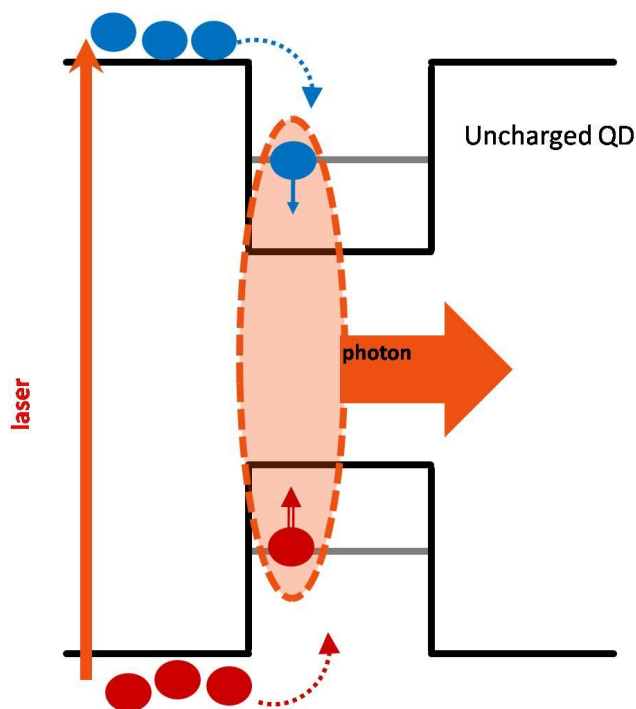


Figure 1.5: Excitation and relaxation process in quantum dots. Electrons and holes are excited in the bulk and then relax in the quantum dot. (Taken from [16].)

the quantum dot material and that of the surrounding material, the former being smaller so that it is more energetically favourable for the charges to remain inside. Inside the dot the carriers tend to relax to the lower energy state available in the dot (ground state) but this process is made difficult by the phonon bottleneck effect. Due to the quantization of energy levels, transitions to one energy to a lower energy by the emission of a single phonon becomes forbidden [17–19]. The main process for relaxation becomes carrier-carrier scattering, thus reducing significantly the relaxation rate in the quantum dots and leading to the usual emission lifetime of ~ 1 ns. The exciton recombines by emitting a photon having an energy that depends on the shape, size and atomic characteristics of the quantum dot. This property in particular makes quantum dots very attractive as controlled single photon emitters [20, 21], and entangled photon sources [22, 23]. The ability to trap and retain charges during a finite amount of time is also one many hope to use to perform operations on the spin of the charge, making it an effective tool for quantum computation [24, 25]. The wide range of wavelength at which QDs can emit also made them attractive for quantum dot lasers [8, 26].

1.2 Motivations: why are quantum dots desirable?

While the fabrication and optical properties of quantum dots are fascinating to study as they bring valuable insight about the electronic behaviour of solids at a quantum level, one might also be motivated by the prospect of finding for these nanostructures a real life application. Though the work presented in this thesis is mainly a work of observation and not oriented towards immediate industrial application, it is still interesting to non-exhaustively review a few applications where quantum dots have or are foreseen to have a significant role.

1.2.1 Quantum dot lasers

The laser, or Light Amplification by Stimulated Emission of Radiation is one of the most important invention of the 20th century. It has a huge range of applications in our everyday life, such as communications, medical probing and surgery, military, and it is also an essential element for scientific research. The gain medium which forms the main part of the laser can be made of various materials, the most used being gas (like helium-neon), doped crystal (titanium-sapphire), or semiconductor (diode lasers). Recently there has been interest in building lasers using quantum dots as their amplification material. Performances of quantum dot lasers has been investigated, and compare well to that of gas lasers. The advantages of QD lasers compared to quantum well lasers dwell in the quantized energy levels of QDs. It offers a high temperature stability of the threshold current density (up to 180 K), as well as an optimized gain [27]. Since QDs have properties similar to atoms, QD lasers avoid the negative aspects of bulk and quantum well semiconductor lasers, while having the huge advantage that the wavelength of the emitted light depends on the size and composition of the quantum dots. This widely opens the wavelength operation range for this type of laser compared to other types [28–30].

1.2.2 Entangled photon emitters

Entanglement is a theoretical quantum state of two particles where the properties of one can be measured through the other, independently of the physical distance separating them. Many applications could ensue from this phenomenon, including quantum computation [24, 25, 31], quantum teleportation for instant communication [32, 33], or superdense coding which consists in coding two classical bits of information into one quantum bit [34].

Recently bi-excitons in quantum dots have been proposed as entangled photon pair emitters [23], and later a system consisting of a quantum dot diode has been implemented, providing a compact and controllable source of entangled photon pairs [22]. Quantum dot emitters would prove an invaluable system for generating entangled photons, as it can generate them on demand and trigger emissions one by one, a feature not matched by other systems using optical parametric down conversion [35, 36].

1.2.3 Quantum bit: a possible candidate?

Quantum information theory has been imagined as a possible enhancement of current classical binary computation, by using the counter-intuitive properties of quantum mechanics [37]. The principle is to consider in the place of classical bit assuming values of only zero or one, a quantum bit (q-bit) that could not only take the values $|0\rangle$ and $|1\rangle$, but also a linear combination $|0\rangle + |1\rangle$ of both. By implementing circuits with newly imagined logic gates like Hadamard and Control-Not, it is possible for certain computational operations like factorisation of large numbers or database searching to be achieved much faster than with a classical method [25].

Though the theory has been well defined for a few decades now, we are still looking to physically implement the system. Electron spins have been proposed as q-bits due to their impressive coherence time ($\sim 200 \mu\text{s}$) [31]. The spin could then be transmitted through photons emitted by quantum dots. Electron spins in coupled quantum dots have also been considered as a possible quantum gate for computation [38].

1.3 Quantum dot fabrication

A low dimensional structure can only be of use for large scale application if we manage to reproduce it. For the last two decades various techniques have emerged and evolved to produce high quality quantum dot structures. The present section describes the main techniques used to obtain the samples the main chapters of this thesis are based upon, as well as some other widely studied types of quantum dots.

1.3.1 Epitaxial techniques

The typical semiconductor sample is a disc comprised of a thin (less than 1 mm) substrate with the active layers on top. The substrate is obtained from ingots of highly pure semiconductor grown by crystallization of melted material. The ingot is then sliced into thin discs by a wire saw. Wafers made of silicon are widely used in industry but compound semiconductor wafers can also be obtained with the same technique. The growth of the active layers on top of this wafer requires more complex techniques, the two main ones being molecular beam epitaxy (MBE) and metal-organic vapour phase epitaxy (MOVPE) also called metal-organic chemical vapour deposition (MOCVD) [39, 40].

MBE has been developed in 1968 in Bell Telephone Laboratories [41], it is a process by which elements (such as Gallium, Arsenic, Phosphorus...) are heated up to sublimation and deposited on the surface of the wafer, maintained at a high temperature of several hundreds of °C. There the atoms assemble epitaxially (in an ordered crystalline way). The operation relies primarily on high or ultra-high vacuum (10^{-8} Pa) and slow deposition rate to achieve a very high level of material purity. MOCVD on the other hand, is a different process that removes the need for high vacuum. The material is grown by a chemical process rather than depositing sublimated pure components. Elements like Indium or Phosphorus are provided to the wafer through pure gases such as Trimethylindium ($\text{In}(\text{CH}_3)_3$) or Phosphine (PH_3), which react at the surface leaving the atom of interest ordered in the crystal and a gaseous by-product of the reaction (like methane), later evacuated. For this reaction to take place, the wafer needs to be heated at temperature of 500 or 600 °C, in order to break the atomic bonds of the gaseous reactants.

MOCVD is particularly useful for the growth of P-based materials, as phosphorus is difficult to evaporate through MBE. A more complete comparison of the two techniques can be found in a 1984 work by Dapkus [42]. These techniques allow growth of semiconductor material on a monolayer rate, and therefore have been used extensively for the growth of thin layers (among which quantum wells) as well as micro and nanostructures as we'll see in the next paragraph.

1.3.2 Self-assembled quantum dots

The layer-by-layer growth process described in the previous paragraph is well adapted for the formation of thin layers like quantum wells, but they can also be used to

grow more complicated nanostructures like quantum wires and quantum dots. The formation of quantum dots uses interesting surface physics effects that will be qualitatively described in this paragraph.

It has been discovered in the late eighties that quantum dots formed naturally during the growth of epitaxial layers [43]. This phenomenon called Stranski-Krastanov regime has been studied and originates from lattice mismatch at the interface of different materials. Since the growth of the material is epitaxial, the atoms arrange themselves in a crystal lattice, but when a material is deposited on top of a different one, with different lattice size, there is formation of strain at the interface: the atoms of the new material have to adapt to the lattice size of the material onto which they are grown, but physically they tend to arrange with their own lattice size. Such situation occurs for example in the case when InAs is grown on top of GaAs, the two materials having $\sim 7\%$ mismatch between their respective lattice characteristic sizes. After the deposition of the new material reaches a critical thickness (which depends on the amplitude of the mismatch) [44], the strain becomes such that it is more energetically favourable for the atoms to form islands. The process is described in figure 1.6.

After the islands have grown into pyramidal aggregates of the desired size (depending on the concentration of material deposited, but generally between 5 and 100 nm on the side of the base), they are capped with the same material onto which they have been grown. Those dots are levelled by the newly grown layers until they reach a shape of truncated pyramid, or sometimes that of a lens, depending on how the islands were formed. The layer below the critical thickness is similar to a quantum well and is called wetting layer. Self-assembled quantum dots are composed of 10^4 to 10^6 atoms.

Such quantum dots are called self-assembled, due to the minimal human intervention during their formation. As stated above, self-assembled quantum dots can be made of silicon, germanium, or be compounded of III and V elements (GaAs, InP, GaN) or II and VI elements (CdSe, ZnTe, etc...). The works depicted in this thesis are focused exclusively on III-V quantum dots. Typical emission wavelengths of III-V QDs span from 690 nm (InP) to 950 nm (InGaAs), this wavelength does not only depend on the material used but also on the shape and size of the dot, which can be controlled by varying growth parameters like substrate temperature or deposition rate [44].

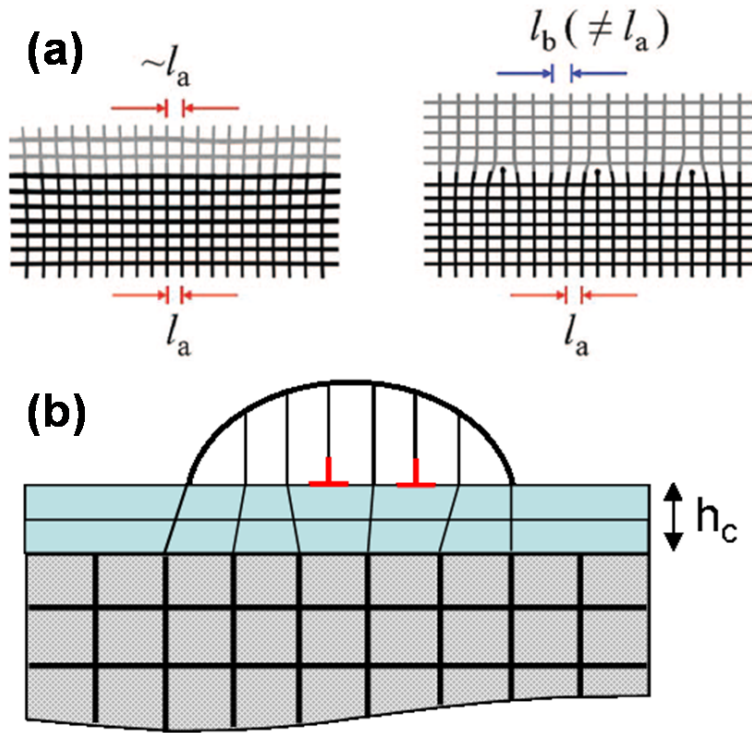


Figure 1.6: Illustration of the Stranski-Krastanov process: a) lattice mismatch between two materials causes strain (left) and dislocations (right) if it is large enough. (Taken from [7].) b) After deposition of a critical thickness h_c , strain relaxation induces the formation of an island. (Taken from [45].)

1.3.3 Interface fluctuations from quantum wells

Some structures can present the same properties of charge confinement without actually being clearly limited in all three directions. It is the case for the so-called interface quantum dots, formed by interface fluctuations of ultra-thin layers (usually quantum wells). In the growth direction the charges are confined due to the difference in material bandgaps, and in the lateral directions the difference of one monolayer of the material makes it more spatially confined, and therefore it requires more energy for the trapped charge to escape. The principle is illustrated in the image in figure 1.7.

It is noteworthy that the width of the well must be smaller than the exciton radius in bulk material (of the order of 10 nm in GaAs [6]) in order for the exciton to be confined and effectively trapped in the interface fluctuations. Such nanostructures have been discovered in quantum wells in the early nineties [46] and have been the first zero-dimensional semiconductor structures studied, shortly before the

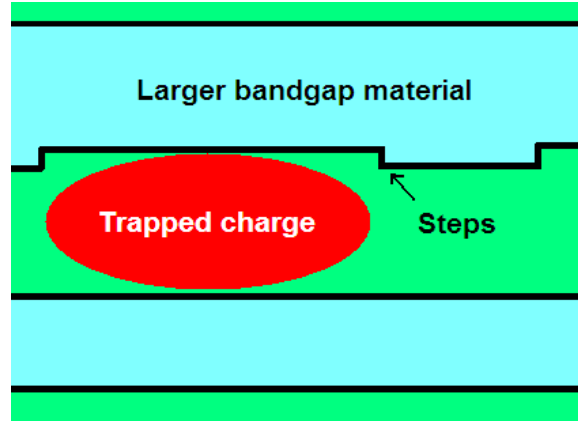


Figure 1.7: Illustration of a lateral view of a quantum dot created by interface fluctuation of thin layers of alternating semiconductor materials.

self-assembled kind. They present many differences with self-assembled. They are not strained, which can be an advantage as their formation does not create dislocations. Although they are well confined in the growth direction due to the small thickness of the quantum wells, their confinement in the lateral direction is weaker as it originates from a thickness fluctuation of the quantum well. The main reason why they are much less attractive compared with self-assembled is that unlike the latter, it is not possible to easily control their shape and size, and through that their optical properties. Chapter 3 of this thesis is based on a sample exhibiting interface fluctuations quantum dots.

1.3.4 Other types of quantum dots

There are other types of zero-dimensional nanostructures not addressed in this work, a non-exhaustive list of which is provided in this paragraph:

- **Colloidal quantum dots** are semiconductor nanocrystals obtained by a chemical synthesis. Precursor compounds are dissolved in a solution and start agglomerating upon heating into clusters of 10^2 to 10^5 atoms. The particularity of those quantum dots is that they are in liquid form, unlike the other types which are in solid state form. Colloidal quantum dots are one of the most promising methods for large-scale commercial applications, their synthesis is also known to be the least toxic. Colloidal quantum dots are interesting for biomedical applications, due to their free particle nature [47].
- Another way to obtain in a material the properties of quantum dots is to electrically pattern a two-dimensional electron gas. An electrode is litho-

graphically designed on top of a 2D structure filled with charges, typically a quantum well, and by applying a voltage between the gate and back electrodes, the charges, already confined in one direction due to the nature of the quantum well, are confined in the other two directions by the electric field. This kind of structure is called **gated quantum dot**.

- Within the same material different kind of crystal structures can grow. It has been demonstrated that when growing a nanowire of InP, the atoms could be ordered as a zinc-blende structure, much similar to most bulk semiconductors, but also as a wurtzite structure. Alternating the growth of both structures in a quantum wire would confine the charges in the direction of the wire, due to the difference in bandgap between the two types of crystal. Such quantum dots have been dubbed **crystal phase quantum dots** [48].

1.4 Experimental work on quantum dots

As seen in section 1.2 quantum dots are attractive in a wide range of domains, but they are not yet ready for large scale industrial applications. To this end, further understanding of their optical properties and the different ways to fabricate them is necessary. This section describes the main experimental techniques used to study quantum dots and what informations we can gather from them.

1.4.1 Micro-photoluminescence

The quantum dots studied in this thesis are all III-V self-assembled or interface fluctuations, emitting in the 700 nm or 950 nm regions. It has been said in the previous sections that quantum dots were good photon emitters. Indeed because of their direct band-gap, III-V materials can easily absorb and emit electromagnetic energy. Studying quantum dot emissions using micro-photoluminescence is the most direct way to obtain informations about their shape and size [49], energy levels [7], and spin polarization [50]. The experiment consists in exciting the sample with a laser while it is cooled at cryogenic temperature below 10 K and observe the resulting photoluminescence. This photoluminescence is diffracted through a spectrometer and directed at a charge-coupled device, providing a complete emission spectrum of the sample. First we'll go through the processes occurring under optical excitation, and then we'll describe the hardware used for the experiment.

Optical processes under excitation In our experiments the QD sample is excited non resonantly, which means the energy of the laser is greater than the bandgap of the semiconductor material surrounding the dots. Electrons and holes are excited in the bulk and then can either recombine at any point to emit a photon, or be trapped in a quantum dot (see section 1.1.4). When an electron and a hole relax into a quantum dot they form a Coulombic bond and result in an electron-hole pair that is usually called exciton. The exciton eventually recombines by emitting a photon with a frequency corresponding to the bandgap of the quantum dot. This phenomenon is best observed at a low temperature of below 10 K. At higher temperatures thermal processes becomes non-negligible and dominate optical emissions, resulting in a quenching of the photoluminescence. The average recombination time or lifetime can vary depending on size and shape of the dot, type of material and external factors but is generally of the order of the nanosecond for InGaAs self-assembled quantum dots [51].

If the surrounding bulk is saturated with charge carriers (which happens when the sample is excited with a high number of photons, or in other terms in the case where we use a high power of laser excitation) additional carriers can relax into the quantum dot before the first exciton recombines. The new electron and hole each fill the next available energy states, following the Pauli exclusion principle. The quantum dot then contains a bi-exciton, and with more electron-hole pairs a tri-exciton, etc... [52, 53]. It can also happen that a single electron or a single hole is trapped in the quantum dot. This can occur naturally due to the imperfect shape of the dot but it is also possible to control the charge in the dot by using an electric field. This technique is described in section 1.4.3 and in chapter 4. When an electron-hole pair relaxes into the dot it produces a trion, negatively or positively charged, depending on the nature of the particle present at ground state [52, 54, 55]. The study of charged exciton is very attractive for the purpose of implementing spin q-bit with the spin of single electrons or holes [56, 57]. The hole being a quasiparticle with a spin angular momentum of $3/2$, unlike the electron whose spin angular momentum is $1/2$, the exciton can have either a total spin of ± 1 (bright exciton), a state which can emit or absorb a photon, or a total spin of ± 2 (dark exciton), which is a state having a low probability of emitting a photon. Charged excitons can also be dark, it corresponds to the cases where the two electrons(holes) have identical spin, and to the cases where the electrons(holes) have different spins but the single hole(electron) has opposite spin from the electron(hole) at ground state [58–60]. Dynamics of dark excitons will not be described further in this thesis.

Experimental setup The sample is placed into a cryostat filled or flowing with liquid helium, decreasing its temperature to less than 10 K. It is excited with a HeNe red laser emitting at 650 nm and collimated by a microscope objective. The setup is described on figure 1.8.

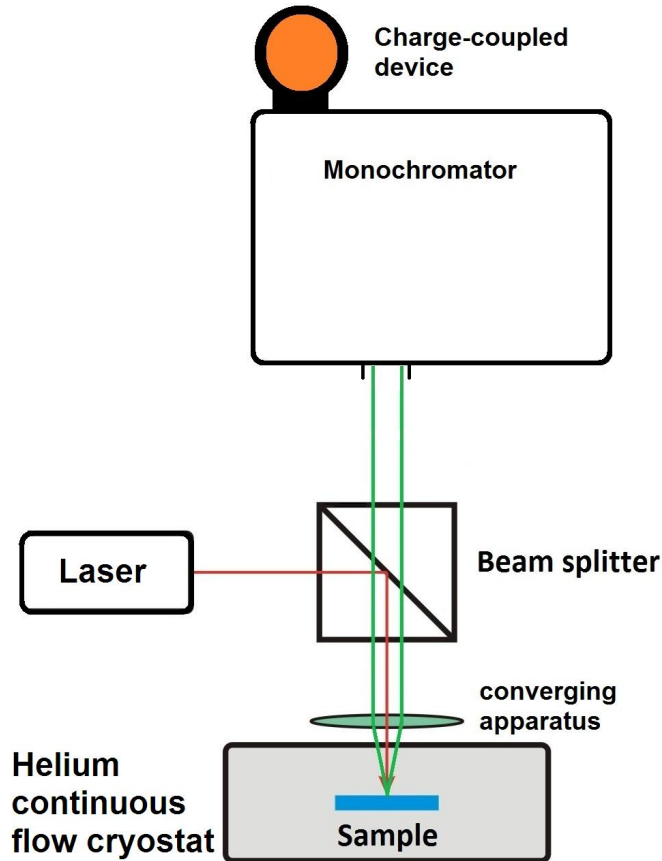


Figure 1.8: Schematics of the experimental photoluminescence setup.

The radiative efficiency of the quantum dot is almost 100% but it can happen in any direction upon a solid angle of 720° . The fraction of that angle that is not totally reflected at the interface between semiconductor and vacuum (around 2% for GaAs) is then collected through the microscope objective and directed at a monochromator. A charge coupled device at the exit of the monochromator allows to see a spectrum of light emitted by the sample. Such a spectrum is comprised of an inhomogeneously broad emission from recombinations happening in the bulk semiconductor (usually between 800 and 850 nm for GaAs), at lower energy we find the broad emission of the wetting layer and on the higher energy side of this emission the quantum dots. Studying the spectrum emitted by a sample containing

quantum dots would in principle allow the observation of specific lines of energy corresponding to the various excitonic complexes that can be trapped inside quantum dots. The intensity of those lines depends on the number of photons emitted by the dots, which in turn depends on the quality of the growth, the nature of the materials used, the quantum dots recombination rate and the intensity of the excitation source. The dot lines are not exactly homogeneous because of electrical noise, instead taking the form of a broad line with width spanning between 50 and 200 μeV [61, 62].

The microscope objective is a key element for the observation of single dot emission lines. Without it, due to the large sample area covered by the laser spot (of the order of the hundreds of μm), and the high density of dots yielded by the Stranski-Krastanov growth method (from 10^8 cm^{-2} to 10^{12} cm^{-2}) the number of quantum dots actually observed would be too high to be able to observe them individually, resulting in an inhomogeneously broadened ensemble PL. The microscope objective focuses the beam on the sample to a spot size as small as 1 μm of diameter. This allows single quantum dots to be observed individually. To observe and fully study single quantum dots it is desirable to have an even smaller density of lines. This can be achieved by using a metal mask containing apertures with a diameter of a few hundreds of nm. With this apparatus the lines are well isolated and can be studied separately.

1.4.2 Measurement of fine structure splitting

When an electron in a neutral quantum dot becomes excited, it can have a spin up or down (corresponding respectively to a $|-1\rangle$ and $|+1\rangle$ exciton). The same is true for charged excitons: the spin of the single hole (electron) of the excited state can have a spin up or down. Those are two states having the same energy which means the spectral line observed by photoluminescence is actually two-fold degenerate [55]. This degeneracy can be lifted using a magnetic field since it adds a linear term depending on the total spin of the exciton to its energy. This lifting of degeneracy is called Zeeman effect, and is illustrated on figure 1.9.

There are two main experimental approaches to apply magnetic field, along the quantisation or growth axis (Faraday geometry) and perpendicular to it (Voigt geometry). Voigt geometry can be interesting because it breaks the circular symmetry of the dot: self-assembled dots can be approximated to have a lens shape, so they can be considered to have one axis of symmetry along the growth direction. Ap-

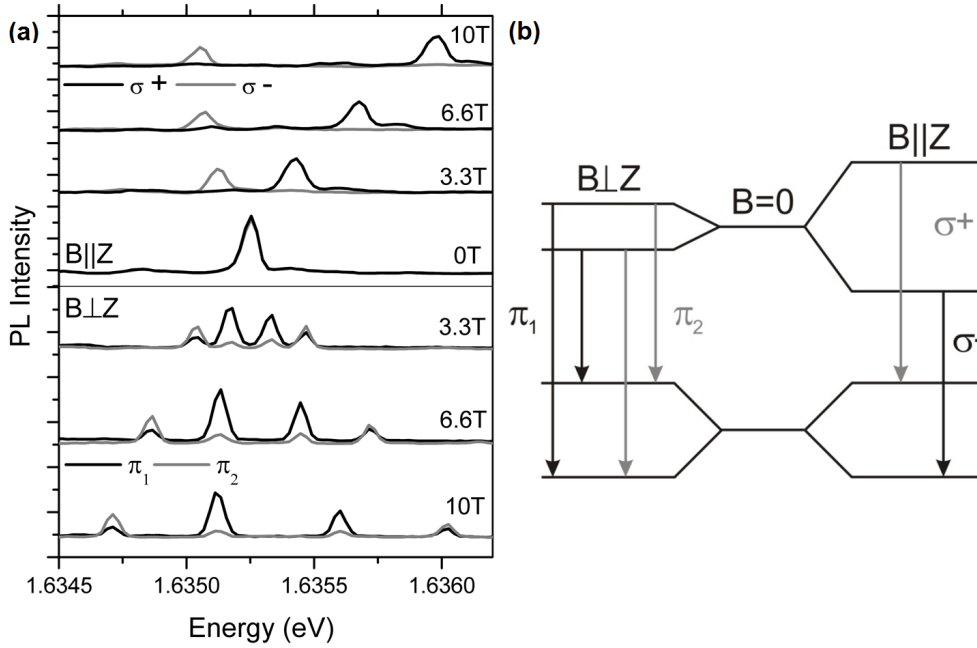


Figure 1.9: Illustration of the Zeeman effect: the application of a magnetic field lifts the degeneracy on energy levels (b), splitting the original spectral line into several (a). From Del Pozo-Zamudio et al. [63].

plying a magnetic field in the Faraday geometry conserves this symmetry whereas a magnetic field in Voigt geometry creates an in-plane anisotropy. It allows for the observation of dark excitons (fig. 1.9 (a) bottom and (b) left) [55]. Zeeman splitting can give us information about the electronic and hole g-factor, as well as the diamagnetic shift, a quantity useful for the determination of dot shape and dimensions [50].

The degeneracy can also be lifted naturally when the dot's shape cannot be approximated to be symmetric. The fine structure splitting that results is generally of the order of $50 \mu\text{eV}$ [64, 65]. For neutral excitons the light emitted by the two states is linearly polarized. If the fine structure splitting is smaller than the broadening of the lines it is not possible to observe it, but since one state is horizontally polarized and the other vertically, the shift in energy from one state to the other can be observed using a linear polarizer. Such an experiment is described in chapter 3.

1.4.3 Charge control using electric field

To observe one specific excitonic complex can prove difficult if we have no way to trigger them on demand. One of the main experimental approaches to tune the

charge occupancy of a dot is through an electric field. In a quantum dot sample processed as a Schottky diode the electric field is applied between the quantum dot region and a doped region and allows control over the resident charge in the dot [52]. This principle is described in figure 1.10: a gate contact and a back contact are fabricated respectively on the surface of the sample and under the quantum dot region.

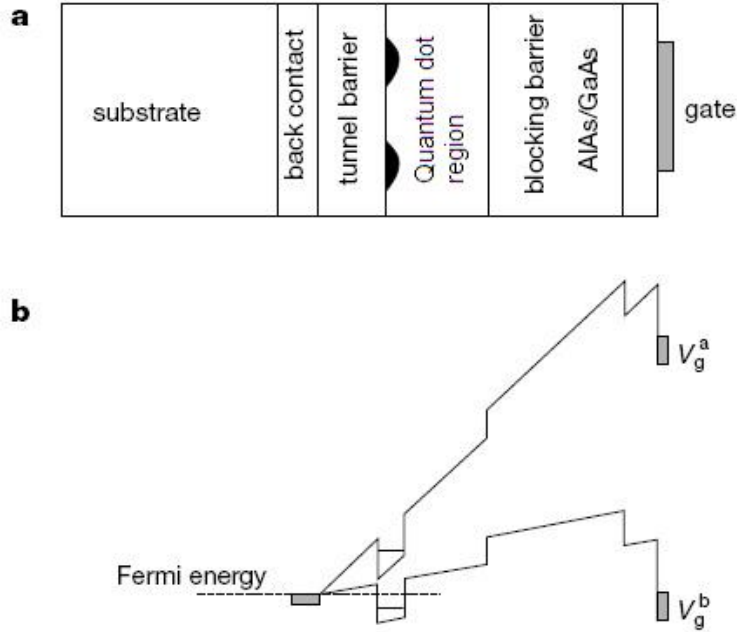


Figure 1.10: Illustration of electrically controlled charging of quantum dots. (a) The layer structure of the sample shows that a voltage applied at the gate (right) would create a current of charges between the dots and the back contact (left), modifying the energy diagram in (b). Depending on the applied voltage, the ground state level of the dot can be above or below the Fermi level, in which latter case electrons would be able to tunnel into the dot. Figure taken from [54].

The layer structure is illustrated in figure 1.10(a), the sample then acts as a Schottky diode due to the presence of a doped (n or p) layer just below the back contact. As can be seen in 1.10(b), a modification in the voltage applied on the gate contact will change the energy level of the dot, bringing it on demand below or above the Fermi level of charge carriers originating from the doped layer. If the quantum dot level is brought below the Fermi level, electrons (or holes in the case of p-doping) tunnel into the dot, allowing us to engineer a dot into a neutral, positively or negatively charged dot. The barrier between the dots and the back contact is usually of the order of 50 nm thick [52]. Schottky diode structures are widely used in the study of quantum confined Stark effect [66, 67]. They are the

main topic of chapter 4.

1.5 Organization of the thesis

The present thesis is organized in the following way. Three projects are presented in three different chapters. Though they can be only slightly correlated and not always based on the same sample, they have in common to investigate the optical properties of quantum dots grown in a way that has not been done before, or with a material not widely studied before.

Chapter 2 relates to the study of self-assembled InAs quantum dots grown monolithically on silicon, and their coupling with photonic crystal cavities. The quality of the cavities, fabricated for the first time on a silicon substrate, is asserted as well as the single photon emission ability of the dots. Chapter 3 is based on the same sample, but the investigation focuses on quantum dots formed by interface fluctuations of GaAs/AlGaAs thin layer superlattices. Optical properties, fine structure splitting and photon anti-bunching are studied. Finally, in chapter 4 characterization of quantum dots grown from a new combination of material, InPAs, is conducted. Samples with various concentrations of arsenic have their emission spectra compared, and Schottky diode fabrication allows for study of the dots under controlled electric field.

References

- [1] Wgsimon, “Transistor Count and Moore’s Law - 2011.” http://en.wikipedia.org/wiki/File:Transistor_Count_and_Moore%27s_Law_-_2011.svg, May 2011.
- [2] G. E. Moore, “Cramming more components into integrated circuits,” *Electronics*, vol. 38, 1965.
- [3] Michler, Peter, *Single Quantum Dots*. Topics in Applied Physics, Springer, 2003.
- [4] M. S. Skolnick and D. J. Mowbray, “SELF-ASSEMBLED SEMICONDUCTOR QUANTUM DOTS: Fundamental Physics and Device Applications,” *Annual Review of Materials Research*, vol. 34, no. 1, pp. 181–218, 2004.
- [5] D. leadley, “Electronic band structure.” <http://www2.warwick.ac.uk/fac/sci/physics/current/postgraduate/regs/mpags/ex5/bandstructure/>, Jul 2011.
- [6] M. Fox, *Optical Properties of Solids (Oxford Master Series in Physics, 3)*. Oxford University Press, USA, 2001.
- [7] A. N. Vamivakas and M. Atatüre, “Photons and (artificial) atoms: an overview of optical spectroscopy techniques on quantum dots,” *Contemporary Physics*, vol. 51, pp. 17–36, Dec. 2009.
- [8] D. Bimberg, *Quantum dot heterostructures*. Berlin: John Wiley and Sons, 1999.
- [9] Masumoto, Y and Takagahara, T, *Semiconductor Quantum Dots*. Nanoscience and Technology, Springer, 2002.
- [10] V. A. Shchukin and D. Bimberg, “Spontaneous ordering of nanostructures on crystal surfaces,” *Reviews of Modern Physics*, vol. 71, pp. 1125+, July 1999.

- [11] P. Reiss, M. Protière, and L. Li, “Core/Shell Semiconductor Nanocrystals,” *Small*, vol. 5, pp. 154–168, Jan. 2009.
- [12] M. Bruchez, M. Moronne, P. Gin, S. Weiss, and A. P. Alivisatos, “Semiconductor Nanocrystals as Fluorescent Biological Labels,” *Science*, vol. 281, pp. 2013–2016, Sept. 1998.
- [13] S. Kumar and T. Nann, “Shape Control of II-VI Semiconductor Nanomaterials,” *Small*, vol. 2, pp. 316–329, Mar. 2006.
- [14] I. A. Akimov, K. V. Kavokin, A. Hundt, and F. Henneberger, “Electron-hole exchange interaction in a negatively charged quantum dot,” *Physical Review B*, vol. 71, pp. 075326+, Feb. 2005.
- [15] J. Shah, *Ultrafast Spectroscopy of Semiconductors and Semiconductor Nanostructures*. Springer, 1999.
- [16] A. I. Tartakovskii, “Nuclear magnetic resonance in quantum dots.” Symposium on Semiconductor Nano-Photonics for Quantum Information Science, Sep 2013.
- [17] U. Bockelmann and G. Bastard, “Phonon scattering and energy relaxation in two-, one-, and zero-dimensional electron gases,” *Phys. Rev. B*, vol. 42, pp. 8947–8951, Nov 1990.
- [18] H. Benisty, C. M. Sotomayor-Torrès, and C. Weisbuch, “Intrinsic mechanism for the poor luminescence properties of quantum-box systems,” *Phys. Rev. B*, vol. 44, pp. 10945–10948, Nov 1991.
- [19] J. Urayama, T. B. Norris, J. Singh, and P. Bhattacharya, “Observation of phonon bottleneck in quantum dot electronic relaxation,” *Phys. Rev. Lett.*, vol. 86, pp. 4930–4933, May 2001.
- [20] J. Kim, O. Benson, H. Kan, and Y. Yamamoto, “A single-photon turnstile device,” *Nature*, vol. 397, pp. 500–503, Feb. 1999.
- [21] A. J. Shields, “Semiconductor quantum light sources,” *Nat Photon*, vol. 1, pp. 215–223, 2007.
- [22] C. L. Salter, R. M. Stevenson, I. Farrer, C. A. Nicoll, D. A. Ritchie, and A. J. Shields, “An entangled-light-emitting diode,” *Nature*, vol. 465, pp. 594–597, June 2010.

- [23] R. M. Stevenson, R. J. Young, P. Atkinson, K. Cooper, D. A. Ritchie, and A. J. Shields, “A semiconductor source of triggered entangled photon pairs,” *Nature*, vol. 439, pp. 179–182, Jan. 2006.
- [24] D. Deutsch, “Quantum theory, the church-turing principle and the universal quantum computer,” *Proceedings of the Royal Society of London. A. Mathematical and Physical Sciences*, vol. 400, no. 1818, pp. 97–117, 1985.
- [25] T. Hey, “Quantum computation: an introduction.” https://www.researchgate.net/publication/3363605_Quantum_computing_an_introduction?ev=srch_pub, Sept. 1999.
- [26] D. Liang and J. E. Bowers, “Recent progress in lasers on silicon,” *Nat Photon*, vol. 4, no. 8, pp. 511–517, 2010.
- [27] N. N. Ledentsov, V. M. Ustinov, V. A. Shchukin, P. S. Kop’ev, Z. Alferov, and D. Bimberg, “Quantum dot heterostructures: Fabrication, properties, lasers (Review),” *Semiconductors*, vol. 32, no. 4, pp. 343–365, 1998.
- [28] Y. Arakawa and H. Sakaki, “Multidimensional quantum well laser and temperature dependence of its threshold current,” *Applied Physics Letters*, vol. 40, no. 11, pp. 939–941, 1982.
- [29] “Fujitsu, university of tokyo develop world’s first 10gbps quantum dot laser featuring breakthrough temperature-independent output.” <http://www.fujitsu.com/global/news/pr/archives/month/2004/20040910-01.html>.
- [30] A. Banerjee, T. Frost, and P. Bhattacharya, “Nitride-based quantum dot visible lasers,” *Journal of Physics D: Applied Physics*, vol. 46, pp. 264004+, July 2013.
- [31] J. L. O’Brien, A. Furusawa, and J. Vuckovic, “Photonic quantum technologies,” *Nat Photon*, vol. 3, pp. 687–695, Dec. 2009.
- [32] C. H. Bennett, G. Brassard, C. Crépeau, R. Jozsa, A. Peres, and W. K. Wootters, “Teleporting an unknown quantum state via dual classical and Einstein-Podolsky-Rosen channels,” *Physical Review Letters*, vol. 70, pp. 1895–1899, Mar. 1993.
- [33] X.-S. Ma, T. Herbst, T. Scheidl, D. Wang, S. Kropatschek, W. Naylor, B. Wittmann, A. Mech, J. Kofler, E. Anisimova, V. Makarov, T. Jennewein, R. Ursin, and A. Zeilinger, “Quantum teleportation over 143 kilometres using active feed-forward,” *Nature*, vol. 489, pp. 269–273, Sept. 2012.

- [34] C. H. Bennett and S. J. Wiesner, “Communication via one- and two-particle operators on Einstein-Podolsky-Rosen states,” *Physical Review Letters*, vol. 69, pp. 2881–2884, Nov. 1992.
- [35] Y. H. Shih and C. O. Alley, “New Type of Einstein-Podolsky-Rosen-Bohm Experiment Using Pairs of Light Quanta Produced by Optical Parametric Down Conversion,” *Physical Review Letters*, vol. 61, pp. 2921–2924, Dec. 1988.
- [36] T. E. Kiess, Y. H. Shih, A. V. Sergienko, and C. O. Alley, “Einstein-Podolsky-Rosen-Bohm experiment using pairs of light quanta produced by type-II parametric down-conversion,” *Physical Review Letters*, vol. 71, pp. 3893–3897, Dec. 1993.
- [37] C. Cohen-Tannoudji, B. Diu, and F. Laloë, *Mécanique quantique*. Enseignement des sciences, Hermann, 1973.
- [38] D. Loss and D. P. DiVincenzo, “Quantum computation with quantum dots,” *Physical Review A*, vol. 57, pp. 120–126, Jan. 1998.
- [39] Aixtron, *How MOCVD works. Deposition Technology for Beginners*. Aixtron SE, 2011.
- [40] P. M. Petroff and S. P. DenBaars, “MBE and MOCVD growth and properties of self-assembling quantum dot arrays in III-V semiconductor structures,” *Superlattices and Microstructures*, vol. 15, pp. 15+, Jan. 1994.
- [41] A. Y. Cho and J. R. Arthur, “Molecular beam epitaxy,” *Progress in Solid State Chemistry*, vol. 10, pp. 157–191, Jan. 1975.
- [42] P. D. Dapkus, “A critical comparison of MOCVD and MBE for heterojunction devices,” *Journal of Crystal Growth*, vol. 68, pp. 345–355, Sept. 1984.
- [43] P. M. Petroff, A. Lorke, and A. Imamoglu, “Epitaxially self-assembled quantum dots,” *Physicstoday*, vol. 54, pp. 46+, May 2001.
- [44] A. Baskaran and P. Smereka, “Mechanisms of Stranski-Krastanov growth,” *Journal of Applied Physics*, vol. 111, pp. 044321–044321–6, Feb. 2012.
- [45] Acarlso3, “Adsorbate island showing interfacial dislocations.” <http://en.wikipedia.org/wiki/File:DislocatedIsland.png>, Dec 2007.

- [46] A. Zrenner, L. V. Butov, M. Hagn, G. Abstreiter, G. Böhm, and G. Weimann, “Quantum dots formed by interface fluctuations in AlAs/GaAs coupled quantum well structures,” *Physical Review Letters*, vol. 72, pp. 3382–3385, May 1994.
- [47] J. . M. Klostranec and W. . C. . W. Chan, “Quantum Dots in Biological and Biomedical Research: Recent Progress and Present Challenges,” *Adv. Mater.*, vol. 18, pp. 1953–1964, Aug. 2006.
- [48] N. Akopian, G. Patriarche, L. Liu, J. C. Harmand, and V. Zwiller, “Crystal Phase Quantum Dots,” *Nano Lett.*, vol. 10, pp. 1198–1201, Mar. 2010.
- [49] J. Shumway, A. J. Williamson, A. Zunger, A. Passaseo, M. DeGiorgi, R. Cingolani, M. Catalano, and P. Crozier, “Electronic structure consequences of In/Ga composition variations in self-assembled $\text{In}_x\text{Ga}_{1-x}\text{As}/\text{GaAs}$ alloy quantum dots,” *Physical Review B*, vol. 64, pp. 125302+, Sept. 2001.
- [50] M. N. Makhonin, K. V. Kavokin, P. Senellart, A. Lemaître, A. J. Ramsay, M. S. Skolnick, and A. I. Tartakovskii, “Fast control of nuclear spin polarization in an optically pumped single quantum dot,” *Nat Mater*, vol. 10, pp. 844–848, Nov. 2011.
- [51] I. J. Luxmoore, R. Toro, O. Del Pozo-Zamudio, N. A. Wasley, E. A. Chekhovich, A. M. Sanchez, R. Beanland, A. M. Fox, M. S. Skolnick, H. Y. Liu, and A. I. Tartakovskii, “III-V quantum light source and cavity-QED on Silicon,” *Sci. Rep.*, vol. 3, p. 1239, 2013.
- [52] O. D. D. Couto, J. Puebla, E. A. Chekhovich, I. J. Luxmoore, C. J. Elliott, N. Babazadeh, M. S. Skolnick, A. I. Tartakovskii, and A. B. Krysa, “Charge control in $\text{InP}/(\text{Ga,In})\text{P}$ single quantum dots embedded in Schottky diodes,” *Physical Review B*, vol. 84, pp. 125301+, Sept. 2011.
- [53] N. A. J. M. Kleemans, J. van Bree, A. O. Govorov, J. G. Keizer, G. J. Hamhuis, R. Notzel, Silov, and P. M. Koenraad, “Many-body exciton states in self-assembled quantum dots coupled to a Fermi sea,” *Nat Phys*, vol. 6, pp. 534–538, July 2010.
- [54] R. J. Warburton, C. Schafflein, D. Haft, F. Bickel, A. Lorke, K. Karrai, J. M. Garcia, W. Schoenfeld, and P. M. Petroff, “Optical emission from a charge-tunable quantum ring,” *Nature*, vol. 405, pp. 926–929, June 2000.

- [55] M. Bayer, G. Ortner, O. Stern, A. Kuther, A. A. Gorbunov, A. Forchel, P. Hawrylak, S. Fafard, K. Hinzer, T. L. Reinecke, S. N. Walck, J. P. Reithmaier, F. Klopff, and F. Schäfer, “Fine structure of neutral and charged excitons in self-assembled In(Ga)As/(Al)GaAs quantum dots,” *Physical Review B*, vol. 65, pp. 195315+, May 2002.
- [56] A. J. Ramsay, S. J. Boyle, R. S. Kolodka, J. B. B. Oliveira, J. Skiba-Szymanska, H. Y. Liu, M. Hopkinson, A. M. Fox, and M. S. Skolnick, “Fast Optical Preparation, Control, and Readout of a Single Quantum Dot Spin,” *Physical Review Letters*, vol. 100, pp. 197401+, May 2008.
- [57] T. M. Godden, J. H. Quilter, A. J. Ramsay, Y. Wu, P. Brereton, S. J. Boyle, I. J. Luxmoore, J. Puebla-Nunez, A. M. Fox, and M. S. Skolnick, “Coherent Optical Control of the Spin of a Single Hole in an InAs/GaAs Quantum Dot,” *Physical Review Letters*, vol. 108, pp. 017402+, Jan. 2012.
- [58] C. Schüller, K. B. Broocks, C. Heyn, and D. Heitmann, “Oscillator strengths of dark charged excitons at low electron filling factors,” *Physical Review B*, vol. 65, pp. 081301+, Jan. 2002.
- [59] D. Andronikov, “Charged exciton complexes (trions) in low dimensional structures,” *conference paper*, June 2005.
- [60] A. J. Shields, M. Pepper, M. Y. Simmons, and D. A. Ritchie, “Spin-triplet negatively charged excitons in GaAs quantum wells,” *Physical Review B*, vol. 52, pp. 7841+, Sept. 1995.
- [61] P. Borri, W. Langbein, S. Schneider, U. Woggon, R. L. Sellin, D. Ouyang, and D. Bimberg, “Ultralong Dephasing Time in InGaAs Quantum Dots,” *Physical Review Letters*, vol. 87, pp. 157401+, Oct. 2001.
- [62] A. V. Kuhlmann, J. Houel, A. Ludwig, L. Greuter, D. Reuter, A. D. Wieck, M. Poggio, and R. J. Warburton, “Charge noise and spin noise in a semiconductor quantum device,” *Nat Phys*, vol. 9, pp. 570–575, Sept. 2013.
- [63] O. Del Pozo-Zamudio, J. Puebla, E. Chekhovich, R. Toro, A. Krysa, R. Beanland, A. M. Sanchez, M. S. Skolnick, and A. I. Tartakovskii, “Growth and magneto-optical characterization of InPAs/GaInP Quantum Dots,” *Unpublished*, 2013.

- [64] D. Gammon, E. S. Snow, B. V. Shanabrook, D. S. Katzer, and D. Park, “Fine Structure Splitting in the Optical Spectra of Single GaAs Quantum Dots,” *Physical Review Letters*, vol. 76, pp. 3005–3008, Apr. 1996.
- [65] R. Toro, O. Del Pozo-Zamudio, M. N. Makhonin, J. Dixon, A. M. Sanchez, R. Beanland, H.-Y. Liu, M. S. Skolnick, and A. I. Tartakovskii, “Visible light single photon emitters monolithically grown on silicon,” *Unpublished*, 2013.
- [66] P. W. Fry, I. E. Itskevich, D. J. Mowbray, M. S. Skolnick, J. J. Finley, J. A. Barker, E. P. O’Reilly, L. R. Wilson, I. A. Larkin, P. A. Maksym, M. Hopkinson, M. Al-Khafaji, J. P. R. David, A. G. Cullis, G. Hill, and J. C. Clark, “Inverted electron-hole alignment in InAs-GaAs self-assembled quantum dots,” *Physical Review Letters*, vol. 84, pp. 733+, Jan. 2000.
- [67] P. W. Fry, I. E. Itskevich, S. R. Parnell, J. J. Finley, L. R. Wilson, K. L. Schumacher, D. J. Mowbray, M. S. Skolnick, M. Al-Khafaji, A. G. Cullis, M. Hopkinson, J. C. Clark, and G. Hill, “Photocurrent spectroscopy of InAs/GaAs self-assembled quantum dots,” *Physical Review B*, vol. 62, pp. 16784+, Dec. 2000.

Chapter 2

Optical characterization and cavity coupling of InAs/GaAs quantum dots monolithically grown on silicon substrate

2.1 Introduction

Silicon chips have been used as our main computing technology for the last four decades, with a number of transistors per chip doubling every two years as predicted by Moore's law. Since last decade though the scalability of bulk silicon technology has reached a limitation, prompting the fake solution of dividing computational tasks between multiple cores. To reach the next level of computing one must find a way of making operations that differ from the usual open/closed electricity current flow. Encoding bits of data into the spin of photons is one way of doing it that is heavily investigated since the nineties [1]. It would also allow for entanglement of particles (in this case photons) leading to a new, more effective way of computing, the so-called quantum information processing (QIP) [2]. Photonic technology is also of prime importance for domains such as quantum lithography and quantum cryptography. To replace silicon complementary metal-oxide semiconductor (CMOS) technology, the same type of material has been used, only in the form of nanostructures instead of bulk [3, 4]. Indeed a group IV semiconductor like silicon is praised by industry for its low cost of fabrication, its robustness and the possibility to easily create insulation layers by growing silicon oxide. Also being a state of the art technology, silicon processing is much more attractive for industry. On the other hand, silicon's indirect band gap makes it a mediocre light emitter, whereas compound

semiconductors like III-V have direct band gap providing best opto-electronic capabilities, and better electron mobility. Furthermore, single photon emission have been demonstrated [5], a feature essential for any quantum manipulation.

A straightforward solution is to integrate III-V quantum emitters with existing silicon technology, feasibility of which is demonstrated in this chapter through the optical and structural study of InGaAs quantum dots monolithically grown on a silicon substrate, and embedded in photonic crystal microcavities [6].

First the sample structure will be discussed, then the quantum dots and the quality of cavities, then single photon emission demonstration, and finally strong coupling opening door to quantum electrodynamics.

2.2 Structural study

2.2.1 Previous attempts at growing III-V on IV

As explained in the introduction, the integration of compound semiconductors (III-V, or II-VI) with group IV is desirable among other things for quantum and classical computation. Though the first attempts can be traced back as early as 1962, the purpose there was to make hybrid heterojunctions with better characteristics for electronic applications [7]. Also the growth of GaAs on an intermediate substrate of germanium, due to the similar lattice constant of the two materials [8], does not present the same challenges as with silicon, whose lattice mismatch with III-V ranges from 4% to 8% (see paragraph 2.2.3). In later years, the need of bringing III-V optical capabilities with the high efficiency of state of the art Si technology became more apparent, and in 1984 Wang managed one of the first growths of GaAs/AlGaAs on silicon [9]. Less than a year later Metzger from MIT realized a metal-semiconductor field-effect transistor (MESFET) with good device characteristics from GaAs layers grown directly on silicon [10]. As more studies were being made on the subject [11, 12], growth techniques started to emerge to overcome the issues of semiconductor hybridization and make it more suitable for the growth of complex structures like quantum wells or quantum dots [13]. For the past decade quantum dots fabricated on Si allowed for semiconductor lasers with good characteristics to be integrated with silicon technology, opening the way to the introduction of III-V to silicon photonics [14–16] (see figure 2.1).

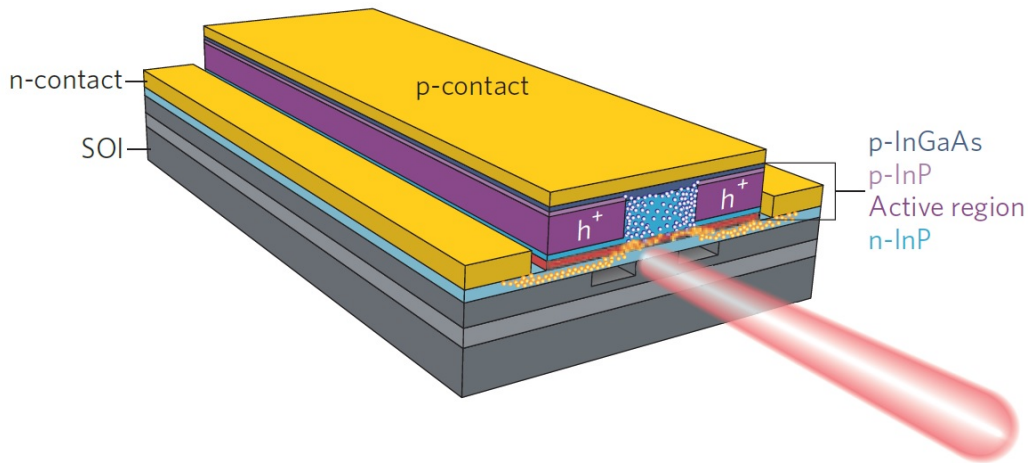


Figure 2.1: Illustration of hybrid III-V/Si technology: in this hybrid Si FabryProt laser, the InP active layers are bonded on a Si waveguide. Adapted from “Recent progress in lasers on silicon” from Di Liang and John E. Bowers [14]

Now that coherent light sources are implemented on silicon, the next step towards optical devices on silicon is the single photon emitter. Only recently was that feature achieved, on one hand by Cavigli et al. using the method of droplet epitaxy dots, grown on top of a Ge-on-Si virtual substrate [17] and on the other hand by our team at University of Sheffield [6] based on a InAs quantum dots sample monolithically grown on Si substrate by Hui-Yun Liu at University College London [16]. The present chapter is based on this last work.

2.2.2 Structure description

Now we will explore the structure of the sample grown by Liu et al.. It consists of a phosphorus-doped silicon substrate oriented in the (100) direction, with a 4 °offcut towards the [110] plane. To remove surface oxidation, sample was maintained at a high temperature of 900 °C for 10 minutes. After cooling down the wafer, the III-V part of the sample has been realized using molecular beam epitaxy (MBE), starting with a 30 nm nucleation layer grown at 400 °C with a low growth rate of 0.1 monolayers per second (ML/s). The remaining 970 nm of the GaAs were grown at high temperature at a rate of 0.7 ML/s, accounting for a total contact layer of 1 μm , as can be seen on figure 2.2.

Next layers to be grown were dislocation filters [11, 18]. The strain filters consist of a fourfold repetition of a more complex structure, composed of five layers of 10 nm thick $\text{In}_{0.15}\text{Al}_{0.85}\text{As}$, alternating with five layers of 10 nm thick GaAs, all of this

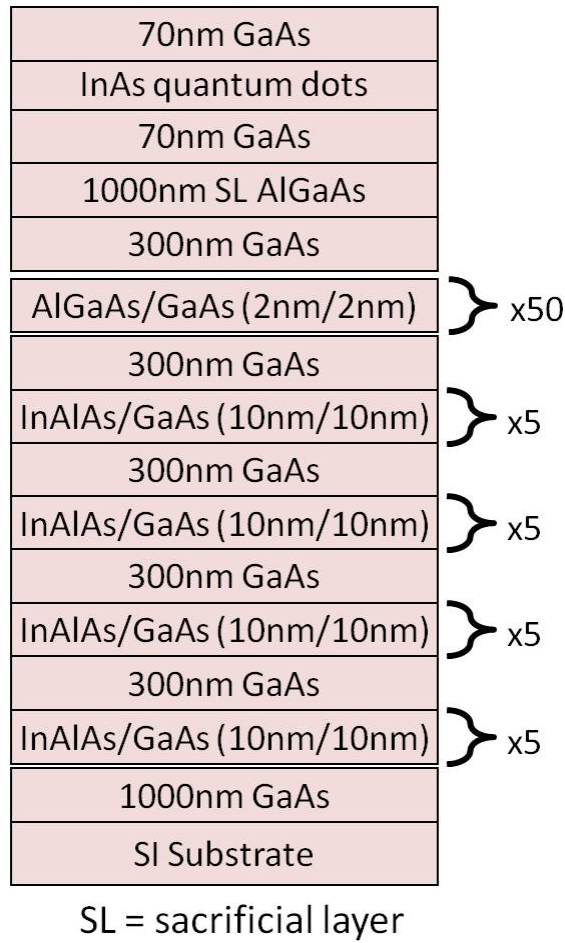


Figure 2.2: Layer structure of the sample.

capped with 300 nm of GaAs. On top of that is grown a short period superlattice comprised of 50 times a 2 nm layer of $\text{Al}_{0.4}\text{Ga}_{0.6}\text{As}$ topped with a 2 nm layer of GaAs.

On top of all that after a capping layer of 300 nm GaAs is a 1 μm thick $\text{Al}_{0.6}\text{Ga}_{0.4}\text{As}$ sacrificial layer, which is used for the fabrication of photonic crystals described in paragraph 2.4.2, and on which lay the active layer of InAs self-assembled quantum dots embedded in 140 nm GaAs (70 nm below and 70 nm above). The quantum dots height has been engineered through the indium flush technique [19], thus three samples have been grown with heights of 2 nm, 2.5 nm and 3 nm.

2.2.3 Structure discussion

Due to huge lattice mismatch between silicon and GaAs, one finds it very difficult to obtain high quality quantum dots and other nanostructures. Indeed the lattice mismatch, of near 4% between Si and GaAs and 8% for Si and InP, favours the creation of threading dislocations (they can be seen clearly on fig. 2.4), which act as non-radiative recombination sites, thus potentially dramatically lowering PL efficiency. Many a feature of this complex growth structure (described above) is aimed at reducing the natural drawbacks of the semiconductor hybridization, mainly by reducing the density of dislocations.

Nucleation layer

First to be taken into account is the growth temperature of the GaAs nucleation layer. On top of the silicon substrate is grown a 1 μm layer of GaAs, and to introduce this layer, the first 30 nm of GaAs are grown at a low temperature and slow rate of 0.1 MonoLayer per second (ML/s) against the faster 0.7 ML/s for the rest of the GaAs. The temperature at which the nucleation layer is grown has been specifically engineered to reduce strain. Test growths at different temperatures have shown a distinct reduction in strain density at 400 $^{\circ}\text{C}$ [16], as can be seen in fig. 2.3. Three different samples have been grown, with nucleation layer temperature of 380 $^{\circ}\text{C}$, 400 $^{\circ}\text{C}$ and 420 $^{\circ}\text{C}$, cross-sectional TEM image of the samples revealed a significantly smaller density of defects in the 400 $^{\circ}\text{C}$ sample, prompting the growth of all subsequent samples at this temperature.

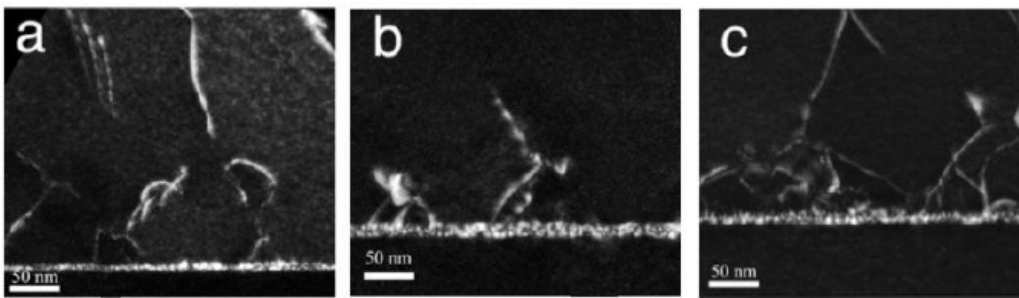


Figure 2.3: cross-sectional TEM image of Si/GaAs interface. The nucleation layer is grown at different temperatures: (a) 380 $^{\circ}\text{C}$, (b) 400 $^{\circ}\text{C}$, (c) 420 $^{\circ}\text{C}$. Images taken from [16].

Strain filter

Though being an optimized parameter for the growth of the nucleation layer, this temperature of 400 °C does not prevent the formation of a high density of defects propagating through the full thickness of III-V material and greatly lowering photon emission. To reduce the number of such dislocations a strain filter is still necessary. An InAlAs/GaAs strained layer superlattice (SLS) is grown for that purpose. The SLS have started to see a lot of studies and applications from the 70s when interest was growing on mismatched compound semiconductor growth [13, 18, 20]. The principle is to create an array of thin layers, alternating materials of mismatched lattice parameter. Because of this mismatch, strain is naturally created in the SLS, though due to the small thickness of the layers it does not propagate to the upper layers. These strains capture or deviate the dislocations coming from the lower layers. These strains capture or deviate the dislocations coming from the lower layers, eventually reducing them by a huge percentage.



Figure 2.4: TEM image of the layer structure. The clearer layer on the bottom of the image is Si, strain formation can be seen on the upper III-V layers.

Indeed the effect can clearly be seen on figure 2.4 representing a cross-sectional TEM image of the sample realized by A. Sanchez and R. Beanland from University

of Warwick. In a clear color, is the Si substrate. On top of it is the 1 μm layer of GaAs presenting a high density of dislocations, which propagate along the growth axis. The four InAlAs/GaAs superlattices can be observed located one after the other in the middle top of the TEM image. After each of these SLS a smaller number of dislocations is observed, finally giving a density of $\sim 6 \times 10^6 \text{ cm}^{-2}$ at the sample surface (measured from etch-pit density).

Antiphase disorder

Another source of dislocations is caused by the polar nature of III-V semiconductor. Indeed III-V lattice is formed of two poles, an anion (arsenic in the case of GaAs) and a cation (gallium) whereas silicon is a non-polar substrate. Since there is no or little preference as to which ion is bound to the surface during the early stages of the growth, it can lead to situations where a region starts with the cation plane and another region starts with the anion plane, leading to atom mismatch (see figure 2.5). This phenomenon is called anti-phase disorder [11], and as can be seen on the figure can also be caused by steps on the surface of the substrate. It has been found though that starting the III-V growth with a prelayer of only one of the elements effectively suppresses the formation of anti-phase domains [12].

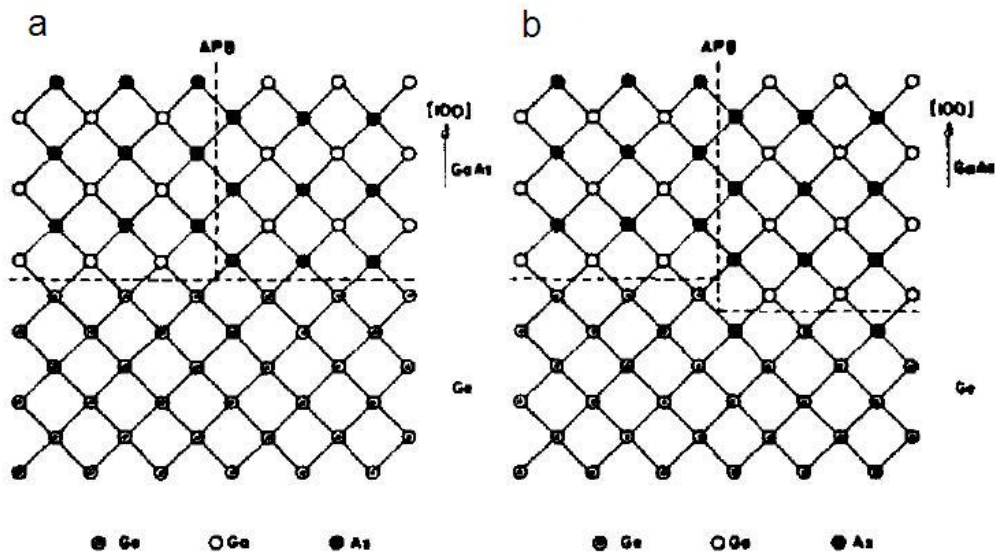


Figure 2.5: Antiphase boundary for GaAs grown on a Ge substrate. (a)The two antiphase domains started on the same plane, but with different atom deposition. (b)The two antiphase domains started with the same atom, but on two different planes separated by a one atom step. Figure taken from [11].

Smoothing layers

Since the main purpose of this sample is to make photonic crystal with cavities as small as a few hundreds of nm, a smooth surface is desired. This is realized by growing a short period superlattice (SPL, see fig. 2.4), alternating super thin layers of GaAs and AlGaAs. This technique, though not tested, has been inspired from Fischer et al. [11]. In this work the growth front after the first GaAs layer on top of Si is revealed (by TEM) to be not planar, but shaped in pyramids and valleys. It was demonstrated that a superlattice of 40-period GaAs/AlGaAs reduces the undulation amplitude of the growth front. It is not at the moment possible to objectively assert of the effectiveness of this technique, but the undeniable great quality and bright emission of QD and photonic crystal cavities on this sample cannot be attributed only to the reduction of threading dislocations.

Additionally, this superlattice is interesting for its ability to show single QD-like emissions. This property will be studied in chapter 3.

Indium flush

QDs can grow in a variety of shapes and sizes. In order to homogenize their emission one can cap their height to a fixed value using a technique such as indium flush [21]. Also, as this material is aimed at silicon photonics applications, it makes sense to limit the emission wavelength to less than 1 μm so that it can efficiently work with silicon photon detectors. Furthermore, the use of this method facilitates the achievement of low dot density, which can prove critical for single dot study.

The QDs in this sample have been capped with a thickness of GaAs smaller than the natural height of the dots. This layer stabilizes around the dots as the InAs islands are energetically unfavourable sites for the growth of GaAs. The sample has then been annealed in an indium environment which caused desorption of the resident indium in the dot parts that still emerged from the GaAs capping. This technique is called indium flush. This resulted in the levelling of the dots at the desired height of the first capping layer. The QDs are then capped with a second layer of GaAs as in the usual growth method.

Techniques consisting of interrupting the capping of the dot layer in the aim of controlling the dots shapes and properties have been called double capping [22] or partial capping and annealing [23], and can be used with desorption of other

elements as well [19]. In our study presented in this chapter, three samples have been realized, with different QD heights, respectively 2 nm, 2.5 nm and 3 nm. The 3 nm sample was chosen due to relatively low and uniform dot densities achieved across the wafer.

Thermal expansion

The lattice constant of silicon crystal is 5.431 Å whereas for GaAs crystal it is 5.65325 Å. (All the values are taken from [24].) The lattice mismatch is therefore 4.09%. This mismatch changes during the growth as both materials have a different thermal expansion coefficient. The linear thermal expansion coefficient α of a material represents how a characteristic length of said material changes with temperature. The coefficient itself is not a constant, but we can approximate the expansion of the materials during the growth. If we take an average α of 3.5×10^{-6} parts per K between 300 K and 675 K (growth temperature) for Si, and 5.73×10^{-6} parts per K for GaAs, we obtain a lattice constant during growth of 5.317 Å and 5.66556 Å for Si and GaAs respectively. The lattice mismatch is then 6.56 %. It has been demonstrated that a difference of lattice mismatch between growth and room temperatures can be the source of dislocations unless cooling rate is reduced [25], this phenomenon is yet another possible cause of the high density of threading dislocations in the sample.

2.3 Spectral landscape and optical properties

2.3.1 Micro-photoluminescence experimental setup

The setup used for the optical characterization (μ PL) of the sample is the one described in the previous chapter (see paragraph 1.4.1), except light can pass through either a single or a double spectrometer. A flipping mirror would allow the light emitted from the sample to be directed at the suitable spectrometer, after which the light is collected by a charge-coupled device. The complete setup used for all PL measurements in this chapter is represented figure 2.6. All measurements are performed at a temperature of 10 K.

The single spectrometer is mounted with three gratings, respectively 300, 600 and 1200 grooves per millimetre (g/mm). While those gratings provide a smaller resolution than the double spectrometer, the single light diffraction also means less signal loss, and the better performances of the new CCD accounts for a much

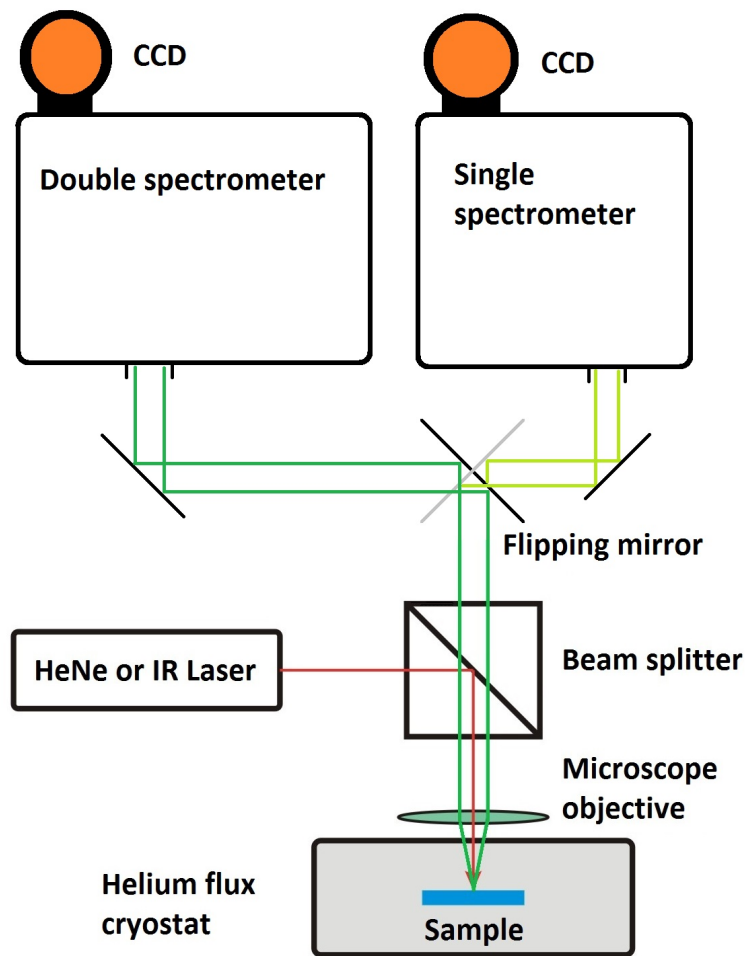


Figure 2.6: Micro-photoluminescence experimental setup.

brighter PL reading. As a rule of thumbs, the single spectrometer would be used first to identify interesting dots on the sample, and afterwards the double spectrometer would be used on those dots, with a longer exposition time, to conduct experiments requiring a higher spectral resolution.

The samples are measured with a red HeNe laser emitting at a wavelength of 633 nm. A rotating attenuating filter allows rough tuning of the excitation power, from the 1 milliwatt output of the laser down to a few tens of nanowatts.

2.3.2 Micro-PL spectra of QD ensembles

This section regroupes characterization studies of the raw surface of the 3 samples with differing QD heights.

Quantum dot height

As explained in section 2.2.3, three samples have been realized with different QD heights, namely 2 nm, 2.5 nm and 3 nm. To make it convenient they will be called 2 nm, 2.5 nm and 3 nm samples from now on. μ PL of those samples was performed at different locations on the wafers to account for dot density non-uniformity. The first striking observation made from this preliminary PL is that the 2 nm and 2.5 nm samples present similar spectra in the region 1.31 eV to 1.44 eV consisting of a broad ensemble of either very dense dots, or a high level of noise. In the same region on the 3 nm sample (figure 2.7) one can observe the InAs dots, with density allowing clear detection of single lines with full width at half maximum (FWHM) as narrow as $50 \mu\text{eV}$ (see inset of figure 2.7). On the 2 nm and 2.5 nm samples no regions with a suitably low QD density were found, so only the 3 nm sample will be studied in this chapter. Therefore all the subsequent data shown in this chapter will be coming from the 3 nm sample, if not otherwise stated.

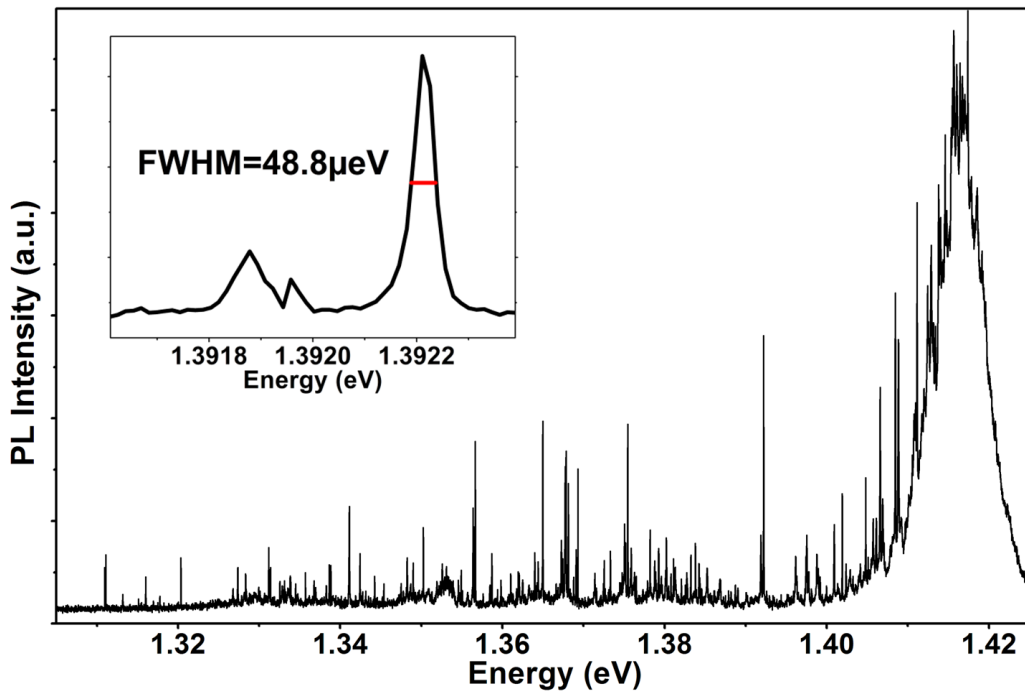


Figure 2.7: μ PL spectrum of the 1.31 eV - 1.44 eV region of (a) the 2 nm sample and (b) the 3 nm sample at excitation power $10 \mu\text{W}$

Description of the broad range PL spectrum

The broad range μ PL spectrum represented on figure 2.8 allows observation of various features, most of which are expected from this kind of sample, but some of unknown origin. InAs QD appear from 1.31 eV and up to 1.42 eV, followed by the InAs wetting layer centred at 1.415 eV with slight variations of the order of the tenth of meV depending on the position of the excitation spot on the surface of the sample. The emission of GaAs bulk is located around 1.48 eV. Weaker PL features can be observed at 1.445 eV and 1.465 eV. These are believed to come from the deep strained layers of GaAs. Due to the structure of the sample (see figure 2.2), many layers of bulk GaAs are grown between the strained layer superlattices besides the GaAs capping layer, and each can have slightly different spectral properties.

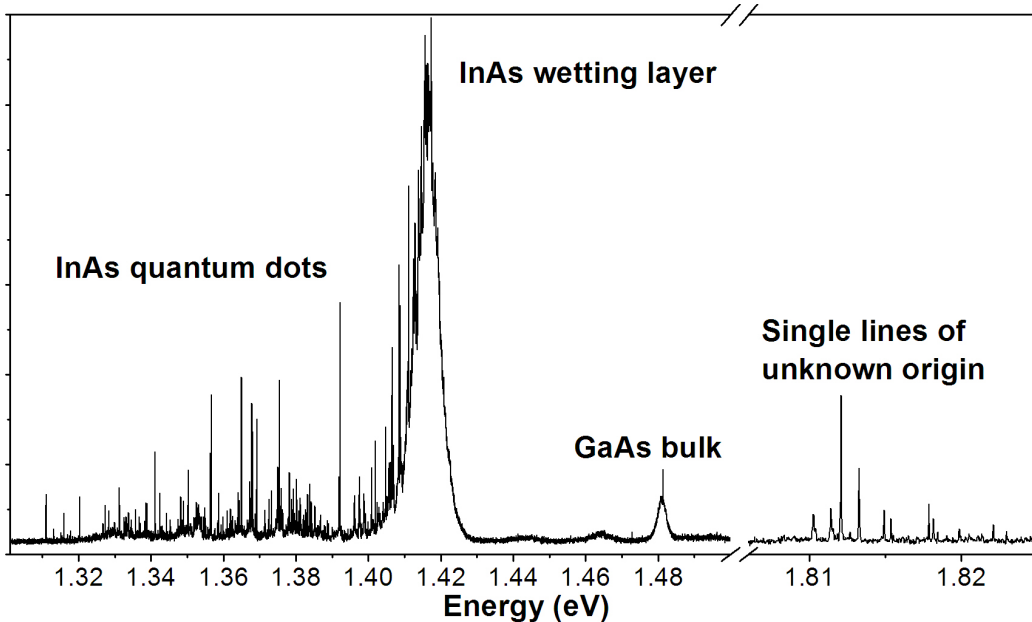


Figure 2.8: Long range spectrum of the sample.

The last but not least feature of this full spectrum is the presence of undefined sharp lines in the 1.81 eV - 1.82 eV region: those lines look identical to QD lines, and also have narrow linewidth of $60 \mu\text{eV}$. They are emitted by QD-like nanostructures formed by the interface fluctuations between the superthin GaAs/AlGaAs superlattices. They have been extensively investigated in a study that is the topic of chapter 3, and therefore will be left aside for the remnant of this chapter. It is interesting to note that the interface dots appear with the same density and the same PL brightness when the excitation spot is focused at any place on the surface

of the wafer, and as well on the 2 nm and 2.5 nm high dots wafers. Indeed those dots being created by a process occurring in the lower layers have uniform characteristics throughout the wafer, independent from the parameters used during the growth of the InAs dots.

Density of dots

The density of dots is varying across the sample surface, following a gradient toward the edge of the wafer. Figure 2.9 shows three different spectra representing the characteristic densities of dots that can be found on the wafer.

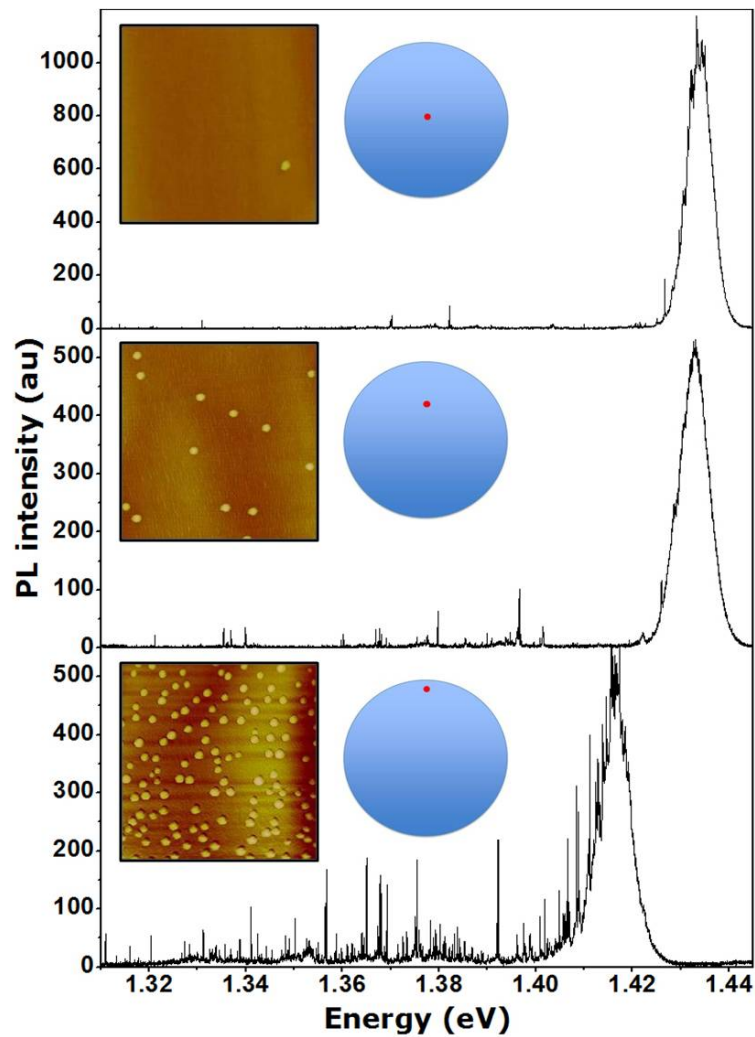


Figure 2.9: μ PL representation of dot density across the surface of the wafer. Inset left: AFM image of the uncapped dots. Inset right: position of the measurements on the surface of the wafer.

From top to bottom the spectra are taken respectively in the centre of the

wafer, between the centre and the edge and at the top edge of the wafer. In the inset of each spectrum is an atomic force microscope (AFM) image of the surface of the sample at the corresponding place on the wafer, taken on uncapped test QDs grown on the sample surface. The place onto which the AFM and μ PL spectrum have been acquired is represented in the right part of the inset, by a red point on the blue wafer. The AFM pictures represent a $1 \mu\text{m}^2$ surface, where uncapped QDs can be seen in a brighter colour. From the AFM data we can extract a dot density of approximately 10^8 cm^{-2} , 10^9 cm^{-2} and 10^{10} cm^{-2} for those places. Each spectrum features a large and bright peak (1.435 eV for the top graph, 1.417 eV for the bottom one) which is associated with the emission of the InAs wetting layer (WL). On the lower energy side of the WL, single lines can be observed that grow more numerous as the position on the wafer is close to the edge. An estimation of the number of those QD lines ranges from a few units (top) to a few hundred (bottom), which considering the laser excitation spot area of the order of $1 \mu\text{m}^2$ accounts for a density of dot consistent with the AFM observations. One can notice by looking at the PL intensity scale on the left that the intensity of the WL decreases with increasing density of dot, and that the WL emission redshifts. The former can be attributed to the higher number of carriers from the WL being captured by the QDs to undergo radiative recombination, while the latter can be explained by a higher In concentration. These observations are similar to the optical behaviour of InGaAs/GaAs QD grown on III-V (GaAs) substrate [26].

Excitonic complexes characterization

Closer optical characterization has been brought to the sample to investigate excitonic complexes and exciton binding energy. Particularly a study of PL intensity of single lines with respect to excitation power allows determination of bi-excitons, as their PL increases with power in a quadratic way, as opposed to neutral and charged excitons increasing linearly. Figure 2.10 shows characterization of such a neutral exciton/bi-exciton (X/XX) pair.

Fig. 2.10 (a) represents three PL spectra of two lines, here denoted X for the exciton and XX for the bi-exciton. Each spectrum was acquired at a different excitation power so the evolution of the photon count can be estimated: indeed it can be seen that X appears and reaches saturation before the other line. The integrated number of photon counts is plotted for each of the two lines against excitation power in figure 2.10 (b). The X line is in black squares while the data representing XX are red dots. Emission of the XX remains low up to $2 \mu\text{W}$. Saturation of X peak is ob-

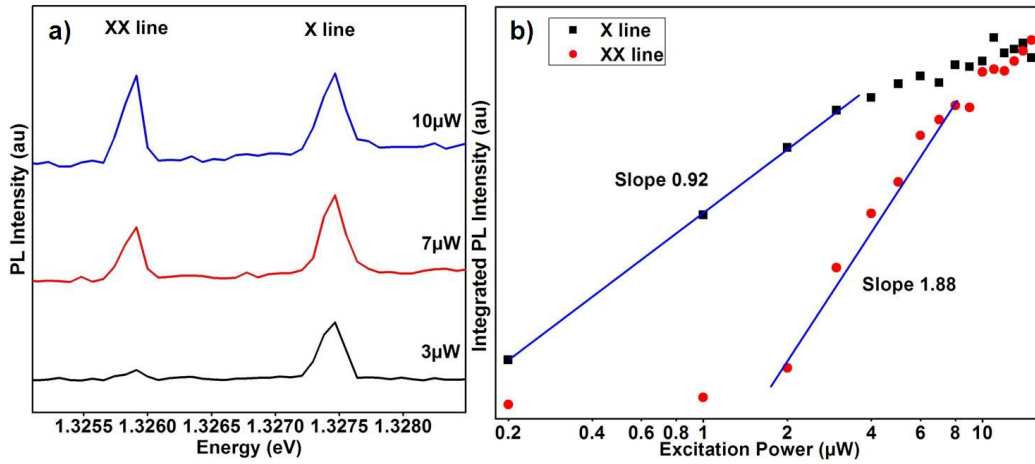


Figure 2.10: Optical characterization of a pair exciton/bi-exciton. (a) μ PL measurement of the pair at three different excitation power, (b) integrated PL intensity of the same pair with respect to excitation power. The scales are logarithmic.

served at lower power than for XX: $\sim 3.5 \mu\text{W}$ and $\sim 8 \mu\text{W}$, respectively. The scales in figure 2.10 (b) being represented logarithmically, it is easy to observe the nature of the power dependent PL: since X increases linearly and XX quadratically [27], before saturation linear slopes can be expected on the logarithmic graph, with a slope of 1 and 2 respectively for X and XX line. The two lines are fitted with a blue straight line, whose slope is calculated to be respectively of 0.92 and 1.88, which fits reasonably with the theory, and confirms the X/XX nature of this pair. Three X/XX pairs measured across the sample exhibited binding energies of 1.18 meV, 1.56 meV and 2.43 meV. These results are reasonably in accordance with what can be found in the literature for InGaAs QDs grown on GaAs substrate [26, 28]. The disparity in binding energies can be explained by variations of quantum dot sizes through the sample [28]. Such a variation in size can indeed be observed on the AFM images in figure 2.9.

2.4 Photonic crystal cavities

Photonic crystal cavities (PCC) are microstructures that can be fabricated on the sample to observe light-matter interactions. They have been fabricated on the sample by Isaac Luxmoore from our group in University of Sheffield. A more extensive description of the device will be found in the next paragraph, after which the fabrication process will be detailed. Finally, the performances of the PCC are revealed through optical experimentation in the last paragraph of this section.

2.4.1 Principle

This paragraph is aimed at providing a general description of the principles of PCC. A more in depth review of the mathematics involved will not be found in this thesis, as the main domain of its author is semiconductor quantum dots, and the PCC are merely used as a tool. The reader will be redirected to the corresponding literature: [29].

The same way the goal of low dimensional semiconductors nanostructures like quantum dots and quantum wells is to gain control over electric charges, photonic crystals are a type of nanostructures that allow control over photons. In any bulk material, the characteristics of the crystal lattice will dictate the behaviour of electron propagation in it. This phenomenon arises from the quantum nature of charges: propagating as waves, their interaction with the periodic crystal of the medium will be different depending on their wavelength characteristics. By extending this concept, any medium can also block the propagation of certain wavelengths, leading to band gaps in the energy band structure. By analogy, photons with specific wavelengths can be trapped or directed within a periodic lattice, hence the name: photonic crystal. In this case, the lattice would be formed of mediums with different refractive indexes, this periodicity of refractive indexes would be to the photon what the periodicity of crystal lattice atomic potential is to a charge carrier. A photonic crystal could be periodic along one dimension, two or three (see figure 2.11).

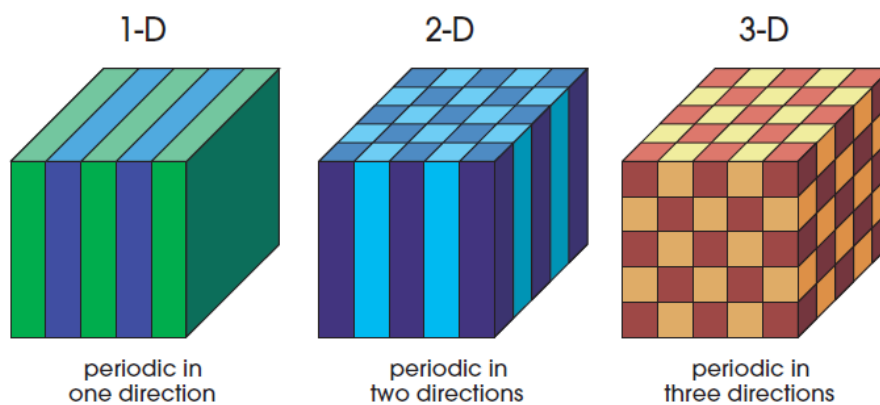


Figure 2.11: Simple cases of one, two and three-dimensional photonic crystals. The different colors represent materials with different dielectric constant. Adapted from “Photonic Crystals: Molding the Flow of Light”, Joannopoulos 2008 [30]

By using the appropriate formation of materials, one can be able to confine photons with specific wavelength, or to guide them in the same way a metallic waveguide directs microwaves. These applications aim at using photons as spin Q-bits. Another well-known application is to use a one-dimensional stack of alternating layers of materials with different dielectric constants to block light with a specific wavelength. This technique is commonly used in dielectric mirrors, dielectric Fabry-Perot filters, and distributed Bragg reflectors. For a more extensive review of the properties and applications of PCC, the reader is invited to read “Photonic Crystals: Molding the Flow of Light” by John Joannopoulos [30].

The goal for this study is to have a QD physically placed inside a PCC, so that an exciton inside the QD can enter in resonance with the photon that is trapped in the cavity (cavity light mode). The interaction between photon and exciton will then be studied in section 2.6.

2.4.2 Fabrication

The fabrication of PCC is enabled by the presence, below the GaAs layer that surrounds the QD, of an AlGaAs sacrificial layer. The aim of this fabrication is to obtain QDs embedded in a micrometric slab of GaAs surrounded by air in all three directions (see figures 2.12, 2.13). The difference in dielectric constant between air and GaAs would allow photons to reflect back into the slab and to interfere destructively with itself, unless its wavelength permits resonance with the cavity.

The fabrication procedure is the following: the cavities are first patterned over the surface of the sample using electron beam lithography (EBL). For that purpose a thin layer of resist is first deposited on the sample, and then the electron flux of the EBL irradiates parts of the polymer, making it sensitive to solvent. The pattern varies according to the type of cavity fabricated, for the L3 cavity represented in the main part of figure 2.13 it consists in a triangular lattice of circular holes, with lattice constant $a = 255 \text{ nm}$ to 260 nm and various hole radii of the order of 50 nm . Within one cavity all holes have exactly the same radius. (It is interesting to note that by varying the exposure time of the EBL, the scattering of electrons on the hard surface of the sample causes wider irradiation of the polymer film, resulting in larger holes. The purpose of making holes with different radii will be explained in paragraph 2.4.3.) The actual cavity is formed by the omission of three aligned holes, effectively making an elongated bulk of GaAs surrounded with air holes (L3 cavity). After solvent dipping, the holes are etched in the sample using inductively coupled

plasma reactive ion etch (ICP-RIE) from the surface down to the underlying sacrificial layer. The sacrificial layer is then removed (hence its name) entirely under the honeycomb lattice by infiltration of hydrofluoric acid. The resulting structure is a membrane of GaAs pierced with holes and containing in its centre the InAs QDs. A side-view representation of the structure is shown in figure 2.12.

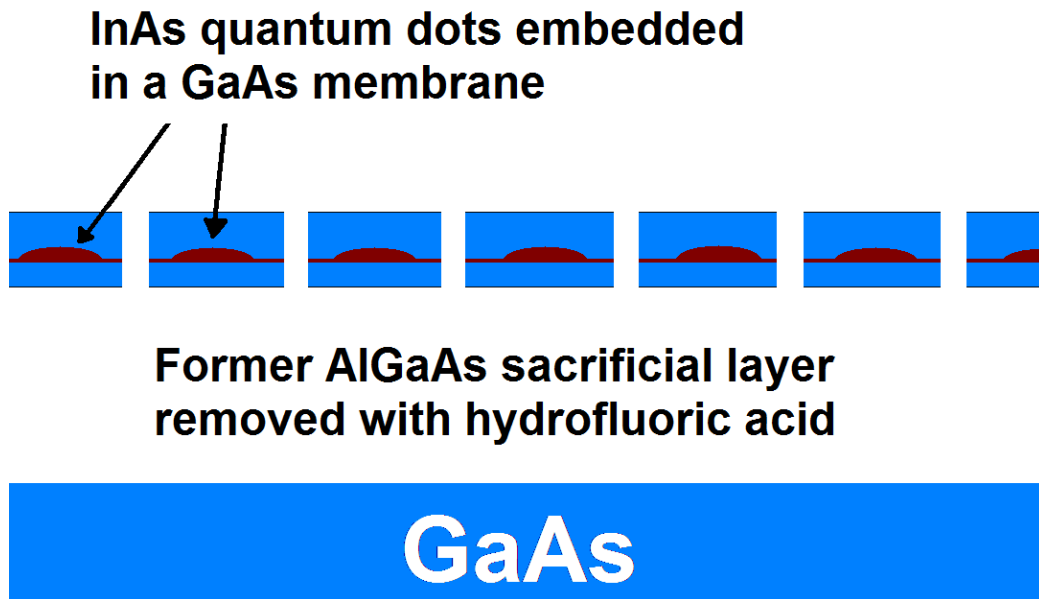


Figure 2.12: Side view schematic of InAs quantum dots embedded in a photonic crystal cavity membrane.

Figure 2.13 shows a top view SEM image of the L3 cavity acquired by I. Luxmoore after the fabrication. Many other types of cavities have been fabricated on the sample, as represented in the inset: (a) H1 cavities with only one missing hole, (b) and (c) microdisks, though only the L3 cavities exhibited good enough characteristics to be studied in detail.

As mentioned before, the aim of this whole fabrication is to have a QD confined into a cavity so that the confined exciton will have strong interaction with the photon mode of the cavity. In practice it is impossible to engineer exactly a self-assembled QD into a cavity, or to fabricate a cavity exactly at the location of a QD without using advanced localization or growth techniques [31, 32]. That is why the method used here is of a more statistical nature: many cavities have been fabricated in an area of relatively high density of QDs ($5 \times 10^9 \text{ cm}^{-2}$ to $1 \times 10^{10} \text{ cm}^{-2}$) and later

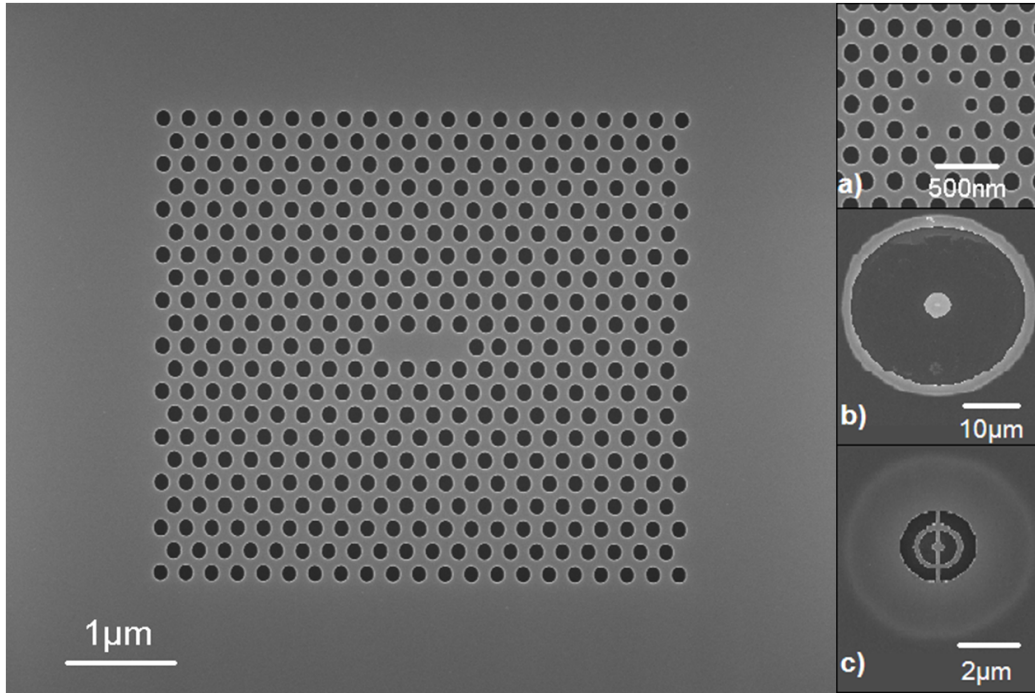


Figure 2.13: SEM images of PCC structures fabricated on the sample. Main: L3 cavity, (a) H1 cavity, (b) microdisk, (c) higher magnification of same microdisk.

in the laboratory environment measured until a suitable QD-in-cavity was found.

2.4.3 Characterization of the performances

A cavity can be characterized by two properties: its mode frequency and its quality factor (Q-factor) [29]. The mode frequency is the frequency at which a photon is in resonance with the cavity, which means the round trip of the photon trapped into the cavity leads to constructive interference. The mode frequency depends on the dimensions of the cavity and the dielectric constant (or refractive index) of the medium. Since the latter is constant in the GaAs membrane, tuning of the cavity mode frequency can be achieved through variations of characteristic lengths. For that purpose the L3 cavities on the sample have been fabricated with various hole radii, the clusters of cavities with a specific radius being sorted in columns on the wafer surface for convenience. The cavities fabricated on the sample have mode frequencies or energies ranging from 1.3 eV to 1.4 eV, effectively covering the range of InAs QD energies (see figure 2.14).

The interesting characteristic here is the Q-factor that reflects the intrinsic quality of the cavity. It is a measurement of the how the cavity is not damped when it

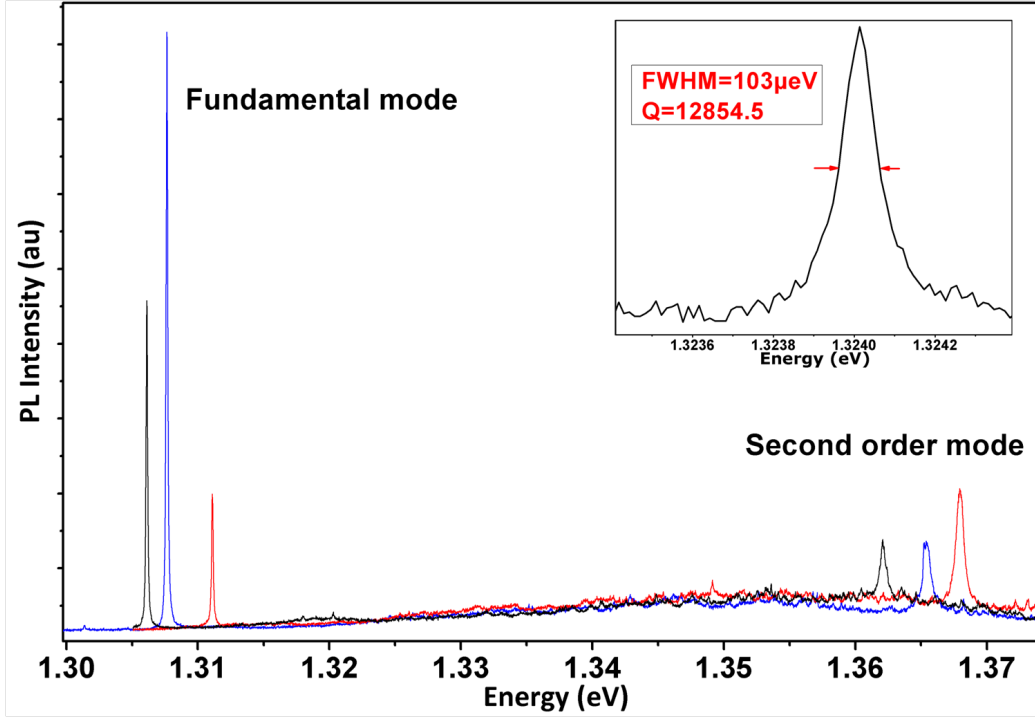


Figure 2.14: PL spectra of three PCC with mode energy in the 1.31 eV region. The first harmonic mode can be seen in the higher energy side, typically at 5.5 eV from the fundamental mode. Inset: PL of cavity with highest Q-factor measured from PCC on the sample.

resonates, in other terms the higher the Q of an oscillator the longer it will resonate [33, 34]. Indeed, in our case the Q is inversely proportional to the photon decay rate of the cavity, which means the higher the Q, the longer a photon stays in the cavity and have a chance to interact with the QD [29]. The properties of the Q-factor and how it affects the performances of the cavity or its interaction with QDs will be discussed in more detailed in the part concerning light-matter interaction, in paragraph 2.6.1. Examples of the best Q-factors measured can be seen in figure 2.14 where they are measured by observing the cavity mode emission in μ PL at low temperature. The Q is estimated by the following formula:

$$Q = \frac{\omega}{\Delta\omega} \quad (2.1)$$

where ω is the frequency of the cavity mode, and $\Delta\omega$ is the FWHM of the cavity mode emission. Among the 30 cavities investigated, Q-factors range from 6000 to a maximum observed of 13000 (figure 2.14 inset), which is comparable with the best quality cavities fabricated on III-V substrate over the last years. At this point it is useful to remind that the whole structure that is studied in this chapter is grown

on silicon, making this quality very good indeed for a first attempt. More than 10% of the observed cavities have Q of at least 10000, while the majority of the cavities exhibit a Q over 9000, number widely accepted to be high enough to observe strong coupling.

2.5 Single photon emission

As explained in the introductory section 2.1, one of the main goals of the study of semiconductor nanostructures is to find a new way of computing, way that can be achieved by manipulating exciton spins. While the electron and/or hole in a QD is a potential good candidate for quantum operation, because of the solid state nature of the material, to transport the information one needs a good carrier, and a photon can accordingly fill this role. Therefore, the first essential ability researched in any new semiconductor nanostructure material is the ability to emit single photons [35], so that information can be passed reliably for example from one QD to another. This study has been conducted on our sample based on auto-correlation data acquired by our fellow group members N. Wasley and I. Luxmoore. It will be described in the present section, first by its experimental procedure and then by the yielded results.

2.5.1 Experimental setup

The photon-correlation experiment, that measures the probability of any two photons to reach a detector at the same time, depending of the delay between their emission, is conducted with a Hanbury Brown and Twiss interferometer (HBT). Figure 2.15 represents a schematic of the HBT setup. The working principle is the following: photons emitted from the sample, excited beforehand with a coherent source, go through a beam splitter, and hit two avalanche photodiodes (APD) placed on either ends of the beam splitter. An APD is a semiconductor device that generates electrical current through photo-generation. It is constituted of a built-in gain system using avalanche multiplication, meaning very low intensity light can be converted into electricity, and therefore detected. This device is ideal for the detection of photons, and that is the reason why it is a choice equipment for an HBT setup. First, one has to make sure that all photons emitted from the sample are coming from the same source, in this case a single QD. To achieve that, the best way is to use a narrow bandpass filter tailored to the wavelength of the measured QD, or to use a monochromator to separate the different frequencies of the light and isolate the exact frequency at which the QD of interest emits. The latter solution

dramatically reduces the emission intensity though, and since photon-correlation requires a lot of intensity to yield results in a timely manner, the former solution is preferred. For this experiment a narrow band-pass filter centred around the source QD emission wavelength and with transmission bandwidth of 2 nm has been used.

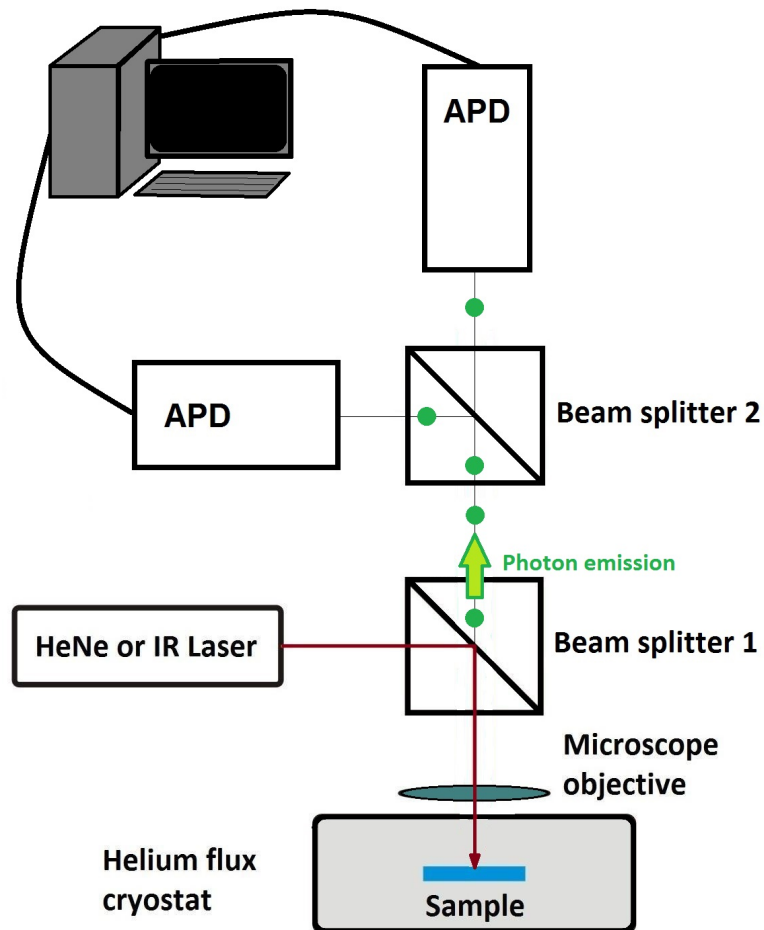


Figure 2.15: Hanbury Brown and Twiss experimental setup.

Upon reaching the separating beam splitter, photons have a 50% probability of going one way or the other, and hit one of the two APDs. APDs are light detectors sensitive enough to count accurately the number of photons. Each of them is connected to a photon-counting module hardware in a computer onto which a software draws the photon auto-correlation function using a method that will be explained in the next paragraph.

2.5.2 Results

To study the photon statistics of light the following function is used:

$$g^{(2)}(\tau) = \frac{\langle I_1(t)I_2(t + \tau) \rangle}{\langle I(t) \rangle^2} \quad (2.2)$$

Where $\langle I_1(t) \rangle$ and $\langle I_2(t) \rangle$ are the time averaged number of photons arriving at APD 1 and APD 2 respectively, and τ is the time delay between the two APD triggers. This function $g^{(2)}(\tau)$ is the second order correlation function, it represents the probability that two photons are emitted with a time delay τ . In an expected ideal case, for a single photon emitter this function would be equal to 0 at $\tau = 0$ ns and for relative time delays larger than the lifetime of the emitter it would be equal to unity. Now it is not possible to generate this exact function as it would require to know the exact photon emission properties of the source at any time, but it can be approximated with a histogram implemented by taking, for each photon hitting APD 1, the time delay until another photon hits APD 2. This method can reasonably approximate $g^{(2)}(\tau)$ if the delays are much less than the average time between two APD triggers. If the source emits photons one by one, the histogram should present a constant value except for a dip around a certain time delay which by taking into account the relative distances of the APD from the source, corresponds to the zero time delay of the emission of two successive photons. Usually in an experimental system the dip will not reach zero due to various factors including noise, parasitic emissions and coupling with charge carriers [36].

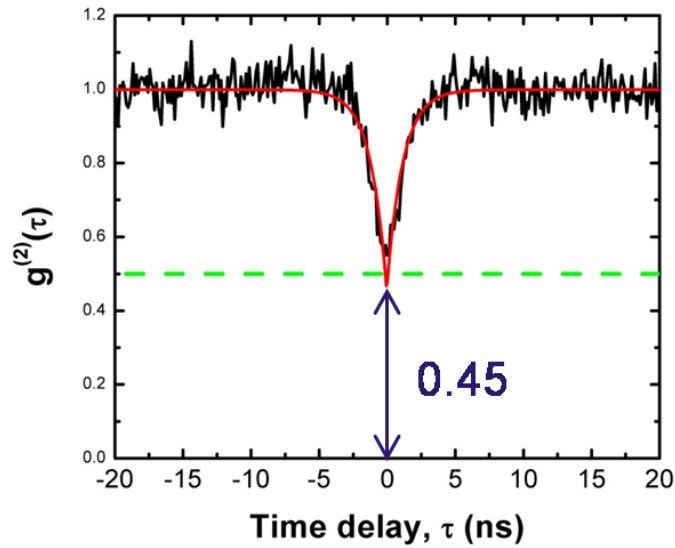


Figure 2.16: Second order correlation function of a single QD under CW excitation.

The result of the experiment realized on an InGaAs single QD located outside the cavities and pumped with continuous-wave (CW) laser is represented figure 2.16. The measurement has been carried out with a HeNe laser at a low excitation power of $2 \mu\text{W}$, and took 1.4 hours to complete. The dip of 55% observed at time delay $\tau = 0 \text{ ns}$ accounts for clear anti-bunching. This demonstrates the single photon emitter nature of the InGaAs dots grown on silicon.

The result is further supported by the same experiment realized with pulsed laser, this time on a QD located in a cavity (figure 2.17). The excitation used here is a titanium-sapphire pulsed laser, with a 82 MHz pulse rate and a pulse duration of 80 fs. The excitation power used for the experiment was 100 nW. The pulsed laser experiment allows a more direct observation of the effect since the pulses are separated in time (by 12 ns) so that only the central pulse (for time delay $\tau = 0 \text{ ns}$) is affected by the quantum nature of the light. Here a clear reduction of the light field of more than 80% achieves to prove single photon emission of the QD on the sample.

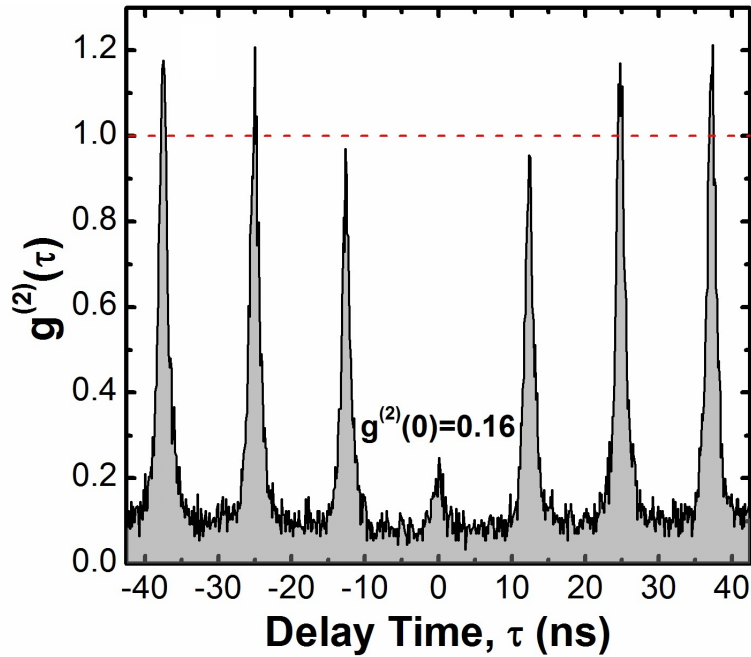


Figure 2.17: Second order correlation function of a single QD under pulsed excitation.

2.6 Light-matter coupling

This section, introduced by section 2.4 about photonic crystals, deals with the most interesting results obtained with this sample: the coupling, at different levels, of light and matter in InAs QD embedded in PCC fabricated directly on silicon substrate. A more in-depth explanation of this phenomenon is to follow, then the two levels of coupling observed will be displayed on subsequent paragraphs.

2.6.1 Principle

The coupling between a cavity mode and an atom (in our case a quantum dot) situated in the centre of the cavity will happen if the transition energy of the atom is in resonance with the photonic mode [29]. The level of coupling depends on three parameters, the atom-photon coupling parameter g_0 , the photon decay rate of the cavity κ and the non-resonant decay rate γ . The condition to have strong coupling is that $g_0 \gg \text{Max}(\kappa, \gamma)$, the condition to have weak coupling is $g_0 \ll \text{Max}(\kappa, \gamma)$. Indeed, the atom-photon interaction represents the ability of the QD to absorb or re-absorb a photon trapped in the cavity. If the QD can absorb a photon faster than the photon being lost out of the cavity mode, there is a reversible process of emission/absorption of photons from the QD. Reversely, if the atom-photon interaction is not strong enough, the photon decays out of the cavity in an irreversible manner. In the intermediate case where g_0 is of the order of the strongest leakage process rate of the cavity, strong coupling evidence can still be seen though not as pronounced. The cavity decay rate is equal to the FWHM $\Delta\omega$ of the cavity mode, so as we've seen in paragraph 2.4.3 κ is related to Q by $Q = \omega/\kappa$. Now we can estimate the necessary Q-factor to observe strong coupling by using the value of g_0 (See chapter 10 from ref [29]):

$$g_0 = \left(\frac{\mu_{12}^2 \omega}{2\epsilon \hbar V_0} \right)^{1/2} \quad (2.3)$$

Where μ_{12}^2 is the electric dipole moment of the quantum dot transition from ground state to the first excited state, $\epsilon = \epsilon_0 \epsilon_r$ is the permittivity of the material, \hbar the reduced Planck constant and V_0 the mode volume of the cavity. The mode volume is the spatial integral over the electric field intensity [37], from previous studies of properties of L3 cavities we can calculate it from:

$$V_0 = 0.64(\lambda/n)^3 \quad (2.4)$$

With λ the wavelength of the photonic mode and n the refractive index of the

material [38]. By substituting g_0 and κ , we find that the condition to be able to observe strong coupling is:

$$Q \approx \left(\frac{2\epsilon_0 \hbar \omega V_0}{\mu_{12}^2} \right)^{1/2} \quad (2.5)$$

By taking $\lambda = 900\text{nm}$ and $n = 3.598$ for GaAs at this wavelength, we obtain an estimate of the mode volume: $V_0 \approx 9.99 \times 10^{-21} \text{ m}^3$. With a value for the relative permittivity of GaAs of 12.9 and for an average value of $\mu_{12}^2 \approx 9 \times 10^{-29} \text{ Cm}$ for the dipole moment, based on literature values both theoretical [39, 40] and experimental [41], we obtain $Q \approx 7890$.

As can be seen from the experimental results of section 2.4.3, the quality of the cavities is good enough to observe strong coupling, provided the QD is located relatively close to the maximum of the cavity mode. An off-centred QD would result in an increased non-resonant decay rate, and a regime of weak coupling instead.

At this point it is good to remind that the procedure for the fabrication of PCC was to pattern them on the surface of the sample without any prior knowledge of the position of the QD. Therefore, the position of QDs relative to cavities is the limiting factor in the observation of any light-matter interaction, and a systematic work had to be done to probe the cavities until an ideal system was found. The next two sections will describe two such cavities, where weak and strong coupling respectively has been observed.

2.6.2 Weak coupling

In the weak coupling regime, as seen in the previous section a photon emitted by the QD quickly decays out of the cavity, making the process of emission irreversible. But what is very interesting in this regime is that the spontaneous emission rate of the QD is significantly modified by the cavity around it. This result has been investigated by E. M. Purcell in 1946, and is therefore called Purcell effect (see E. M. Purcell article on page 681 from ref. [42]). Indeed, the spontaneous emission rate of the QD depends on the density of photon states available outside the dot, density of states which has a different form based whether the QD is in free space or inside a cavity. To calculate the effect of the cavity on the QD emission, we can calculate the Purcell factor F_P :

$$F_P = \frac{W^{cav}}{W^{free}} \quad (2.6)$$

W^{free} and W^{cav} are the spontaneous emission rates of the QD in free space and inside the cavity respectively. The spontaneous emission rate has the following form (calculated using Fermi's Golden rule, see chapter 10.3 from ref. [29]):

$$W = \xi^2 \frac{\pi \omega \mu_{12}^2}{\hbar \epsilon_0 \epsilon_r V_0} g(\omega) \quad (2.7)$$

ξ is a factor that evaluates the orientation of the dipole moment of the QD with respect to the external electric field, and is equal to 1 when perfectly aligned. For a QD that emits randomly in every directions (like in a free space) ξ^2 will be averaged to 1/3.

The main difference comes from the density of state function $g(\omega)$: for free space the available states are a continuum which increases quadratically with ω :

$$g_{free}(\omega) = \frac{\omega^2 V_0}{\pi^2 c^3} \quad (2.8)$$

Whereas in a cavity, the available states for the photon emitted by the QD are reduced to the photonic mode of the cavity, which takes the form of a Lorentzian function:

$$g_{cav}(\omega) = \frac{2}{\pi \Delta \omega_c} \frac{\Delta \omega_c^2}{4(\omega - \omega_c)^2 + \Delta \omega_c^2} \quad (2.9)$$

$\Delta \omega_c$ and ω_c are the FWHM and the frequency of the cavity mode, and are related to the quality factor (equ. 2.1). When substituting into equation 2.6 we obtain:

$$F_P = \frac{3Q(\lambda/n)^3}{4\pi^2 V_0} \xi^2 \frac{\Delta \omega_c^2}{4(\omega - \omega_c)^2 + \Delta \omega_c^2} \quad (2.10)$$

As we can see, if the angular frequency ω of the QD emission is too far off resonance with the cavity mode ω_c , this factor rapidly decreases below unity and close to 0. On the other hand, when the QD is in resonance with the cavity its spontaneous emission rate can dramatically increase. Let's estimate what would be the Purcell factor for a cavity of 8000 Q factor: we assume the QD is in the centre of the cavity, that its emission is perfectly in resonance and that its dipole is aligned with the electric field in the cavity, we therefore have:

$$F_P = \frac{3Q(\lambda/n)^3}{4\pi^2 V_0} \quad (2.11)$$

Which for a $Q = 8000$, emission wavelength of 925 nm and refractive index and

mode volume as calculated in the previous section, gives a Purcell enhancement of 1034.71. Of course this is an ideal value, and is very unlikely to be observed in our sample, due to the facts that it is very difficult to observe a QD located in the maximum of the cavity mode, and that it is not possible to observe with μ PL a dot in resonance, its emission being completely covered by the photonic mode emission line. This last issue can be overcome by using a dot coupled with a second or third-order mode of a cavity. Lesser-order modes are broader and less bright than the fundamental mode, so a QD emission in resonance with the mode can be visible on PL. A reasonable Purcell enhancement has been observed by I. Luxmoore and is illustrated on figure 2.18.

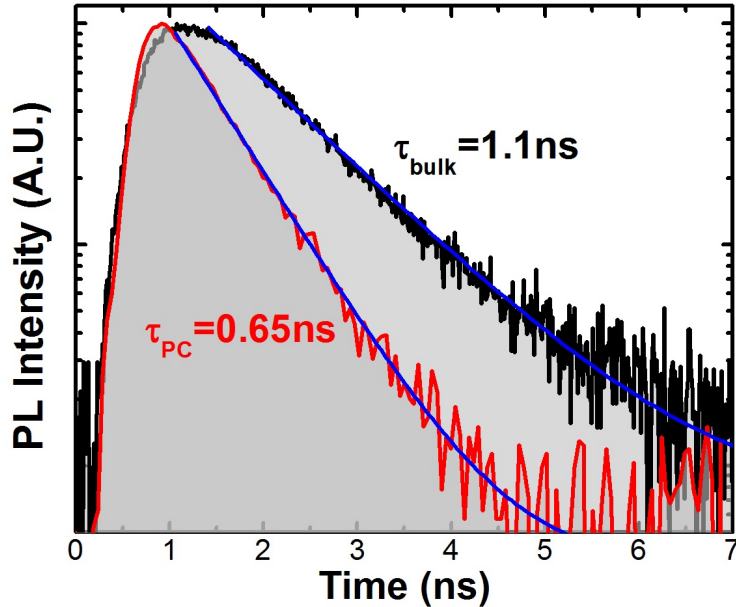


Figure 2.18: Time-resolved μ PL of single dot emission in a photonic crystal cavity (red, lower curve) and in the unprocessed wafer (black, upper curve). The slight difference in rise time could be explained by the difference of the complexes (exciton or bi-exciton) studied in each QD. The experimental conditions like laser pump power were also not exactly the same for the two measurements, one of them having its natural luminescence intensity enhanced by the cavity.

The figure represents a time-resolved μ PL measurements of two dots, one being taken on the raw surface of the wafer without cavity (denominated τ_{bulk}), and the other being weakly coupled with the third-order mode of a cavity (τ_{PC}). The spontaneous emission rate of the QD in cavity is $1/\tau_{PC} \approx 1.54 \times 10^{12} \text{ s}^{-1}$ is increased compared to the one in the bulk $1/\tau_{bulk} \approx 0.91 \times 10^{12} \text{ s}^{-1}$, accounting for a Purcell enhancement of ~ 1.7 , demonstrating weak coupling effect in the cavity. The huge

difference between the theoretical and experimental values of the Purcell enhancement is partly due to the position of the dot off the maximum of the cavity mode, but the main reason is the Q-factor of the third order mode, much smaller than that of the fundamental mode (see equ. 2.1 and 2.11).

This result is important because increasing the photon emission rate of a QD can be extremely useful for numerous applications, one of the main ones being efficient single photon emitters. It is interesting to note that the results from section 2.5.2, figure 2.17 have been obtained on a QD in a cavity, exhibiting such Purcell enhancement.

2.6.3 Strong coupling

When the QD-photon coupling is strong enough, a photon emitted by the QD is reabsorbed before it can escape from the cavity, making the process reversible. This regime of emission/absorption of the photon is called cavity quantum electrodynamics (cavity-QED), a concept that has been studied for the first time by Jaynes and Cummings in 1963 [43]. Such a complex phenomenon will not be mathematically described here, as the aim of this thesis is the study of quantum dots.

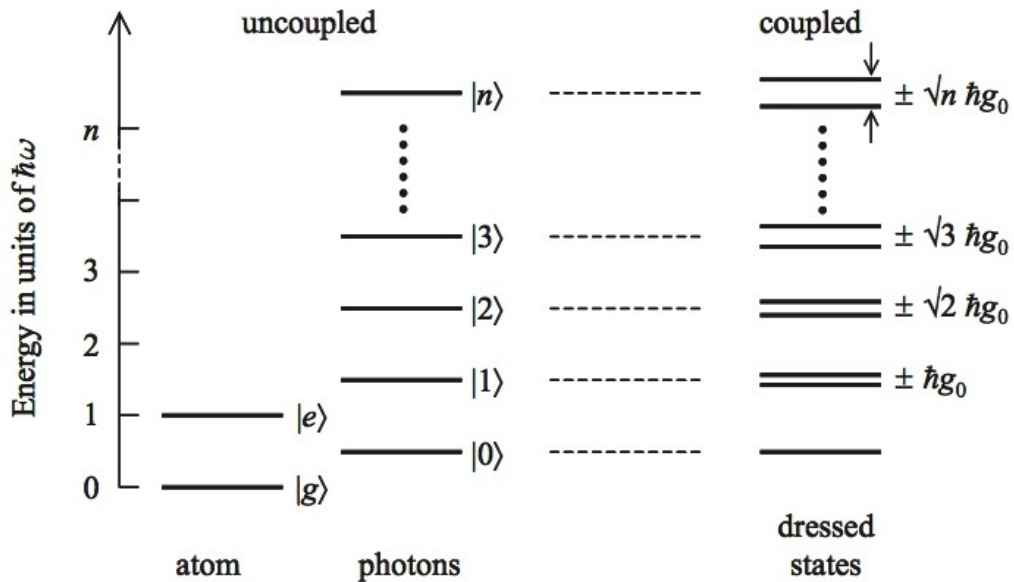


Figure 2.19: The Jaynes-Cummings ladder describing the states of a coupled atom-photon system (right) and the same system without any coupling (left). Taken from figure 10.9 of ref. [29]

The principle can better be understood by looking at figure 2.19: the system comprises an atom (in our case a quantum dot) with two states, ground labelled $|g\rangle$ and excited $|e\rangle$, and a certain number of photons represented by the states $|0\rangle$, $|1\rangle$, ... $|n\rangle$ (in our system the only photon states we will consider will be $|0\rangle$ and $|1\rangle$). The uncoupled states are represented on the left, the excited state of the total system corresponds to either the state $|g, 1\rangle$ or the state $|e, 0\rangle$, which share the energy $(3/2)\hbar\omega$, making this first excited level degenerate. It would be the same for each subsequent level if we had more than one photon in our cavity, the n^{th} energy level being contributed by both $|g, n\rangle$ and $|e, n - 1\rangle$. The effect of strong coupling between the photon and the QD mixes the states and lifts the degeneracy of energies, as depicted on the right part of figure 2.19 called the Jaynes-Cummings ladder: the photon and QD are now one and only mixed system, where the first excited state actually comprises two energies, separated by $\Delta E = 2\hbar g_0$.

Such a system could be compared to the classical analogue, the coupled oscillators depicted figure 2.20: two oscillators with natural (uncoupled) frequencies of ω_1 and ω_2 respectively, linked by a spring giving a coupling strength Ω . The system exhibit two frequencies:

$$\omega_{\pm} = \frac{(\omega_1 + \omega_2)}{2} \pm \sqrt{\Omega^2 + (\omega_1 - \omega_2)^2} \quad (2.12)$$

Which reduces when the natural frequencies of the two oscillators are equal (in our case when the cavity is in resonance with the QD emission) to $\omega_{\pm} = \omega \pm \Omega$, where the frequency of the system is now “split” by the coupling strength of the spring.

In our case we can estimate a possible splitting, provided we find a cavity with a quantum dot strongly coupled to it and located reasonably close to the maximum of the mode. This splitting is called the *vacuum Rabi splitting*, and we can calculate it from the formula:

$$\Delta E = 2\hbar g_0 = \sqrt{\frac{2\mu_{12}^2 \hbar \omega}{\epsilon_0 \epsilon_r V_0}} \quad (2.13)$$

With the values of our system and the same approximations made in paragraph 2.6.1, we obtain a value (ideal) of $\Delta E \approx 349.8 \mu\text{eV}$. This value of course is quite high and would need perfect conditions to be obtained.

The observation of strong coupling in our work has been done experimentally

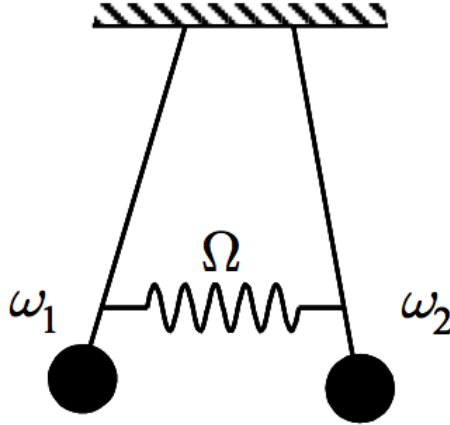


Figure 2.20: Schematics of coupled oscillators. Taken from figure 10.10 of ref. [29]

on the InGaAs QDs embedded in cavities and grown on silicon, by the following method: first a cavity has to be found with a QD emission close enough to the frequency of the fundamental mode of the cavity, on the *higher energy* side. As mentioned earlier, the detected QD needs to be physically inside the cavity, but since this information is impossible to verify, we have to probe cavities until we find a suitable one (only one cavity exhibiting observable strong coupling has been found, out of the 200 measured). The procedure is then to put the QD and mode emission in resonance by raising the temperature, from 4 K and up to 50 K. Indeed, the increase in temperature changes the refractive index of the cavity, redshifting slightly its fundamental mode emission, whereas the quantum dot emission depending on the band gap of the semiconductor material is redshifted at a higher rate. This leads at some point to the resonance of photonic mode and QD emission, such an experiment is represented figure 2.21: the figure represents two μ PL spectra of a cavity mode with a QD emission slightly off-resonance (smaller peak on the higher energy side, at 40 K), at multiple temperatures (increasing from bottom to top).

In fig. 2.21 (a) the QD and the cavity are not strongly coupled, we can see as the temperature rises that the emission lines of the QD and the mode overlap. In fig. 2.21 (b) the QD and the cavity mode are strongly coupled. Around $T = 40$ K where the two emissions would be expected to overlap, instead we can see the lifting of the degenerate energies of the mixed state as two peaks still appear. The QD (mode) is represented at temperatures 35 K and 45 K with a red (blue) Lorentzian fitting. The two peaks are clearly separated and never cross all along the temperature sweep, this “anti-crossing” is the signature of strong coupling between the

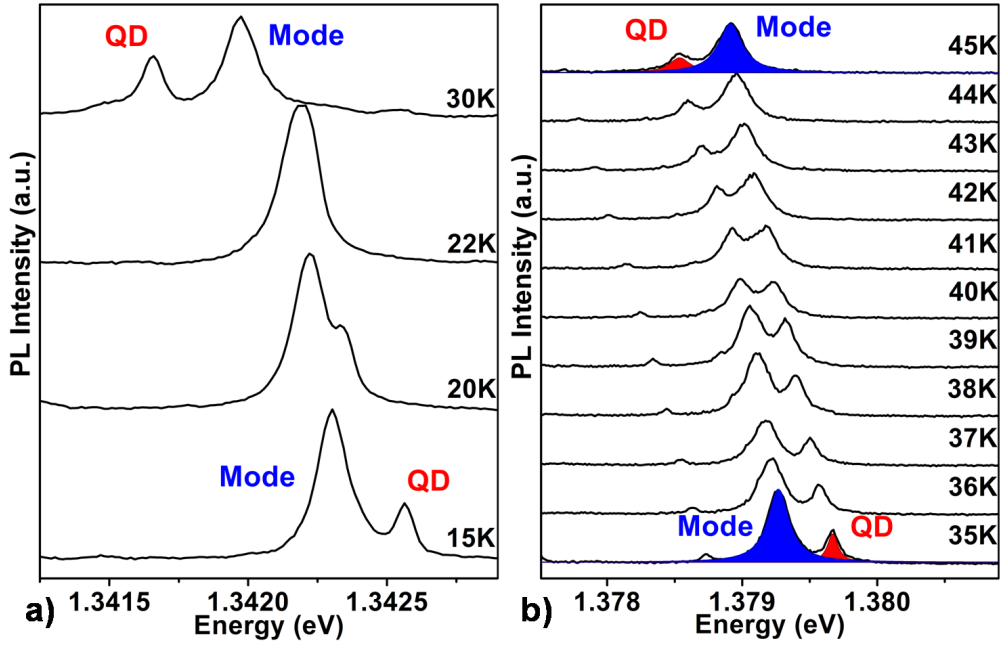


Figure 2.21: μ PL spectra at increasing temperature of a InAs QD slightly off-resonance with a cavity mode. (a) The QD and cavity are not strongly coupled. (b) The QD and cavity exhibit strong coupling.

photonic mode and the QD.

Figure 2.22 shows the plotted energies of the two lines from figure 2.21 (b) with respect to temperature, where the anti-crossing is even more clearly depicted. The red (blue) dashed lines represent the temperature dependence of the QD (cavity mode) emission if they weren't coupled. The upper and lower ensembles of plotted values are fitted with the frequencies ω_+ and ω_- from equ. 2.12 of the classical coupled oscillators (grey curves).

A reading of the energy splitting at the cross-section of the red and blue dashed lines gives a vacuum Rabi splitting of: $\Delta E = 212 \mu\text{eV}$, which is reasonably close to the theoretical estimation of $350 \mu\text{eV}$ we have done earlier. This result is also comparable to the highest Rabi splittings obtained with InGaAs QDs grown on GaAs substrate [32, 44, 45], which is attributed to the high quality of our sample.

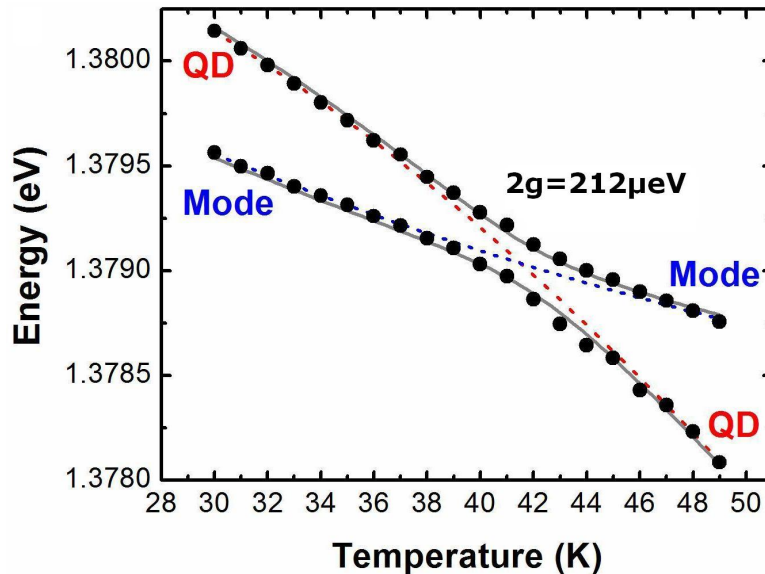


Figure 2.22: Energy dependence on temperature of the QD emission and photonic mode. The red (blue) dashed line represent the temperature dependence of the uncoupled QD (mode).

2.7 Conclusion

To summarize, we have studied InGaAs/GaAs quantum dot structures monolithically grown on a silicon substrate, without use of germanium virtual substrate nor wafer bonding technique. Optical characterization of the sample with microphotoluminescence showed very good single quantum dot emission lines with a variable density across the wafer suitable both for single dot study and observation of QD / photonic crystal cavity coupling, as well as unexpected but nevertheless interesting high energy QD-like lines. Single photon emission from the InGaAs dots have been demonstrated with photon correlation experiment showing clear anti-bunching. Photonic crystal cavities fabricated on the sample exhibited very high quality factor up to 13000 with a large percentage of cavities having Q-factors over 9000. This allowed observation of Purcell effect for single photon emitting QDs and strong light-matter coupling between InGaAs QDs and cavities.

This work is one of the precursors in the study of single QDs grown on silicon, and the first comprising photonic crystals, and is opening the way to future studies in the fields of integration of III-V single photon emitters on silicon and cavity quantum electrodynamics in hybrid III-V/Si structures.

References

- [1] D. Deutsch, “Quantum theory, the church-turing principle and the universal quantum computer,” *Proceedings of the Royal Society of London. A. Mathematical and Physical Sciences*, vol. 400, no. 1818, pp. 97–117, 1985.
- [2] T. Hey, “Quantum computation: an introduction.” https://www.researchgate.net/publication/3363605_Quantum_computing_an_introduction?ev=srch_pub, Sept. 1999.
- [3] J. E. Sharping, K. F. Lee, M. A. Foster, A. C. Turner, B. S. Schmidt, M. Lipson, A. L. Gaeta, and P. Kumar, “Generation of correlated photons in nanoscale silicon waveguides,” *Opt. Express*, vol. 14, pp. 12388–12393, Dec 2006.
- [4] D. Bonneau, E. Engin, K. Ohira, N. Suzuki, H. Yoshida, N. Lizuka, M. Ezaki, C. M. Natarajan, M. G. Tanner, R. H. Hadfield, S. N. Dorenbos, V. Zwiller, J. L. O’Brien, and M. G. Thompson, “Quantum interference and manipulation of entanglement in silicon wire waveguide quantum circuits,” *New J. of Phys.*, vol. 14, p. 045003, 2012.
- [5] O. Benson, C. Santori, M. Pelton, and Y. Yamamoto, “Regulated and entangled photons from a single quantum dot,” *Phys. Rev. Lett.*, vol. 84, pp. 2513–2516, Mar 2000.
- [6] I. J. Luxmoore, R. Toro, O. Del Pozo-Zamudio, N. A. Wasley, E. A. Chekhovich, A. M. Sanchez, R. Beanland, A. M. Fox, M. S. Skolnick, H. Y. Liu, and A. I. Tartakovskii, “III-V quantum light source and cavity-QED on Silicon,” *Sci. Rep.*, vol. 3, p. 1239, 2013.
- [7] R. Anderson, “Experiments on ge-gaas heterojunctions,” *Solid-State Electronics*, vol. 5, no. 5, pp. 341 – 351, 1962.
- [8] L. Knuuttila, A. Lankinen, J. Likonen, H. Lipsanen, X. Lu, P. McNally, J. Rikonen, and T. Tuomi, “Low Temperature Growth GaAs on Ge,” *Japanese Journal of Applied Physics*, vol. 44, pp. 7777+, Nov. 2005.

- [9] W. I. Wang, “Molecular beam epitaxial growth and material properties of GaAs and AlGaAs on Si (100),” *Applied Physics Letters*, vol. 44, no. 12, pp. 1149–1151, 1984.
- [10] G. M. Metzger, H. K. Choi, and B.-Y. Tsaur, “Metal-semiconductor field-effect transistors fabricated in GaAs layers grown directly on Si substrates by molecular beam epitaxy,” *Applied Physics Letters*, vol. 45, no. 10, pp. 1107–1109, 1984.
- [11] R. Fischer, W. T. Masselink, J. Klem, T. Henderson, T. C. McGlenn, M. V. Klein, H. Morkoç, J. H. Mazur, and J. Washburn, “Growth and properties of GaAs/AlGaAs on nonpolar substrates using molecular beam epitaxy,” *Journal of Applied Physics*, vol. 58, no. 1, pp. 374–381, 1985.
- [12] R. Fischer, H. Morkoç, D. A. Neumann, H. Zabel, C. Choi, N. Otsuka, M. Longobardi, and L. P. Erickson, “Material properties of high-quality GaAs epitaxial layers grown on Si substrates,” *Journal of Applied Physics*, vol. 60, no. 5, pp. 1640–1647, 1986.
- [13] Z. Mi and Y.-L. Chang, “III-V compound semiconductor nanostructures on silicon: Epitaxial growth, properties, and applications in light emitting diodes and lasers,” *J. Nanophoton.*, vol. 3, p. 031602, 2009.
- [14] D. Liang and J. E. Bowers, “Recent progress in lasers on silicon,” *Nat Photon*, vol. 4, no. 8, pp. 511–517, 2010.
- [15] S. Sakai, T. Soga, M. Takeyasu, and M. Umeno, “Room-temperature laser operation of AlGaAs/GaAs double heterostructures fabricated on Si substrates by metalorganic chemical vapor deposition,” *Applied Physics Letters*, vol. 48, no. 6, pp. 413–414, 1986.
- [16] T. Wang, H. Y. Liu, A. Lee, F. Pozzi, and A. Seeds, “1.3- μ m InAs/GaAs quantum-dot lasers monolithically grown on Si Substrates,” *Opt. Express*, vol. 19, p. 11381, 2011.
- [17] L. Cavigli, S. Bietti, N. Accanto, S. Minari, M. Abbarchi, G. Isella, C. Frigeri, A. Vinattieri, M. Gurioli, and S. Sanguinetti, “High temperature single photon emitter monolithically integrated on silicon,” *Applied Physics Letters*, vol. 100, no. 23, p. 231112, 2012.
- [18] G. C. Osbourn, “Strained-Layer Superlattices: A Brief Review,” *IEEE J. Quantum Electron.*, vol. 9, p. 1677, 1986.

- [19] C. Paranthoen, N. Bertru, O. Dehaese, A. L. Corre, S. Loualiche, B. Lambert, and G. Patriarche, “Height dispersion control of InAs/InP quantum dots emitting at 1.55 μm ,” *Applied Physics Letters*, vol. 78, no. 12, pp. 1751–1753, 2001.
- [20] J. W. Matthews and A. E. Blakeslee, “Defects in epitaxial multilayers, I: Misfit dislocations,” *J. Cryst. Growth*, vol. 27, pp. 118–125, 1974.
- [21] S. Fafard, Z. R. Wasilewski, C. N. Allen, D. Picard, M. Spanner, J. P. McCaffrey, and P. G. Piva, “Manipulating the energy levels of semiconductor quantum dots,” *Phys. Rev. B*, vol. 59, pp. 15368–15373, Jun 1999.
- [22] J. M. Ulloa, P. M. Koenraad, E. Gapihan, A. Létoublon, and N. Bertru, “Double capping of molecular beam epitaxy grown InAs/InP quantum dots studied by cross-sectional scanning tunneling microscopy,” *Applied Physics Letters*, vol. 91, no. 7, p. 073106, 2007.
- [23] L. Wang, A. Rastelli, and O. G. Schmidt, “Structural and optical properties of in(ga)as/gaas quantum dots treated by partial capping and annealing,” *Journal of Applied Physics*, vol. 100, no. 6, p. 064313, 2006.
- [24] Ioffe Physical Technical Institute, “Characteristics of semiconductors.” <http://www.ioffe.ru/SVA/NSM/Semicond/>.
- [25] M. Tachikawa and H. Mori, “Reduction of dislocation generation for heteroepitaxial III-V/Si by slow cooling,” *Journal of Crystal Growth*, vol. 183, p. 89, 1997.
- [26] R. Oulton, *Optical Spectroscopy of Single Self-Assembled InGaAs/GaAs Quantum Dots*. PhD thesis, The University of Sheffield, 2003.
- [27] K. Brunner, G. Abstreiter, G. Böhm, G. Tränkle, and G. Weimann, “Sharp-line photoluminescence and two-photon absorption of zero-dimensional biexcitons in a gaas/algaas structure,” *Phys. Rev. Lett.*, vol. 73, pp. 1138–1141, Aug 1994.
- [28] M. Bayer, V. D. Kulakovskii, T. Gutbrod, and A. Forchel, “Exciton complexes in InGaAs/GaAs quantum dots,” *Physica B: Condensed Matter*, vol. 249-251, pp. 620–623, June 1998.
- [29] M. Fox, *Quantum Optics: An Introduction (Oxford Master Series in Physics, 6)*. Oxford University Press, USA, June 2006.

- [30] J. D. Joannopoulos, S. G. Johnson, J. N. Winn, and R. D. Meade, *Photonic Crystals: Molding the Flow of Light*. Princeton University Press, second ed., February 2008.
- [31] A. Badolato, K. Hennessy, M. Atatüre, J. Dreiser, E. Hu, P. M. Petroff, and A. Imamoglu, “Deterministic Coupling of Single Quantum Dots to Single Nanocavity Modes,” *Science*, vol. 308, pp. 1158–1161, May 2005.
- [32] K. Hennessy, A. Badolato, M. Winger, D. Gerace, M. Atature, S. Gulde, S. Falt, E. L. Hu, and A. Imamoglu, “Quantum nature of a strongly coupled single quantum dot-cavity system,” *Nature*, vol. 445, pp. 896–899, Feb. 2007.
- [33] J. H. Harlow, *Electric Power Transformer Engineering*. CRC Press, 2004.
- [34] M. Tooley, *Electronic Circuits : Fundamentals and Applications*. Routledge, 2006.
- [35] A. J. Shields, “Semiconductor quantum light sources,” *Nat Photon*, vol. 1, pp. 215–223, 2007.
- [36] A. Kiraz, S. Fälth, C. Becher, B. Gayral, W. V. Schoenfeld, P. M. Petroff, L. Zhang, E. Hu, and A. Imamoglu, “Photon correlation spectroscopy of a single quantum dot,” *Phys. Rev. B*, vol. 65, p. 161303, Mar 2002.
- [37] K. Vahala, *Optical Microcavities (Advanced Series in Applied Physics, 5)*. World Scientific Publishing Co Pte Ltd, Dec. 2004.
- [38] A. R. A. Chalcraft, S. Lam, D. O’Brien, T. F. Krauss, M. Sahin, D. Szymanski, D. Sanvitto, R. Oulton, M. S. Skolnick, A. M. Fox, D. M. Whittaker, H.-Y. Liu, and M. Hopkinson, “Mode structure of the l3 photonic crystal cavity,” *Applied Physics Letters*, vol. 90, no. 24, p. 241117, 2007.
- [39] J. Wang, D. Shang, H. Mao, J. Yu, Q. Zhao, P. Yang, and H. Xing, “Influence of strain on built-in dipole moment in asymmetric $\text{In}_x\text{Ga}_{1-x}\text{As}$ quantum dot molecules,” *Applied Physics A*, vol. 109, no. 2, pp. 391–394, 2012.
- [40] F. Bernardot, E. Aubry, J. Tribollet, C. Testelin, M. Chamarro, L. Lombez, P.-F. Braun, X. Marie, T. Amand, and J.-M. Gérard, “Linear and dynamical photoinduced dichroisms of InAs/GaAs self-assembled quantum dots: Population relaxation and decoherence measurements,” *Phys. Rev. B*, vol. 73, p. 085301, Feb 2006.

- [41] P. W. Fry, I. E. Itskevich, D. J. Mowbray, M. S. Skolnick, J. J. Finley, J. A. Barker, E. P. O'Reilly, L. R. Wilson, I. A. Larkin, P. A. Maksym, M. Hopkinson, M. Al-Khafaji, J. P. R. David, A. G. Cullis, G. Hill, and J. C. Clark, "Inverted electron-hole alignment in InAs-GaAs self-assembled quantum dots," *Phys. Rev. Lett.*, vol. 84, pp. 733–736, Jan 2000.
- [42] E. M. Purcell, "Spontaneous Emission Probabilities at radio Frequencies," *Physical Review Online Archive (Prola)*, vol. 69, p. 681, June 1946.
- [43] E. T. Jaynes and F. W. Cummings, "Comparison of quantum and semiclassical radiation theories with application to the beam maser," *Proceedings of the IEEE*, vol. 51, pp. 89–109, Jan. 1963.
- [44] A. Laucht, F. Hofbauer, N. Hauke, J. Angele, S. Stobbe, M. Kaniber, G. Böhm, P. Lodahl, M. C. Amann, and J. J. Finley, "Electrical control of spontaneous emission and strong coupling for a single quantum dot," *New Journal of Physics*, vol. 11, pp. 023034+, Feb. 2009.
- [45] M. Winger, A. Badolato, K. J. Hennessy, E. L. Hu, and A. Imamoglu, "Quantum dot spectroscopy using cavity quantum electrodynamics," *Physical Review letters*, vol. 101, pp. 226808+, Nov. 2008.

Chapter 3

GaAs/AlGaAs single photon emitters from interface fluctuations of short period superlattice monolithically grown on silicon substrate

3.1 Introduction

Chapter 2 introduced the need to merge existing silicon technology with more efficient semiconductor photon emitters. Back then the single photon emitters in question were self-assembled quantum dots, but although they are the most widely studied quantum dots since 1993-1994 [1, 2], the first referenced study or prediction of zero-dimensional nanostructures traces back to the early 80s [3–6], when Weisbuch predicted that interface fluctuations in the well-known two-dimensional quantum well structure could cause trapping of charges leading to exciton confinement in all three directions. Later the phenomenon was experimentally observed and described in AlGaAs/GaAs quantum wells by Zrenner et al. in 1994 [5], who coined the “interface fluctuation quantum dot” term.

Discovering such nanostructures in our sample provides a very good and unexpected opportunity for two reasons: first III-V on silicon is getting a lot of attention, and a more complete understanding and mastery of the techniques to grow such structures can only be acquired through the study of various different combinations

of materials. Indeed research on quantum technologies is still at an early stage, and no contender for physical implementation of quantum devices has taken a significant lead over the others. Secondly, the usually higher energy emission of interface dots (in the region of visible red light or near infrared) compared to InGaAs self-assembled dots, make them good candidates for other applications like a new type of free-space communication [7], and they are also in the higher sensitivity range of Si detectors.

The present chapter is dedicated to the optical study of interface dots discovered in a hybrid III-V on Si sample. We start with the description of the sample and experimental setup, then continue with formal identification of the origin of the unknown QD-like emission, that will demonstrate their interface nature. A more comprehensive optical study of the emission lines with polarization detection is to follow, and finally the ability to emit single photons will be demonstrated and discussed.

3.2 Sample structure and experimental setup

3.2.1 Sample structure

The sample grown by H.-Y. Liu from UCL on which this study is based is the same as in chapter 2, and the reader should be referred to section 2.2 for a more complete review of the sample structure, the III-V-to-silicon merging history, and the growth techniques employed. In this paragraph though we will emphasize on the other parts of the sample that will be of interest. Figure 3.1 shows the same layer structure drawing as figure 2.2 except the height of each layer is now depicted in the scale. The silicon substrate is represented in green at the bottom, on top of it a layer of 1000 nm of GaAs, then the four dislocation filters are represented in one block in orange. These 10 nm InAlAs / 10 nm GaAs strained layer superlattices are meant to capture and reduce the threading dislocations arising from the huge lattice mismatch ($\sim 4\%$) between Si and GaAs [8–10]. The small magenta slab above it is the AlGaAs/GaAs short period superlattice composed of 50 alternating layers of 2 nm AlGaAs and GaAs. The purpose of those layers is to smooth the surface of the sample to increase quality of subsequent growth [11]. The top layers contain the InGaAs QDs, an intermediate 300 nm layer of GaAs and a sacrificial layer of 1000 nm AlGaAs. Represented in gray on the figure, they are not of interest to this chapter, and will be ignored.



Figure 3.1: Schematics of the layer structure of the sample.

3.2.2 Experimental setup

The experimental setup used for micro-photoluminescence is the same as in chapter 2, it is illustrated on fig. 2.6 and described in section 2.3.1. Only the single spectrometer was used in experiments presented in this chapter, since it provided sufficient spectral resolution.

3.3 Optical identification of the internal layers

3.3.1 Principle

The first micro-photoluminescence spectra of the sample showed, on top of the expected InGaAs quantum dot emissions in the 1.3 - 1.4 eV region, some unexpected features in the higher energy region (see figure 3.2). Those single lines spread from 1.7 eV to 1.8 eV, are followed by a broad band similar to a quantum well emission, and have a full width at half maximum as small as $50 \mu\text{eV}$. They present all characteristics of zero-dimensional quantum structures. Nevertheless, such quantum dots were not intentionally included during the growth process of the sample.

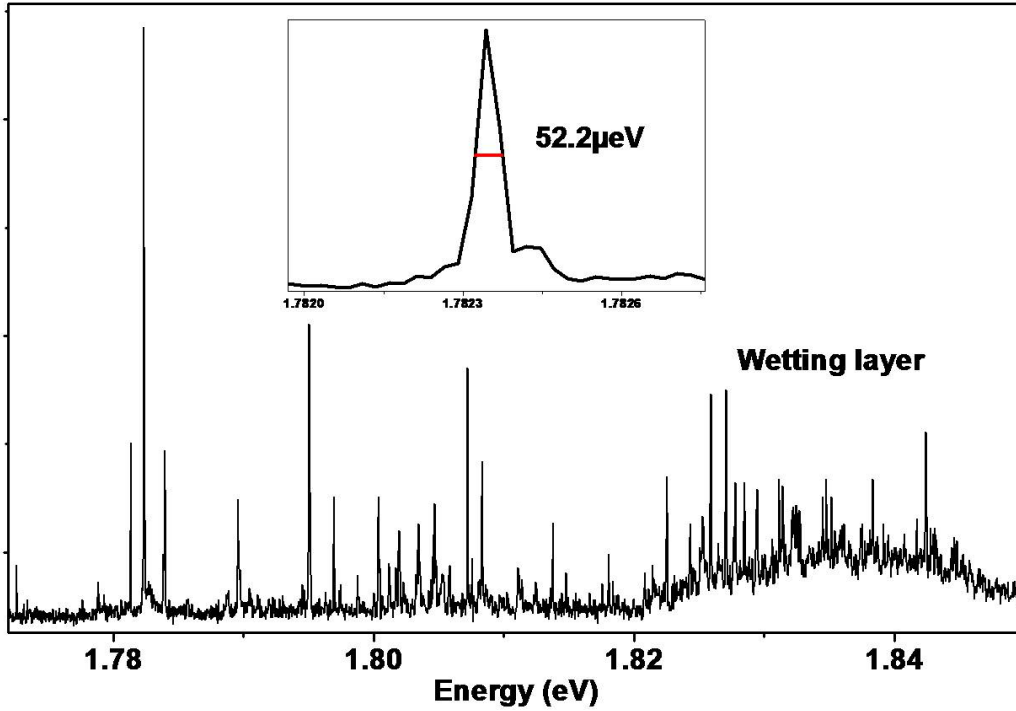


Figure 3.2: Micro-photoluminescence spectrum of the sample in the 1.7 - 1.8 eV region. Single lines with linewidth as narrow as $50 \mu\text{eV}$ appear in this region where nothing would have been expected.

The first step in the study of these emission lines is to determine their source. It is probable that the complex structure of the sample, comprising many superlattices, has allowed formation of nanostructures at some point. The two possible origins are the strained layer superlattice, acting as dislocation filters (orange in figure 3.1) and the AlGaAs/GaAs short period superlattice (magenta on figure 3.1). Indeed the other parts of the sample are all bulk, and cannot host any structure

exhibiting narrow lines.

The strained layer superlattice is formed of alternating 10 nm wide layers of InAlAs and GaAs, such structure has been known to produce self-assembled quantum dots [12, 13]. Indeed the Stranski-Krastanov method relies on the strain between the wetting layer material and the surrounding bulk material to induce self-creation of quantum dots, the accumulated strain being released after a critical number of layers by the formation of islands. Such a strained structure is ideal to capture and eliminate threading dislocations propagating from deeper layers. Reversely, the strain filters used in this sample to diffuse dislocations could very well have released strain by forming nanostructures during growth.

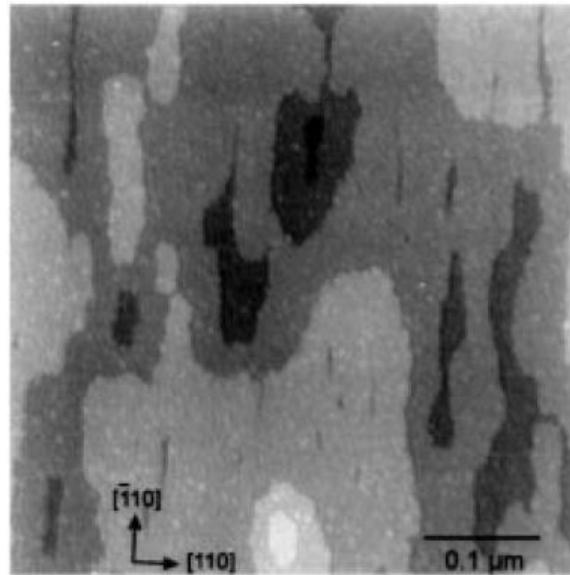


Figure 3.3: Scanning tunnelling microscope image of the surface of a GaAs quantum well layer. The differences in color represent fluctuations of one monolayer. Figure taken from Gammon et al., PRL 1996 [14]

AlGaAs/GaAs short period superlattices, on the other hand, are comprised of 2 nm thick alternating layers, which is the average thickness of many reported quantum wells, from which interface fluctuations formed quantum dot structures [5, 6]. Quantum wells are two-dimensional slabs of semiconductor. Charges in a quantum well encounter a potential barrier that hinders them from escaping in adjacent layers, but are free to propagate in the two dimensions of the well. But in some circumstances, mainly due to imperfect growth, thickness fluctuations may appear at the interface between a well and a neighbouring layer, creating

terraced steps (see figure 3.3). The steps can form a finite area where the well is one monolayer thicker than the surrounding, producing a lateral confinement that would make the propagation of a charge carrier more difficult (though not as much as in the growth direction of the quantum well). When those areas have a size comparable with the exciton Bohr radius of ≈ 10 nm, they can effectively trap excitons, making sharp quantum dot-like emission lines upon recombination. Those nanostructures are called interface quantum dots [5]. The following experiment aims at determining the source of the emission between the two possible candidates, through a basic idea of variable etching.

3.3.2 Variable etching technique

The idea behind this experiment is quite simple: the layers where we suspect nanostructures could have been formed are situated at different depths from the surface of the sample, so by taking a certain number of pieces of the wafer and etching them at different depths, we can observe micro-photoluminescence at different depths, and see clearly which spectral features disappear and which remain.

The study focuses around five samples, four being etched at different depths, and the last one being a raw piece of the wafer to measure photoluminescence of the surface. The samples have been etched using a solution of sulphuric acid and hydrogen peroxyde in a class 10000 clean room. Since this wet etching can be quite non-uniform on the surface, the preferred technique has been to cover the sample with photoresist and to pattern small holes a few hundreds microns wide. After dipping the sample in the etchant, the depth was checked using a Dektak profilometer, an equipment that can measure the surface of objects with a resolution of a few nanometers.

Figure 3.4 depicts the layer structure of the sample (a) along with a transmission electron microscope (TEM) image of a lateral view of the structure (b), provided by A. Sanchez and R. Beanland from University of Warwick. The scale of the layer structure schematic is so that layers correspond between the schematic and the TEM. We can see red arrows numbered from 1 to 4, they represent the depths of the 4 etched samples. For the first arrow the etching has been stopped into the GaAs bulk layer immediately above the AlGaAs/GaAs superthin lattice. At this point, the high energy emission is not expected to disappear yet. The second etching stops within the superthin layers, to check the evolution of the emission lines. The third etching stops in the GaAs bulk layer above the InAlAs/GaAs strained

superlattices of the dislocation filters and the last in the middle of said dislocation filters.

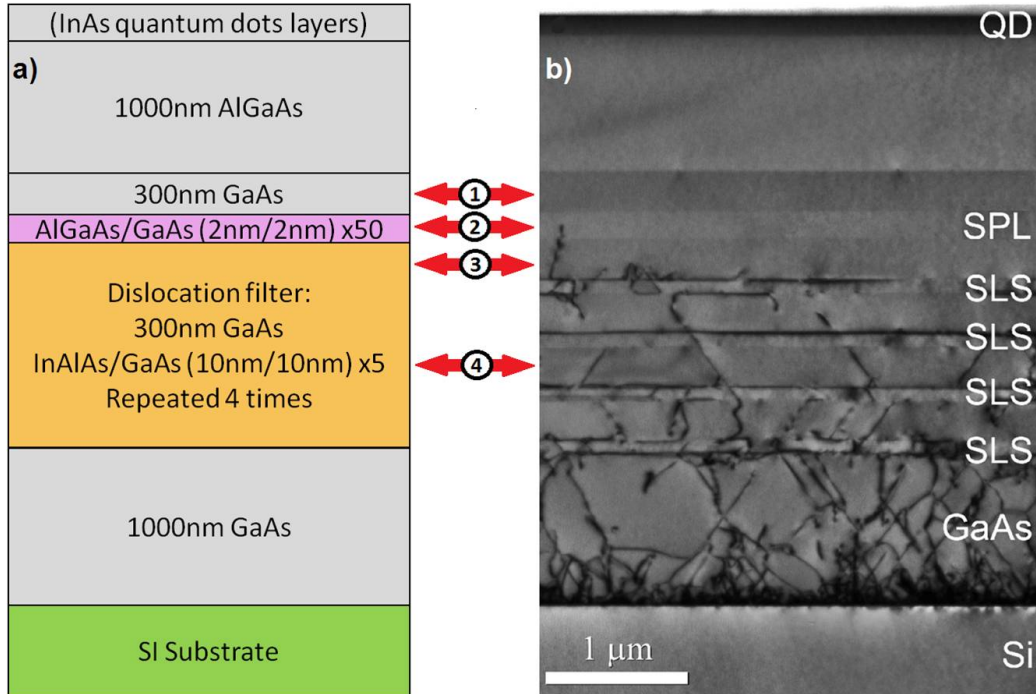


Figure 3.4: Corresponding representations of the structure of the sample. (a) schematic of the layer structure (b) cross-sectional TEM image of the sample. The four markers between part (a) and part (b) indicate the 4 depths at which the sample has been etched to determine the origin of the high energy emissions.

3.3.3 Interpretation of the results

Micro-photoluminescence of the five samples (4 etched plus 1 raw) allows us to see the evolution of spectral features within the internal layers of the sample. Figure 3.5 represents the five spectra organized from top to bottom according to the depth at which they have been measured, with the spectrum of the non-etched sample on top and the one more deeply etched on the bottom (see figure 3.4). The low energy part of the PL spectrum in part (a) gives us insight about the evolution of the different bulk and active layers emissions with depth, while high energy end PL represented on part (b) mainly allows us to determine at which point the high energy QD emission disappear. PL measurements were performed at an excitation power of 300 nW per μm^2 (HeNe laser 633 nm).

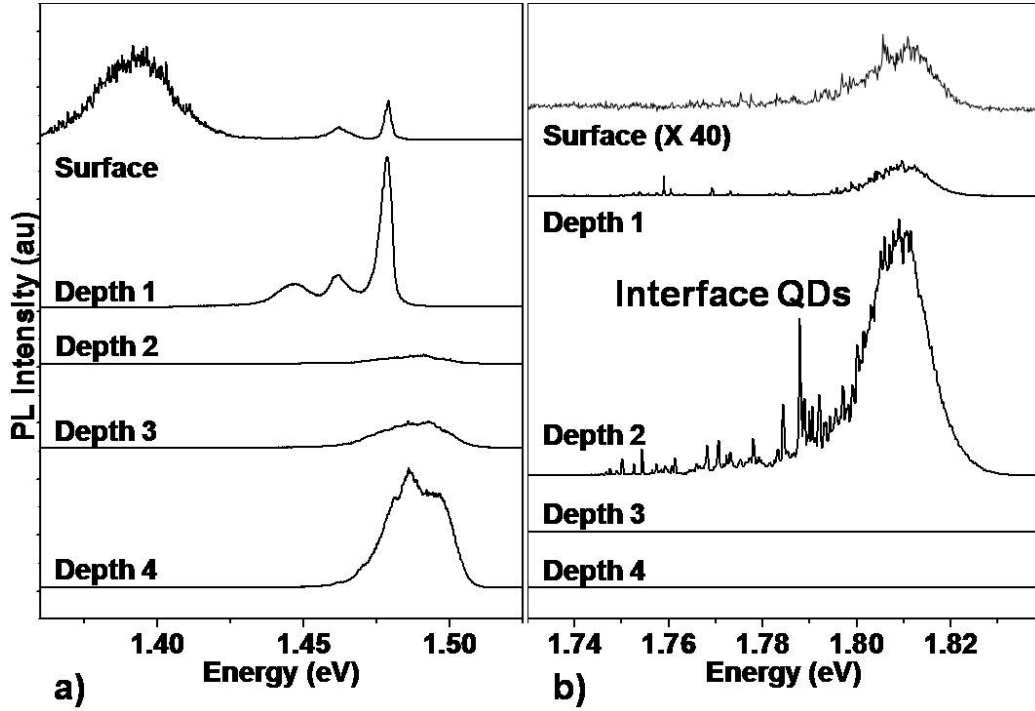


Figure 3.5: PL spectra at low energy (a) and high energy (b) of the sample at different depths after wet etching: from top to bottom: on the raw surface of the wafer, without etching; and at the numbered four depths represented figure 3.4.

On the top spectrum we can see bulk emission at 1.46 eV and 1.475 eV, the presence of multiple bulk peaks is attributed to the several GaAs bulk layers in the structure. The high density cluster of InAs QDs can be observed between 1.32 eV and 1.42 eV, as expected, and the high energy region shows the weak yet unmistakable emission of QD lines (on top of figure 3.5 (b) enhanced 40 times) that interests us. At first depth just above the AlGaAs/GaAs superthin layers we can see complete disappearance of the InAs QDs as expected, and high energy spectrum shows a clear enhancement of the high energy QD emission, justified by the fact that those emissions have higher energy than the bandgap of bulk GaAs. Being closer to the surface (that is, with less bulk GaAs covering their source) makes them less heavily absorbed by the GaAs bulk, and so they appear brighter. In the same fashion, the brighter GaAs bulk emission seen at 1.45 eV, 1.46 eV and 1.475 eV are believed to come from the carrier recombination in the GaAs layer situated below the sacrificial layer. It is confirmed by the disappearance of those emissions at the third depth in the center of the superthin layers. At the two subsequent depths a broad PL band emerges centred around 1.49 eV, probably generated by the heavily strained GaAs layer grown directly on top of silicon. The third depth yields a high energy

dot emission even stronger, with a broad peak at 1.81 eV similar to what would be expected of GaAs/AlGaAs quantum wells, as observed in previous work [5, 6]. The two subsequent samples etched below the AlGaAs/GaAs superlattice do not show any trace of high energy PL. This together with the peak at 1.81 eV constitute the main proofs that the high energy PL lines observed originate from QDs formed by interface fluctuations in the AlGaAs/GaAs superthin lattice.

3.3.4 Further confirmation with temperature dependence

Though the previous experiment shows in a pretty clear fashion that our dots originate from interface fluctuations and not self-assembled, the only way to have full proof of the origin of the dots would be to grow the strain filter and short period superlattice separately. The Dektak's accuracy can vary, particularly when the etching goes as deep as a few μm . To further ascertain our result, a simple test is to observe micro-PL of the emission lines while raising the temperature of the sample. Indeed, at cryogenic temperature, radiative recombination of excitons trapped in dots is the main recombination process, but when temperature raises, a process that was negligible becomes predominant: thermal escape of carriers from the dots. This results in a quenching of the emissions, and as the interface dots are less energetically confined than self-assembled dots, thermal escape becomes effective at much lower temperature. A temperature dependence of both the InAs self-assembled QDs and the high energy emissions would show us which quench the fastest.

The results of this temperature dependent PL are plotted in figure 3.6. The PL spectra at increasing temperature are represented from bottom to top, for low energy InAs dots (a) and high energy interface dots (b). As expected, we can see a much quicker quenching of the high energy emissions, around 40 K while for the InAs dots broadened signal still appears after 70 K. This confirms the shallow nature of the high energy dots, as thermal escape occurs at much lower temperature.

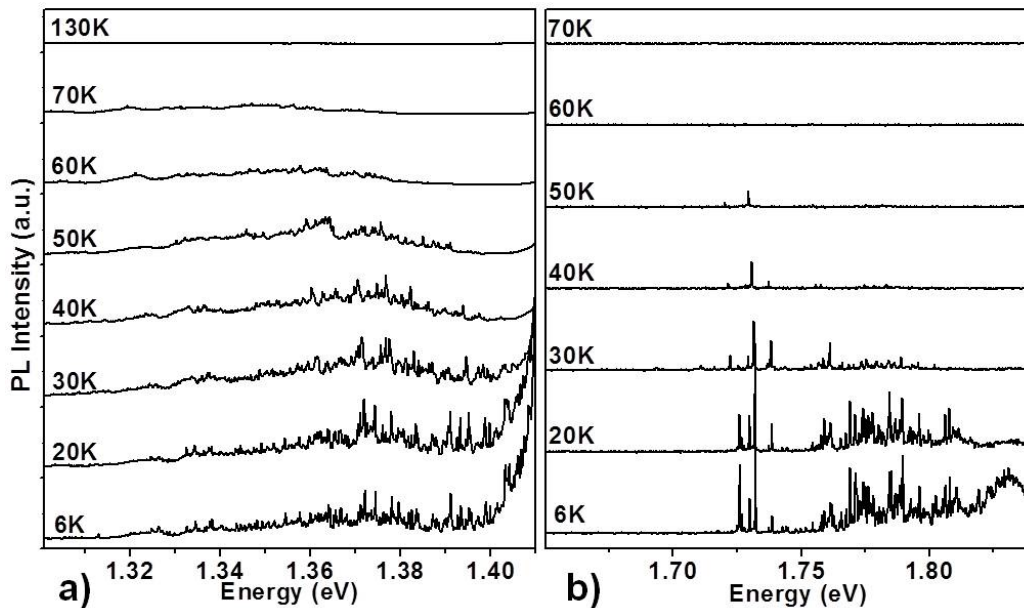


Figure 3.6: Temperature dependent PL of the raw surface of the sample at low energy (a) and high energy (b). Spectra at increasing temperature are represented from bottom to top.

3.4 Polarization study and fine structure of the dots

A more comprehensive study of the optical properties of the dots follows in this section. It will include the observation of the polarization of light emitted by the sample, and dependence of the photoluminescence intensity on excitation power, and will give us insight about the fine structure splitting and the bi-exciton binding energy of the dots.

3.4.1 Principle of light polarization

Light can be polarized in many ways according to how its electric field vector evolves with time. Since the light, in its wave form representation, is composed of a packet of electromagnetic waves, any light coming from a single source can be defined by the characteristic orientations of the electric fields that compose it. Those orientations can be classified into two main types, namely linear polarization and circular polarization. Each other polarization can be seen as a combination of those two components (for more details read about Stokes parameters and Jones calculus). The excitation light will usually not be polarized, which means the ratio between circular and linear polarization is unknown. For our experiment we need to have it

polarized in a certain way, this has been done by using a linear polarizer, a quarter-wave plate and a half-wave plate. The experimental setup for this measurements is illustrated on figure 3.7.

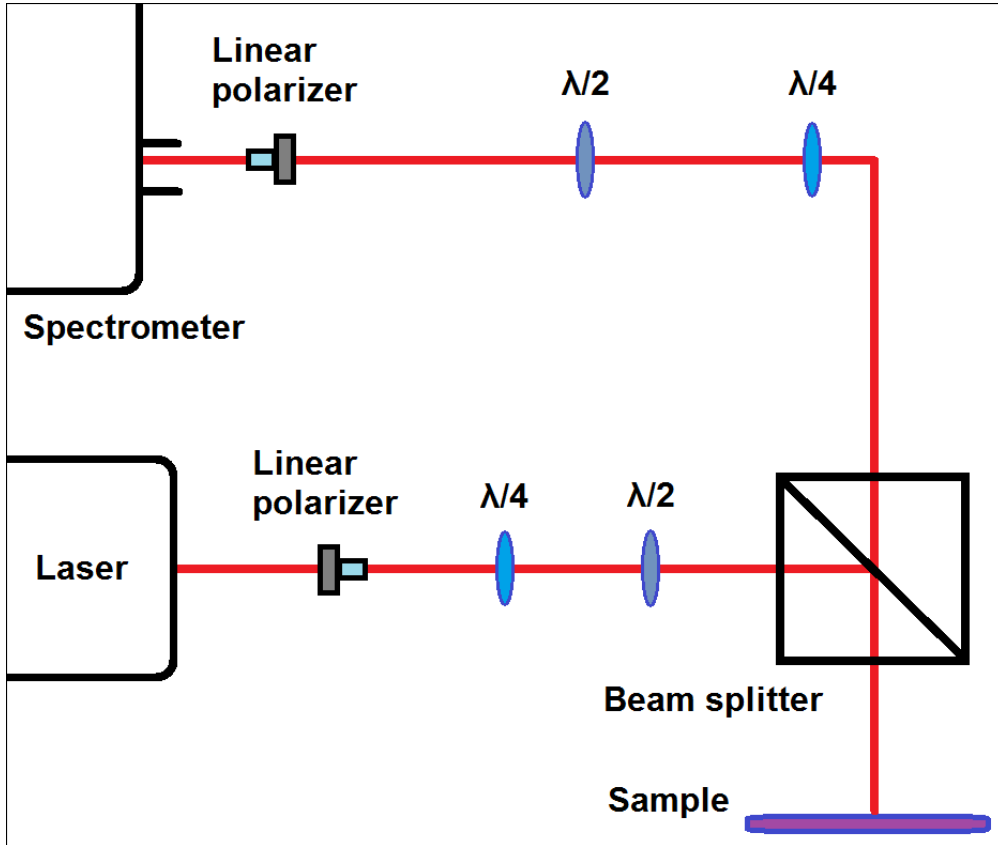


Figure 3.7: Schematic of the setup used to measure polarization dependent μ PL.

The excitation beam first goes through the linear polarizer and then through a quarter-wave plate. The quarter-wave plate inverts the linear and circular components of the polarization, which allows to have a circularly polarized beam. The process is described on figure 3.8. The half-wave plate is used to change the polarization from left-hand circular to right-hand circular. The beam then reaches the sample, pumping it with horizontal, vertical, left-hand or right-hand circular polarization depending on the orientation of the optical equipments on its path.

The light emitted from the sample then goes through another set of quarter-wave plate, half-wave plate, and linear polarizer. This combination ensures that we can filter any component of the polarization of the light emitted by the sample, linear or circular. The filtered beam finally enters the spectrometer and CCD.

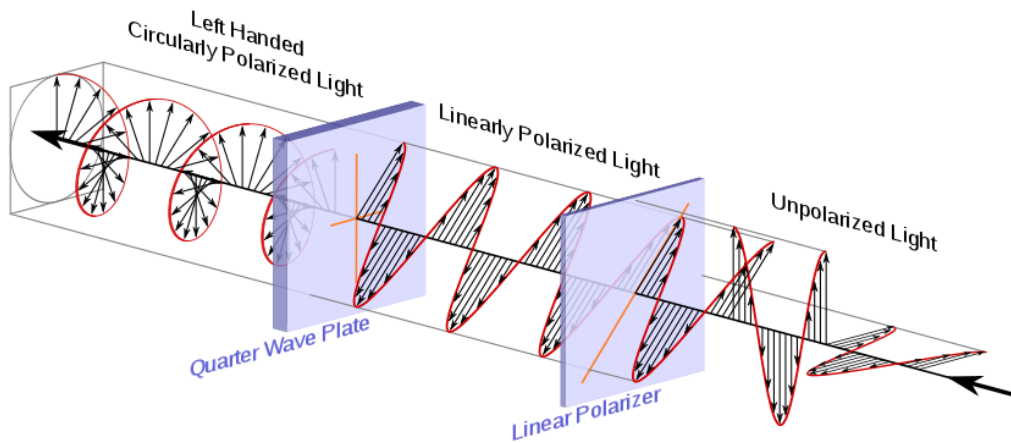


Figure 3.8: An example of light polarization modified by optical equipment: unpolarized light (bottom right) enters a linear polarizer, keeping only the linear component that is aligned with the axis of the polarizer. The linearly polarized light then goes through a quarter-wave plate which changes the polarization to circular. Taken from [15].

3.4.2 Observation of fine structure splitting

The energy levels of a quantum dot are degenerate and can be studied through several orders of precision, namely through the gross, fine and hyperfine structure of the exciton. The gross structure is the zero-order description of energy and doesn't take into account any quantum effect, only relying on the first energy quantum number n [16]. The fine structure is about the interaction between the electron and the hole, and makes use of the spin and angular momentum of the particles [14, 17]. As for the hyperfine structure, it deals with the interaction of the exciton with the nuclei forming the quantum dot [18, 19]. An entire description of the energy levels will not be given in this chapter, but the fine structure behaviour of a quantum dot being unique compared to that of a higher dimension structure, the observation of the fine structure from energy emissions can give us further confirmation of their quantum dot origin.

The exciton in a quantum dot is formed of an electron with spin $\pm 1/2$ and a hole with spin $\pm 3/2$ (heavy holes) or $\pm 1/2$ (light holes). The light hole and heavy hole energies presenting a difference of the order of tens of meV for quantum dots, the former can be neglected, which gives us total angular momentum numbers of +1, -1, +2 and -2. The last two are forbidden transitions that cannot interact with the light field (i.e. emit photons) unless they are mixed with the former two (bright) states by means of a strong non-symmetry of the dot or application of an external

magnetic field in the Voigt geometry [17], and therefore are very difficult to observe, hence their name dark states or dark excitons. Such states are not studied nor observed in this work. The bright states, on the other hand, are degenerate under normal conditions and if the dot has a perfectly circular base. The degeneracy is lifted when a magnetic field is applied in the Faraday geometry, when the +1 and -1 exciton states split (Zeeman effect, see section 1.4.2). When no magnetic field is applied, in the case of reduced symmetry (when the base of the dot is not circular) a smaller fine structure splitting can be observed between the +1 and -1 energy levels [14, 17, 20–22] (for a mathematical demonstration of this read ref.[17]). Furthermore, the two states will emit linearly polarized light, perpendicular to one another.

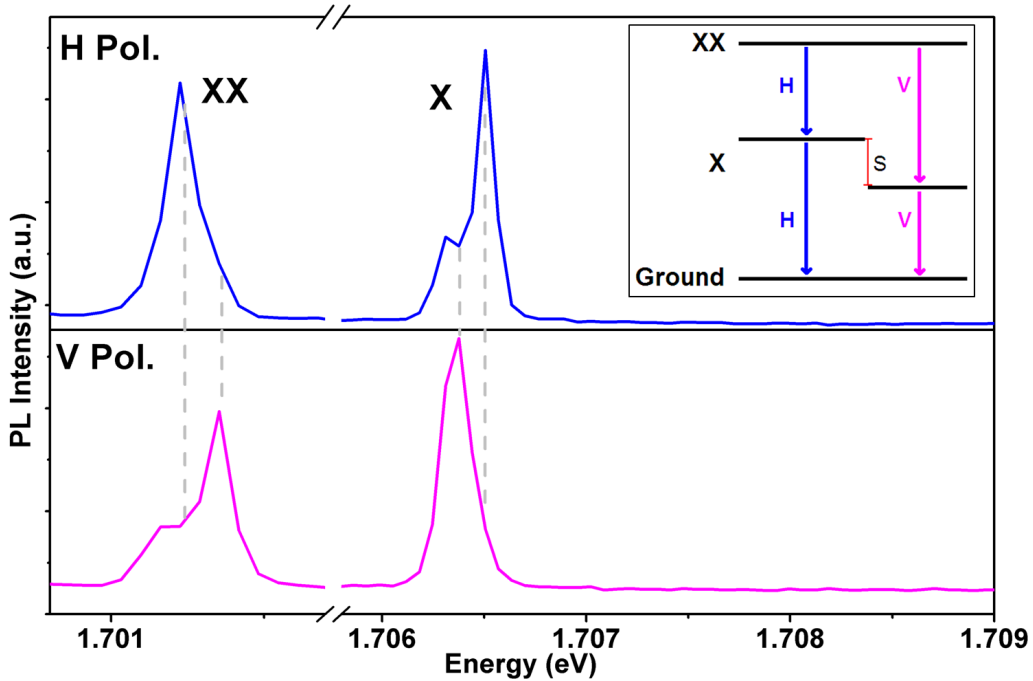


Figure 3.9: Fine structure splitting of a pair exciton (right)/bi-exciton (left) observed under horizontal linear polarization (top) and vertical linear polarization (bottom). The inset displays an energy diagram of the bi-exciton decay. S is the fine structure splitting.

This effect can be observed in figure 3.9, representing photoluminescence spectra of an exciton/bi-exciton pair under different polarization detection. The line on the right, assumed to be the exciton X, is separated from the other line that we assume is the bi-exciton XX by a binding energy of 5 meV, which would be quite high for a self-assembled quantum dot but has been previously observed in interface

fluctuation dots [6]. The top of figure 3.9 represents the horizontal polarization¹ detected from the excitonic states. When detecting vertical polarization of the same states (bottom), we can see a clear shift of the lines, to lower energy for the exciton and higher energy for the bi-exciton. The fine structure splitting showing here cannot be measured accurately as it is close to the best resolution of the single spectrometer used for the experiment, but with the adequate fitting of the lines using Lorentzian curves, we can have a good estimate of the splitting. This particular dot shows the biggest splitting recorded on the sample with 120 μeV . Throughout the sample fine structure splittings ranging from 40 μeV to 100 μeV have been measured, as similarly observed in other works [14].

3.4.3 Power dependence of exciton/bi-exciton pairs

The lines studied in the previous paragraph have been subject to power dependence measurements to confirm that they are indeed exciton and bi-exciton, as well as to gather information on the dynamics of charge carriers. Figure 3.10 shows the result of such an experiment, with photoluminescence integrated intensity of the exciton (black squares) and the bi-exciton (red triangles) plotted against excitation power. Excitation power ranges from 200 nW to 50 μW where phenomenon of saturation begins to appear.

The axis are represented in a logarithmic scale to better understand the relation between excitation power and number of photons emitted by the dot, in the same fashion as in section 2.3.2. Slopes for the exciton and the bi-exciton are calculated to be respectively 0.72 and 1.35, which denotes a sublinear dependence on power for the exciton and super linear though not quadratic dependence for bi-exciton. Those numbers, though related by a ratio of two as would be expected of an exciton/bi-exciton pair, are below the expected values of 1 and 2 [6]. This phenomenon has not been investigated in the present study, but a probable explanation can be given considering the mechanisms involved are not uncommon. The main hypothesis here is that charge carriers in delocalized states interact with charges trapped in the quantum dot. As excitation power increases, so the number of free charge carriers in the surrounding semiconductor, leading to a depletion of quantum dot states and to a sublinear power dependence [23, 24].

¹In this study the terms horizontal and vertical are arbitrary since it is difficult to know the orientation of the crystal lattice. Therefore the terms horizontal and vertical will be used to refer to two linear polarizations normal to one another.

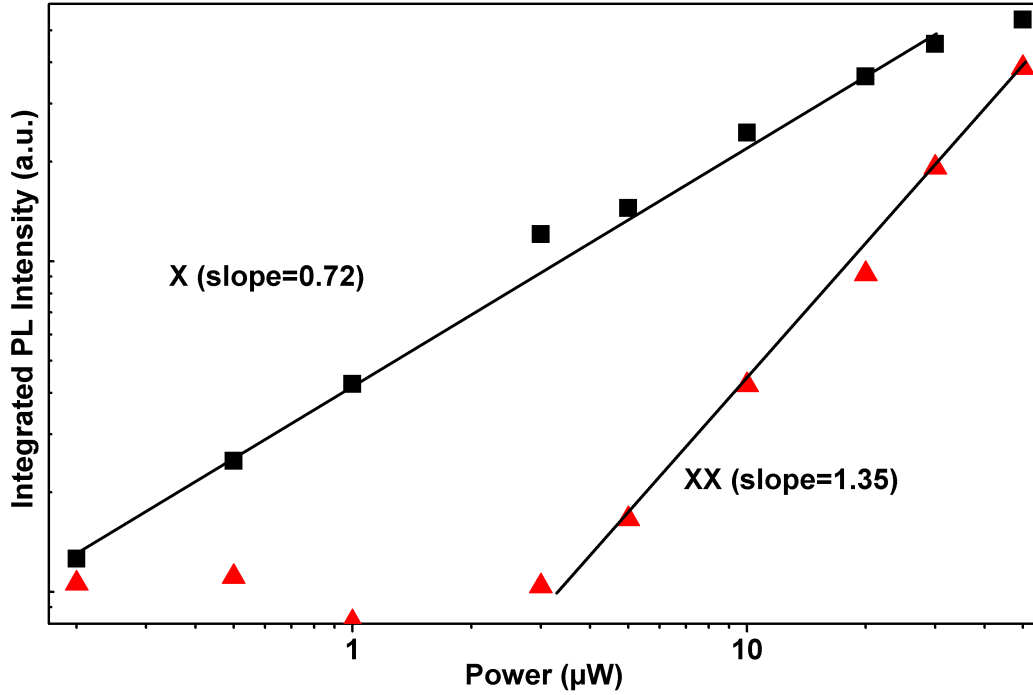


Figure 3.10: Excitation power dependent integrated PL intensity of an exciton (black squares) and a bi-exciton (red triangles).

3.5 Photon emission and lifetime properties

Complementary measurements have been realized to study single photon emission ability of the interface fluctuation quantum dots. They are described in this section, together with complementary information on the lifetime of the dots, based on experiments conducted by J. Chana and M. Sich from our group in Sheffield.

3.5.1 Experimental setup

For the lifetime experiment the sample is pumped with a Titanium-Sapphire 800 nm pulsed laser, with a pulse frequency of 82 MHz and a pulse width of less than 3 ps. The beam goes through a frequency doubler to obtain a blue pulse at 400 nm. Light collected from the sample is directed at a monochromator which is connected to a Hamatsu C5680 streak camera. The aim of the experiment is to measure the lifetime of an isolated quantum dot, and since the density of dots is not variable throughout the sample, the isolation can be achieved only through a custom designed 1 nm wide narrow band-pass filter. Two filters have been designed, based on the wavelength of suitable dots with high intensity count, at 722.9 nm and 713.3 nm. The 722.9 nm one has been successfully used during all the experiments. The

monochromator was first used to verify that the filter was isolating the dot properly (see fig. 3.11 (a) and (b)), and when we were certain that the only light coming to the monochromator was from the dot of interest, the diffraction grating was replaced by a simple mirror to maximize the signal (indeed the grating causes a 50% loss of signal compared to a mirror).

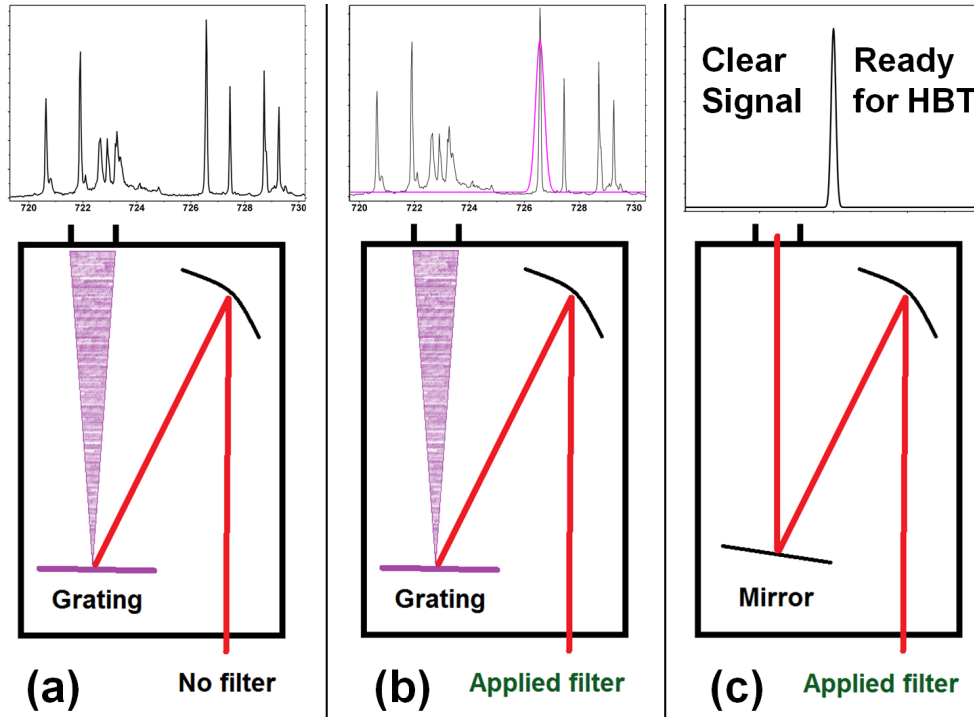


Figure 3.11: Illustration of the setup used to measure lifetime and photon correlation despite the low signal of the sample: (a) the whole spectrum is measured using a monochromator; (b) a narrow band-pass filter is applied to isolate the dot emission of interest and (c) the diffraction grating is replaced by a mirror to obtain a strong clear signal.

For the photon correlation experiment a Hanbury-Brown and Twiss experimental setup has been used, with a continuous excitation using He-Ne laser at 633 nm. The method to maximize the signal is the same as for the lifetime experiment, described in figure 3.11.

3.5.2 Lifetime of interface quantum dots

The lifetimes of the interface fluctuation quantum dots of the sample have been investigated to gain further knowledge of the dynamics of such structures. As explained in section 1.4.1, the lifetime is the average time an exciton exists in the

quantum dot before it recombines to emit a photon. The probability that the exciton recombines is a decreasing exponential, with characteristic time τ being the quantum dot lifetime. During the experiment, a laser pulse illuminates the sample and an electron-hole pair relaxes into the quantum dot. It recombines and the emitted photon is collected by the streak camera. After thousands of pulses the CCD matrix behind the streak camera has reconstituted a histogram of the quantum dot emission times (to obtain our result it took a typical time of 30 s), that can be extracted and is plotted on figure 3.12.

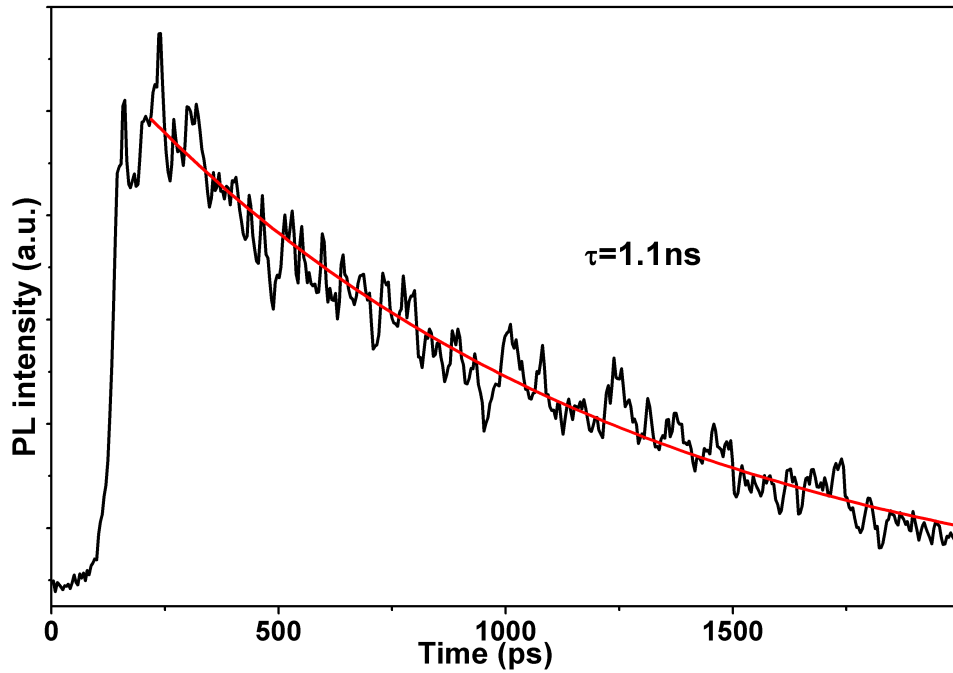


Figure 3.12: Lifetime measurement of a single interface fluctuation quantum dot. The first peak comes from light scattered from the laser, so the fitting starts at the second peak caused by the emission of the QD.

The experiment yielded a lifetime of 1.1 ns, which is comparable to the lifetimes measured in self-assembled InGaAs quantum dots from the same sample [25] and is rather typical for QDs.

3.5.3 Single photon emission

As seen in the previous chapter, the ability to emit single photons is of prime importance for the integration into silicon photonics and many quantum applications of a material [26–29]. It has been demonstrated for the interface fluctuation dots

in the present section.

The experimental setup is a Hanbury-Brown and Twiss interferometer similar to the one used to demonstrate single photon emission for the InAs self-assembled dots on silicon (see paragraph 2.5.1). The time resolution of the avalanche photodiodes used in the setup is 500 ps, which is half the lifetime of the dots in the sample. The measurements has been conducted by exciting the sample with a continuous-wave HeNe 633 nm laser, at 3 μW per cm^2 power. The signal is sent to two avalanche photodiodes using a beam splitter optical fiber. The emission of the quantum dot of interest is isolated from the other emissions by the same narrow band-pass filter used in the previous section.

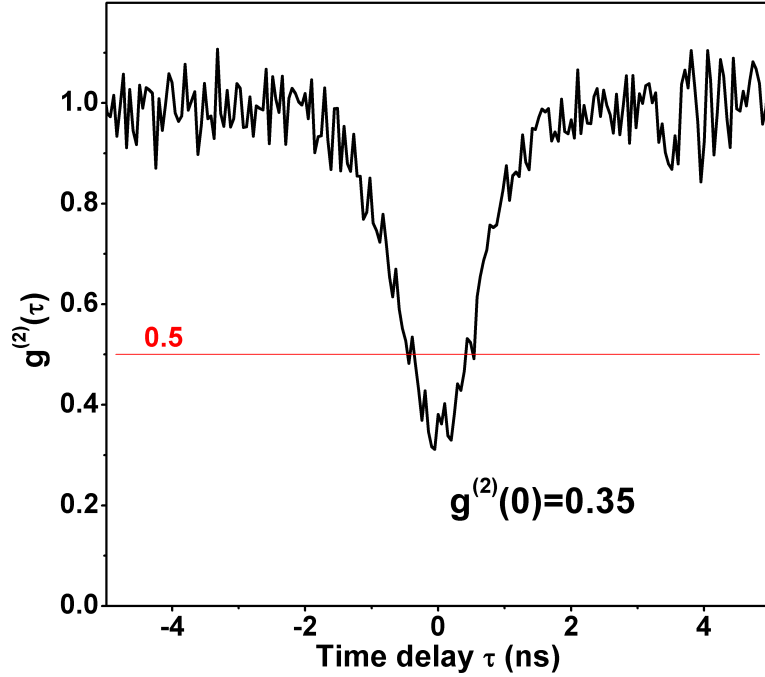


Figure 3.13: Autocorrelation function of a GaAs/AlGaAs single quantum dot. At a time delay of 0 s, a clear anti-bunching of 65% is observed.

Results of these experiments are demonstrated in figure 3.13. As can be seen very clearly, autocorrelation function at a time delay of 0 s shows a 65% dip, thus demonstrating strong anti-bunching. The anti-bunching has a decay time of $t_1 = 0.55$ ns. It is determined by fitting the $g^{(2)}(\tau)$ curve with the following decreasing exponential function:

$$g^{(2)}(\tau) = 1 - \exp(-|\tau|/t_1) \quad (3.1)$$

The fact that the anti-bunching dip doesn't reach 0 at zero time delay is partly due to background noise and the limitations due to the time response of the APDs. The main cause is the intermittent charging occurring in the dot [30]. This charging can be reduced by decreasing the intensity of the excitation laser, but it would also reduce by too much the intensity of the dot photoluminescence. Another way of avoiding trapping of charge carriers would be to use a pulsed laser and to excite the sample closer to resonant excitation [31].

3.6 Conclusion

In conclusion, we have investigated unexpected emission lines on a InAs/GaAs quantum dot sample monolithically grown on silicon. The lines have been identified as originating from interface fluctuations in a GaAs/AlGaAs short period superlattice, by a method of variable etching at different depths from the surface. Further optical characterization confirmed the quantum dot nature of the emissions, and its single photon emitting capabilities.

This work, though not combined with photonic crystals as the previous one was, is interesting in the way that it presents a different way of growing zero-dimensional structures that has not been attempted before, and which yet yielded successful results. Particularly, the energy range of the dots situated in the far visible (1.7 - 1.8 eV) makes them attractive for applications in fields such as free-space communication [7] and provides single photon emitters in the range of high sensitivity of Si detectors.

References

- [1] D. Leonard, M. Krishnamurthy, C. M. Reaves, S. P. Denbaars, and P. M. Petroff, “Direct formation of quantum-sized dots from uniform coherent islands of InGaAs on GaAs surfaces,” *Applied Physics Letters*, vol. 63, no. 23, pp. 3203–3205, 1993.
- [2] P. M. Petroff and S. P. DenBaars, “MBE and MOCVD growth and properties of self-assembling quantum dot arrays in III-V semiconductor structures,” *Superlattices and Microstructures*, vol. 15, pp. 15+, Jan. 1994.
- [3] C. Weisbuch, R. Dingle, A. C. Gossard, and W. Wiegmann, “Optical characterization of interface disorder in multi-quantum well structures,” *Solid State Communications*, vol. 38, pp. 709–712, May 1981.
- [4] D. Bimberg, “Cathodoluminescence atomic scale images of monolayer islands at GaAs/GaAlAs interfaces,” *Journal of Vacuum Science & Technology B: Microelectronics and Nanometer Structures*, vol. 5, pp. 1191+, July 1987.
- [5] A. Zrenner, L. V. Butov, M. Hagn, G. Abstreiter, G. Böhm, and G. Weimann, “Quantum dots formed by interface fluctuations in AlAs/GaAs coupled quantum well structures,” *Physical Review Letters*, vol. 72, pp. 3382–3385, May 1994.
- [6] K. Brunner, G. Abstreiter, G. Böhm, G. Tränkle, and G. Weimann, “Sharp-line photoluminescence and two-photon absorption of zero-dimensional biexcitons in a gaas/algaas structure,” *Phys. Rev. Lett.*, vol. 73, pp. 1138–1141, Aug 1994.
- [7] K. D. Langer and J. Grubor, “Recent Developments in Optical Wireless Communications using Infrared and Visible Light,” in *9th International Conference on Transparent Optical Networks, 2007. ICTON '07.*, vol. 3, pp. 146–151, IEEE, July 2007.
- [8] Z. Mi and Y.-L. Chang, “III-V compound semiconductor nanostructures on

silicon: Epitaxial growth, properties, and applications in light emitting diodes and lasers,” *J. Nanophoton.*, vol. 3, p. 031602, 2009.

- [9] G. C. Osbourn, “Strained-Layer Superlattices: A Brief Review,” *IEEE J. Quantum Electron.*, vol. 9, p. 1677, 1986.
- [10] J. W. Matthews and A. E. Blakeslee, “Defects in epitaxial multilayers, I: Misfit dislocations,” *J. Cryst. Growth*, vol. 27, pp. 118–125, 1974.
- [11] R. Fischer, W. T. Masselink, J. Klem, T. Henderson, T. C. McGlenn, M. V. Klein, H. Morkoç, J. H. Mazur, and J. Washburn, “Growth and properties of GaAs/AlGaAs on nonpolar substrates using molecular beam epitaxy,” *Journal of Applied Physics*, vol. 58, no. 1, pp. 374–381, 1985.
- [12] J. Yang, P. Bhattacharya, and Z. Mi, “High-Performance In_{0.5}Ga_{0.5}As/GaAs Quantum-Dot Lasers on Silicon With Multiple-Layer Quantum-Dot Dislocation Filters,” *Electron Devices, IEEE Transactions on*, vol. 54, pp. 2849–2855, Nov. 2007.
- [13] Z. Mi, J. Yang, P. Bhattacharya, and D. L. Huffaker, “Self-organised quantum dots as dislocation filters: the case of GaAs-based lasers on silicon,” *Electronics Letters*, vol. 42, pp. 121–123, Jan. 2006.
- [14] D. Gammon, E. S. Snow, B. V. Shanabrook, D. S. Katzer, and D. Park, “Fine Structure Splitting in the Optical Spectra of Single GaAs Quantum Dots,” *Physical Review Letters*, vol. 76, pp. 3005–3008, Apr. 1996.
- [15] Dave3457, “Circular Polarization.” <http://en.wikipedia.org/wiki/File:Circular.Polarization.Circularly.Polarized.Light.Circular.Polarizer.Creating.Left.Handed.Helix.View.svg>, Apr 2010.
- [16] C. Cohen-Tannoudji, B. Diu, and F. Laloë, *Mécanique quantique*. Enseignement des sciences, Hermann, 1973.
- [17] M. Bayer, G. Ortner, O. Stern, A. Kuther, A. A. Gorbunov, A. Forchel, P. Hawrylak, S. Fafard, K. Hinzer, T. L. Reinecke, S. N. Walck, J. P. Reithmaier, F. Klopff, and F. Schäfer, “Fine structure of neutral and charged excitons in self-assembled In(Ga)As/(Al)GaAs quantum dots,” *Physical Review B*, vol. 65, pp. 195315+, May 2002.
- [18] A. V. Khaetskii, D. Loss, and L. Glazman, “Electron Spin Decoherence in Quantum Dots due to Interaction with Nuclei,” *Physical Review Letters*, vol. 88, pp. 186802+, Apr. 2002.

- [19] B. Eble, C. Testelin, P. Desfonds, F. Bernardot, A. Balocchi, T. Amand, A. Mirard, A. Lemaître, X. Marie, and M. Chamarro, “Hole-Nuclear Spin Interaction in Quantum Dots,” *Physical Review Letters*, vol. 102, pp. 146601+, Apr. 2009.
- [20] J. J. Finley, D. J. Mowbray, M. S. Skolnick, A. D. Ashmore, C. Baker, A. F. G. Monte, and M. Hopkinson, “Fine structure of charged and neutral excitons in InAs-Al_{0.6}Ga_{0.4}As quantum dots,” *Physical Review B*, vol. 66, pp. 153316+, Oct. 2002.
- [21] R. J. Young, R. M. Stevenson, A. J. Shields, P. Atkinson, K. Cooper, D. A. Ritchie, K. M. Groom, A. I. Tartakovskii, and M. S. Skolnick, “Inversion of exciton level splitting in quantum dots,” *Physical Review B*, vol. 72, pp. 113305+, Sept. 2005.
- [22] A. V. Gaisler, A. S. Yaroshevich, I. A. Derebezov, A. K. Kalagin, A. K. Bakarov, A. I. Toropov, D. V. Shcheglov, V. A. Gaisler, A. V. Latyshev, and A. L. Aseev, “Fine structure of the exciton states in InAs quantum dots,” *JETP Letters*, vol. 97, no. 5, pp. 274–278, 2013.
- [23] S. Khatsevich, D. H. Rich, E. T. Kim, and A. Madhukar, “Cathodoluminescence imaging and spectroscopy of excited states in InAs self-assembled quantum dots,” *Journal of Applied Physics*, vol. 97, no. 12, pp. 123520+, 2005.
- [24] J. Motohisa, J. J. Baumberg, A. P. Heberle, and J. Allam, “Anomalous excitation intensity dependence of photoluminescence from InAs self-assembled quantum dots,” *Solid-State Electronics*, vol. 42, pp. 1335–1339, July 1998.
- [25] I. J. Luxmoore, R. Toro, O. Del Pozo-Zamudio, N. A. Wasley, E. A. Chekhovich, A. M. Sanchez, R. Beanland, A. M. Fox, M. S. Skolnick, H. Y. Liu, and A. I. Tartakovskii, “III-V quantum light source and cavity-QED on Silicon,” *Sci. Rep.*, vol. 3, p. 1239, 2013.
- [26] T. Hey, “Quantum computation: an introduction.” https://www.researchgate.net/publication/3363605_Quantum_computing_an_introduction?ev=srch_pub, Sept. 1999.
- [27] J. L. O’Brien, A. Furusawa, and J. Vuckovic, “Photonic quantum technologies,” *Nat Photon*, vol. 3, pp. 687–695, Dec. 2009.
- [28] C. H. Bennett and S. J. Wiesner, “Communication via one- and two-particle operators on Einstein-Podolsky-Rosen states,” *Physical Review Letters*, vol. 69, pp. 2881–2884, Nov. 1992.

- [29] X.-S. Ma, T. Herbst, T. Scheidl, D. Wang, S. Kropatschek, W. Naylor, B. Wittmann, A. Mech, J. Kofler, E. Anisimova, V. Makarov, T. Jennewein, R. Ursin, and A. Zeilinger, “Quantum teleportation over 143 kilometres using active feed-forward,” *Nature*, vol. 489, pp. 269–273, Sept. 2012.
- [30] C. Santori, D. Fattal, J. Vučković, G. S. Solomon, E. Waks, and Y. Yamamoto, “Submicrosecond correlations in photoluminescence from InAs quantum dots,” *Phys. Rev. B*, vol. 69, p. 205324, May 2004.
- [31] A. J. Shields, “Semiconductor quantum light sources,” *Nat Photon*, vol. 1, pp. 215–223, 2007.

Chapter 4

Effects of arsenic concentration in InPAs/GaInP self-assembled quantum dots

4.1 Introduction

When quantum dots started getting a lot of attention, the main materials used for their fabrication were GaAs/AlGaAs and InGaAs/GaAs. It was also known that InP/GaInP could constitute a possible combination for self-assembled quantum dots, but due to the difficulty of using phosphorus with molecular beam epitaxy, such systems were fabricated using another epitaxy technique called metal-organic chemical vapour deposition (MOCVD) (see section 1.3.1). InP quantum dots have been studied since 1994 [1, 2], and soon displayed properties that made them advantageous comparably to InGaAs dots. The main one being that their emission wavelength range is situated around 650 to 740 nm where lies the maximum efficiency of silicon photon detectors, as opposed to InGaAs dots that emit in the near infrared region (950 nm). The growth of InP dots with MOCVD presents the issue of having a multi-modal distribution of quantum dot sizes that leads to multiple-charge trapping into big quantum dots [3, 4] but this has been addressed by controlling the growth rate and temperature [5].

Recently there has been a growing interest towards incorporating arsenic to this structure to produce InPAs quantum dots embedded in InP nanowires for photonic applications [6–8] or self-assembled for the short-wavelength infrared lasers [9]. InPAs/GaInP self-assembled dots have a strong potential for tuning the emission wavelength by varying the As concentration, from the visible light emission

of InP to the near-infrared emission of InAs. Another interesting property is the high energy confinement they provide, enabling a more effective trapping of charges without necessarily maintaining the sample at a cryogenic temperature (≤ 20 K). This feature makes this material ideal for the study and manipulation of charges, particularly when combined with Schottky diode structures that allow control over the resident charges of the quantum dots [10].

This chapter presents experimental study of such a structure, InPAs/InGaP self-assembled quantum dots embedded in Schottky diodes. The samples have been grown by A. Krysa from the Electronic and Electrical Engineering dpt. The first section offers a description of the samples and experimental setups used for the project, then a second one describes how the concentration of arsenic in the samples modifies the optical and electronic properties of the dots. The third section is about charge control in the dots using Schottky diodes.

4.2 Sample description

Several samples have been grown by A. Krysa using metal-organic chemical vapour deposition, having various arsenic concentrations, and grown at different substrate temperature and deposition rates. These samples have been grown by using the well-known recipe of InP/InGaP MOCVD growth and adding arsine (AsH_3) reactant during the growth of the active quantum dot layer [10]. The samples can basically be divided into two categories. The first category comprises a comparative InP/InGaP sample and 5 samples using the same recipe with additional concentration of As. Those samples can then be compared based only on their arsenic concentration. The second category are two samples with different As concentration but more importantly having a n-doped layer, necessary for the fabrication of Schottky diodes (further described in 4.4.1). The structure of samples from the first category is shown figure 4.1.

The active layers have been grown on top of a GaAs substrate with a cutting inclination of either 3° or 10° . This means semiconductor ingot from which the substrate originates has been cut so the growth direction of the substrate wafer is not normal to the lattice but forms with it an angle of 87° or 80° . Making the substrate with a cutting angle of more than 0° enables to have a terraced surface instead of a flat one, more favourable to the formation of atomic islands. A first layer of 500 nm $\text{Ga}_{0.5}\text{In}_{0.5}\text{P}$ is grown, followed by the dot layer capped by 300

Layer 3	GaInP 50%	300 nm	undoped
Layer 2	InPAs dots	1s InP, 3s InPAs, 1s InP	
Layer 1	GaInP 50%	500 nm	undoped
Substrate	Semi-insulating GaAs, 3°		undoped

Figure 4.1: Schematic of the structure of a regular InPAs quantum dot sample.

nm of bulk $\text{Ga}_{0.5}\text{In}_{0.5}\text{P}$. The quantum dot layer is grown by evaporating reactants (trimethylindium $\text{In}(\text{CH}_3)_3$ and phosphine PH_3) for 5 seconds, a technique already successful for the growth of conventional InP quantum dot samples [10], except AsH_3 is introduced for 3 seconds in the process. The different InPAs samples have been realized with respectively 1.5, 3, 6, 16.7 and 50 standard cubic centimetres of AsH_3 per second (scm). Since the exact dynamic of InPAs growth as not been studied of yet, it is difficult to accurately link the AsH_3 scm with the concentration of As inside the dots.

Layer 7	GaInP	10 nm	undoped
Layer 6	AllnP	100 nm	undoped
Layer 5	GaInP 50%	200 nm	undoped
Layer 4	InPAs dots	1s InP, 3s InPAs, 1s InP	
Layer 3	GaInP 50%	80 nm	undoped
Layer 2	GaInP 50%	200 nm	$N=10^{18}\text{cm}^{-3}$
Layer 1	GaInP 50%	800 nm	undoped
Substrate	Semi-insulating GaAs, 3°		undoped

Figure 4.2: Schematic of the structure of an InPAs quantum dot sample presenting a doped region.

The two doped samples have a different structure, represented figure 4.2. Under the active quantum dots layer is 200 nm of $\text{Ga}_{0.5}\text{In}_{0.5}\text{P}$ doped with 10^{18} atoms of silicon per cm^3 to provide a sea of negative charge carriers. The doped layer is

separated from the dots by a layer of 80 nm undoped InGaP, and a barrier layer of AlInP is grown 200 nm above the quantum dots layer. The larger bandgap provided by the aluminium helps maintaining the holes in the layers surrounding the dots. The AsH₃ deposition rates for those doped samples were 6 sccm and 13.2 sccm. The doped samples are designed to be used with an electric field in order to manipulate the charge carriers inside the dots. For that purpose a Schottky diode structure has to be fabricated out of the sample. Their fabrication is described in section 4.4.1.

4.3 Spectral distribution of quantum dot emissions

Micro-photoluminescence has been performed at cryogenic temperature on the five InPAs samples as well as the test sample InP.

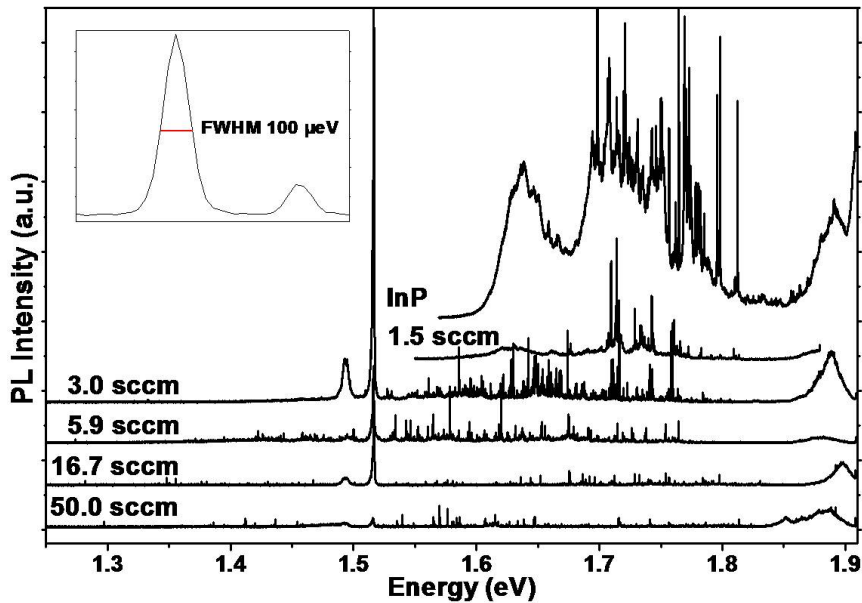


Figure 4.3: Micro-photoluminescence of the 5 InPAs samples along with the test InP sample. Labels on the graphs indicate the sccm level for each sample (except the InP sample labelled “InP”). Inset gives an average FWHM of the quantum dot lines.

The experimental setup used to perform these measurements is the one described in chapter 1 figure 1.8. The results of the experiment are represented on figure 4.3, where we can see the six curves corresponding to the aforementioned six samples, each labelled with the number of sccm of AsH₃ used during growth (except for the

InP sample, labelled InP). All spectra exhibit single quantum dot emission lines, with an typical linewidth of $100 \mu\text{eV}$. Two features are striking when reviewing this data. First the emission range changes with the increase in As concentration by spreading on the low energy side (see fig. 4.4).

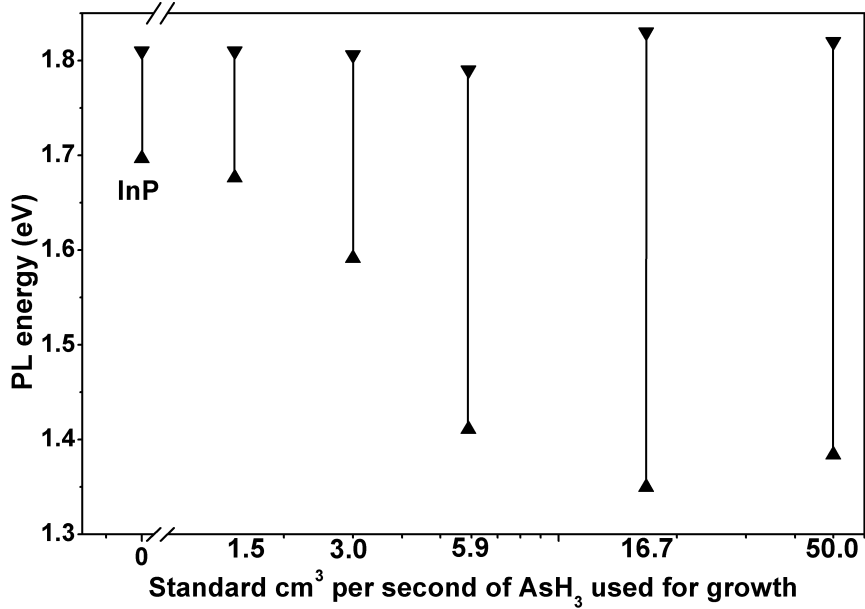


Figure 4.4: Energy range of the quantum dot emissions as a function as AsH_3 sccm for all 5 InPAs samples. The energy range of InP is represented on the left of the figure.

Usual InP quantum dot emission is situated between 1.7 eV and 1.8 eV. With 3 sccm of As the dot PL are between 1.5 eV and 1.8 eV, while at higher As concentrations PL can be seen down to 1.4 eV. It is convenient to remind at this point that the usual emission of InGaAs/GaAs quantum dots ranges between 1.05 eV and 1.4 eV [11], so it makes good sense that the introduction of As into InP dots would shift the emission energies more toward the InAs QD emission region. On the other hand, the fact that the highest emission remains in the same region for all InPAs samples and for InP denotes that there are dots in the InPAs samples that are unaffected by As. The energy of the emission could depend on either the size of the dot (it decreases as the dot is bigger) or the concentration of As (as with more As the dots are assumed to have properties more similar to InAs dots). We can have a rough estimation of the dot size by using magneto-optical characterization. This experiment is described in section 4.5. The InPAs samples display a wide range of evenly spread emission energies, which could signify either an inhomogeneous

distribution of As among dots, or a large range of dot sizes but it will be shown in section 4.5 that the latter is more probable.

The second notable observation is that the emission intensity decreases dramatically as the concentration of As increases. This phenomenon has been explained by the formation of type-II (core-shell) quantum dots with increasing As concentration [12]. Type-II quantum dots are comprised of a core wrapped in a shell of a different material (InAs-rich core in InP-rich shell in this case [12]), and electrons (holes) are confined in the InP (InAs) region, reducing the rate of radiative recombination. The ideal concentrations of As to observe bright lines in the region from 1.6 eV to 1.8 eV are 3 sccm and 5.9 sccm.

Having emission lines in a range stretching from 1.4 eV to 1.8 eV is particularly interesting as no previous self-assembled QDs provide such a wide range of emission energies. Wideband light sources are desirable for a range of applications and particularly optical coherence tomography (OCT) [13, 14]. OCT is a non-invasive imaging technique for biological and medical tissues used in ophthalmology. The principle is to detect the interferences of infrared light scattered into the medium (retina) with a micrometre resolution. Wide band light source would prove effective as depth resolution of the technique is inversely proportional to the FWHM of the source [15, 16].

4.4 Study of excitonic complexes through charge-controlled PL

As previously seen in chapter 1, charged excitons are of prime interest due to the prospect of using a single charge carrier as a spin q-bit [17, 18]. It is also desirable to be able to control charges in single quantum dots to enable study of quantum confined Stark effect [19, 20] as well as many-body interactions [21]. To achieve charge control in InPAs quantum dots, a Schottky diode structure will be used. The aim of this project is to determine whether the InPAs samples are suitable for charge control, if Schottky diodes can be fabricated using this material and show good I/V characteristics, and if different excitonic complexes can be observed and isolated on demand.

4.4.1 Schottky diode fabrication

The fabrication of a diode structure is enabled by the doped layer below the InPAs QDs layer (see fig. 4.2).

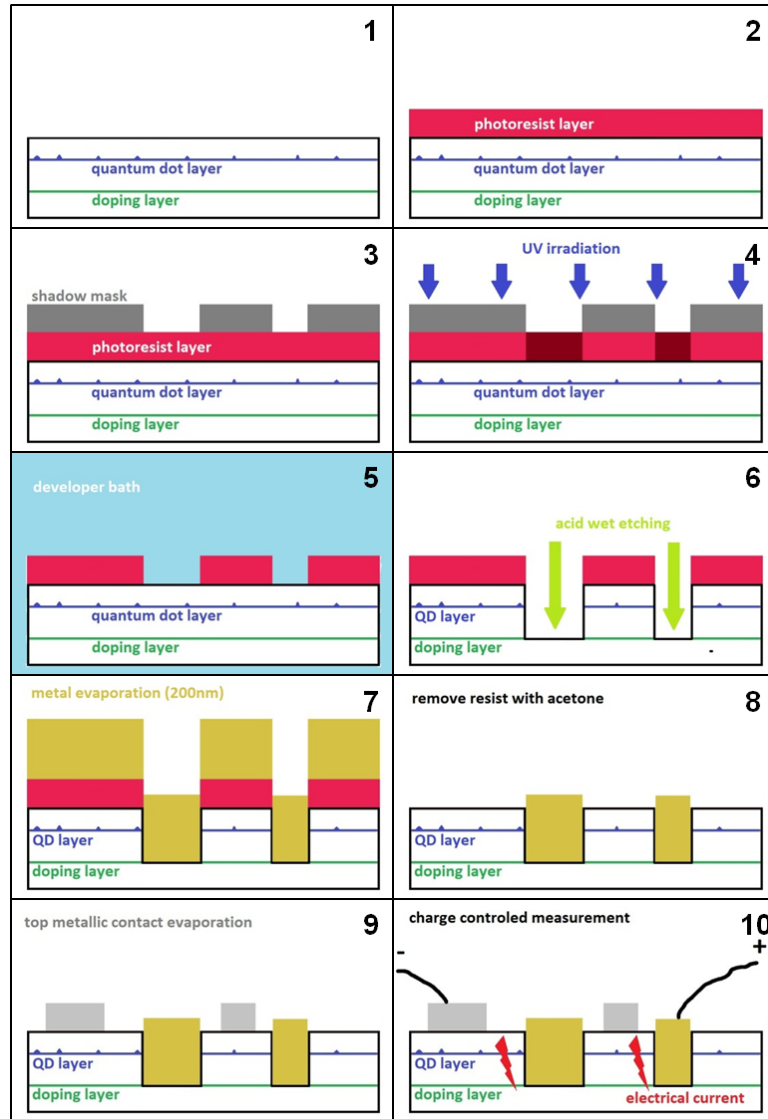


Figure 4.5: The ten steps of the fabrication of Schottky diodes.

The fabrication is a work of precision and must be carried out in a clean-room environment. The device fabrication laboratory of the EPSRC National Centre for III-V Technology in Sheffield is the ideal place to do it. The aim here is to make an electrical connection between the doping layer and the dots. For that metallic contacts need to be implemented on each of the two layers. The whole process is described on figure 4.5. First the sample must be etched down to the doping layer.

To do that the etching zone is patterned on the sample using a layer of photoresist covered with a shadow mask and irradiated using ultra-violet light (steps 1 to 5). The sample is now entirely covered in photoresist except in the places where the etching will be done. These places form the back contact, depicted on figure 4.6 (A).

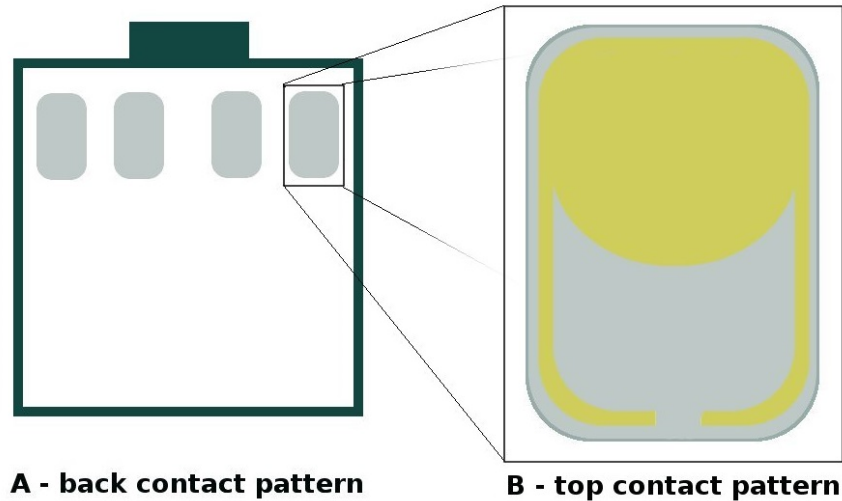


Figure 4.6: Drawing of the Schottky diode patterns. (A) Back contact pattern, connected to the doping layer. (B) Top contact pattern, connected to the surface of the sample.

The sample is etched using a solution of diluted sulfuric acid and hydrogen peroxyde until the doping layer is exposed (step 6). After that a metallic contact consisting of gold, nickel and titanium is deposited on the surface of the sample using a monolayer metal evaporator. The photoresist is removed using acetone, leaving only the back contact parts covered with metal (steps 7, 8). The top contact is evaporated from titanium and gold following the pattern on figure 4.6 (B) (step 9). The sample is now ready to be connected to a voltage controller using the connectors plugged into the helium continuous flow cryostat (step 10).

4.4.2 Principle of charge control by electric field

The Schottky diode allows to exploit the benefits of the doping layer by applying a gradient of electric potential between the surface of the sample and the sea of electrons provided by the doping silicon. The effect of the electric field on the energy diagram of the sample are illustrated in figure 4.7: in zero electric field condition (a) the dot is hosting a certain number of positive and negative charges. When a negative bias is applied (b) the electrons and holes tunnel out of the dot as the

potential barriers on either side become thinner.

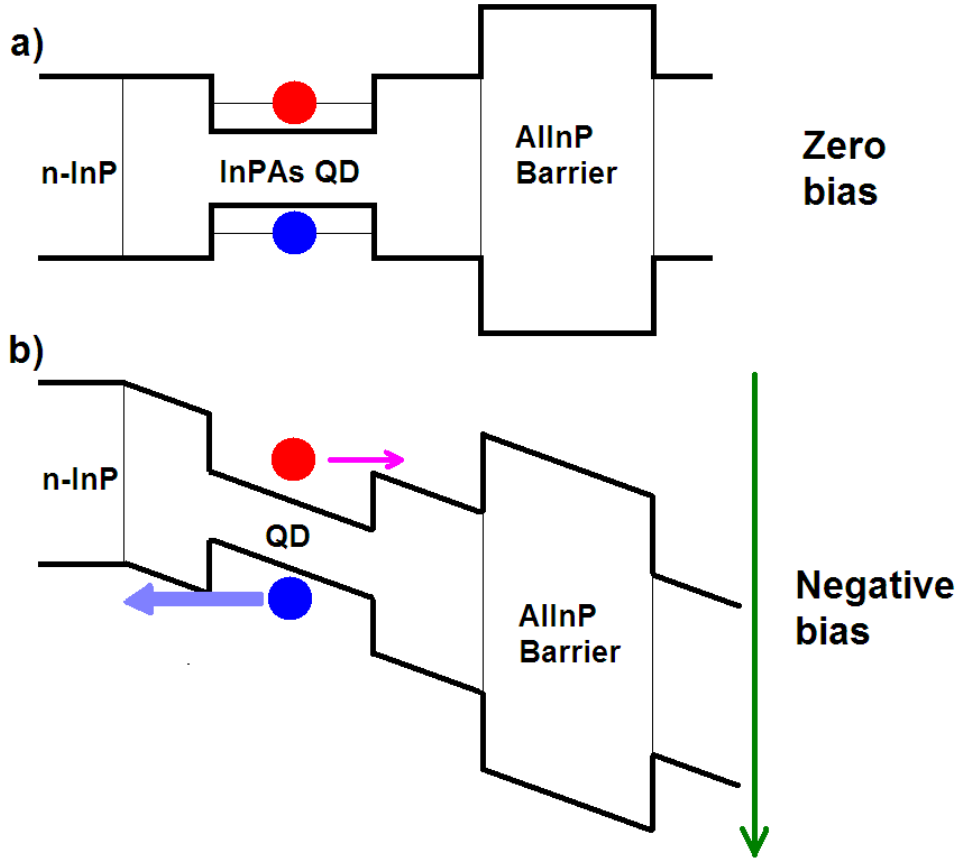


Figure 4.7: Energy diagram of the sample submitted to an electric field. (a) without bias and (b) with an applied reverse bias.

The AllnP barrier layer provides a higher potential to limit the escape of negative charge carriers, theoretically favouring the observation of singly (X^{-1}), doubly (X^{-2}) and even triply (X^{-3}) negatively charged excitons [10, 21]. In forward bias, the high electrical current flowing into the diode results in a high number of charges, which in turn decreases signal-to-noise ratio. For that reason, only reverse bias is used for the observation of single dots.

4.4.3 Results

First the diodes have been tested at room temperature to assert that the current/voltage (I/V) characteristic was suited for the charge control experiment. The ideal behaviour of the diode is to have a current flow of 0 in reverse bias, an infinite one in forward bias. In practice, the I/V slope in the reverse bias region is not

zero due to leakage current. A good diode should have a leakage of less than $10 \mu\text{A}\cdot\text{cm}^{-2}$ over the voltage region used for the experiment, in our case from 0 V to -1.7 V [17, 22].

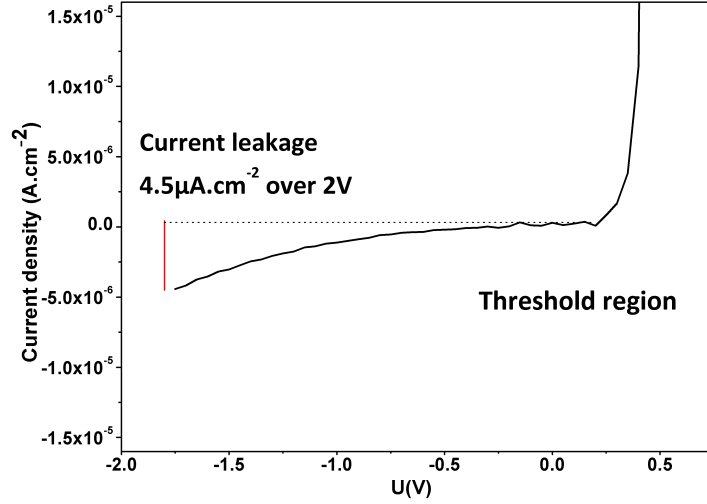


Figure 4.8: J/V characteristic of the Schottky diode fabricated on the sample. A reasonably low leakage current density of $4.5 \times 10^{-6} \text{ A}\cdot\text{cm}^{-2}$ over the first 2 V of reverse bias is demonstrated.

The I/V curve depicted on figure 4.8 demonstrates the acceptability of the fabricated diode with a current leakage of only 500 pA over the region we will use for the experiment.

Experiments have been conducted on the sample grown with 13.2 sccm of AsH_3 . Several dots have been measured, micro-photoluminescence of one of them is plotted against energy and applied bias on figure 4.9.

First a strong negative bias of -1.7 V is applied, causing the tunneling of all charge carriers out of the dot. Then the bias is gradually reduced. At -0.35 V a line can be seen with an energy of 1.418 eV, and with further reduction of the bias a second line appears on the low-energy side of the first. Considering the very low density of QD lines, it is safe to assume that the two clear lines appearing are emitted by the same quantum dot. The first line is believed to be a neutral exciton X_0 and the second line its associated negatively charged exciton X^{-1} . The fact that X^{-1} is on the low-energy side of X_0 is in accordance with what has been previously observed for InP/GaInP quantum dots [10]. The PL lines are represented for three different biases in figure 4.10.

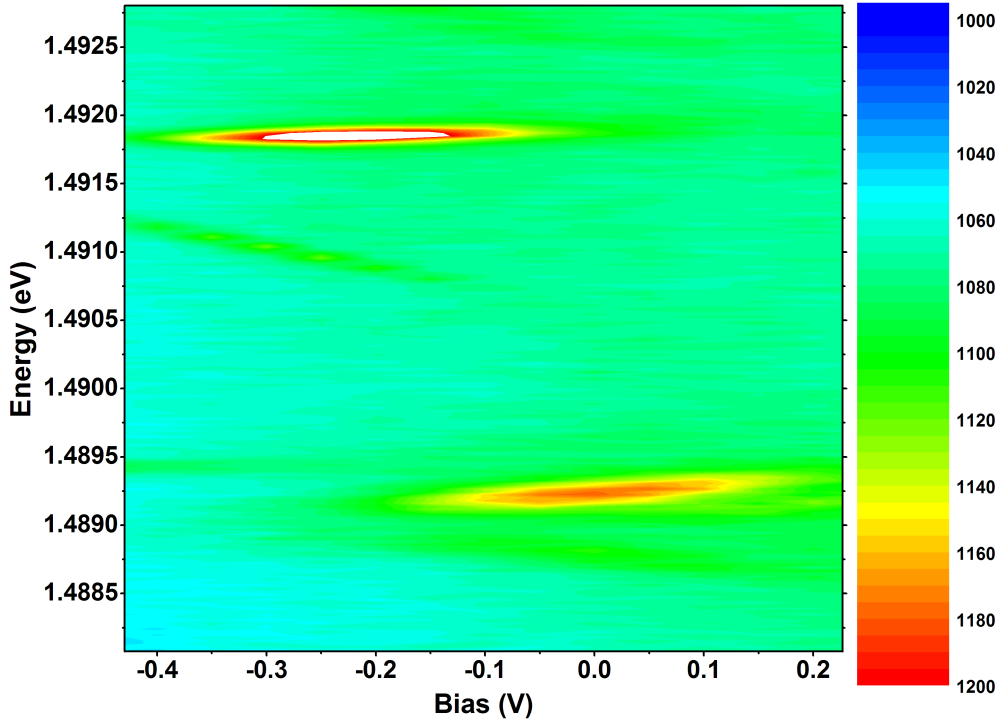


Figure 4.9: Micro-photoluminescence of a quantum dot on the Schottky diode sample as a function of applied voltage bias.

The X_0 and X^{-1} lines exhibit linewidths of $109 \mu\text{eV}$ and $142 \mu\text{eV}$ respectively, and are separated by 2.8 meV . The same line switching behaviour is observed for two additional dots emitting at 1.735 eV and 1.663 eV . The trion binding energy for those two dots is respectively 7.9 and 9.7 meV . This is in the same order of magnitude as the binding energies observed in InP [10] and also in previous charge-tunable work done with InGaAs dots [23].

What we can gather from this result is that the fabrication of Schottky diodes with InPAs/GaInP quantum dots is possible, and charge control works. This result is important as this material combines the reduced QD bandgap enabled by the introduction of As with the large bandgap of the GaInP surrounding bulk. The enhanced confinement provided by InPAs/GaInP compared to previously studied InAs/GaAs and InP/GaInP Schottky structures allows for a better trapping of charges, making it a more effective material for the study of spin processes in quantum dots.

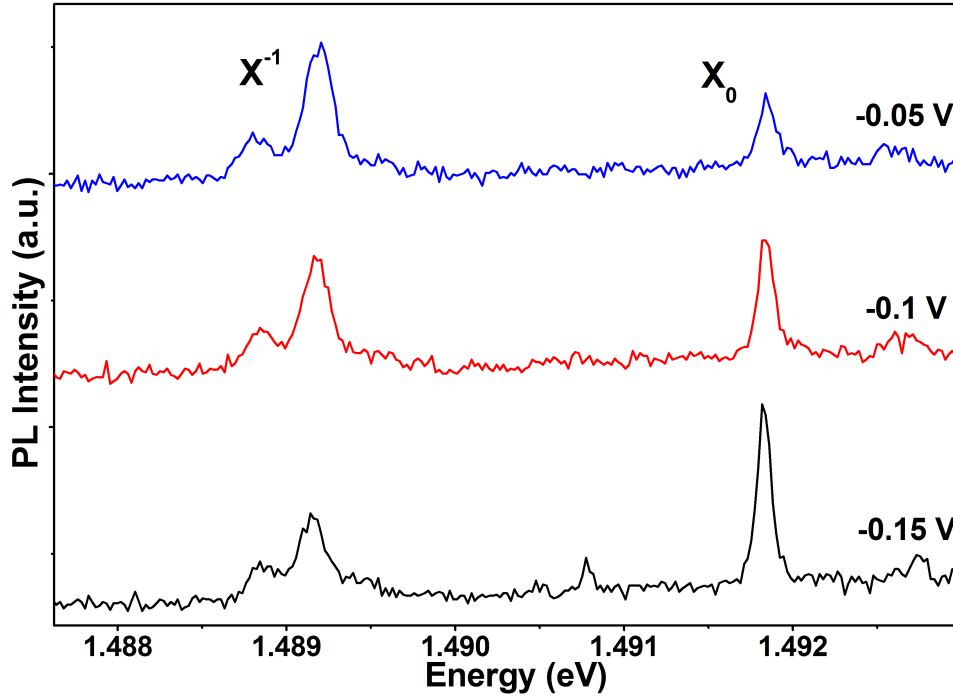


Figure 4.10: PL spectrum of the X_0 and X^{-1} lines for biases of -0.15, -0.1 and -0.05 V.

4.5 Study of the effect of As concentration on magneto-optical properties

This section describes how the concentration of arsenic of the samples changes the photoluminescence features, as well as diamagnetic shift and exciton g-factor under magnetic field. The magnetic field lifts degeneracy of the Zeeman energies, allowing us to calculate the diamagnetic shift of the dots. The diamagnetic shift can then be used to calculate shape and size properties of the dots. This will provide information about how the concentration of As in the dots changes their size.

4.5.1 Experimental setup

To study the sample under magnetic field we have used the setup described on figure 4.11.

To study the optical behaviour of the dots in a high magnetic field environment, a superconducting magnet displaying magnetic field of as high as 10 T has been used. The magnet is a cylinder 2 m tall and 60 cm wide containing superconducting coils in a chamber filled with liquid helium. Inside the chamber the sample is mounted

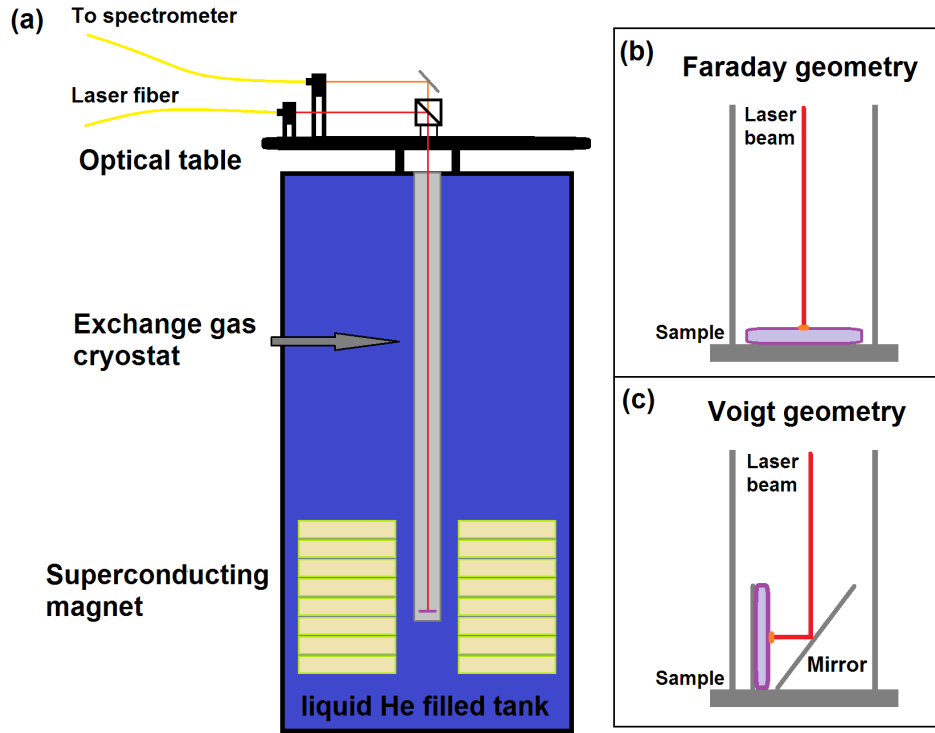


Figure 4.11: (a) Schematic of the superconducting magnet and sample holder system. The sample can be mounted in Faraday (b) or Voigt (c) geometry.

in an exchange gas cryostat. This tube is put under vacuum then inserted with a few mm^3 of gaseous helium. The liquid helium acts as a cooling system for both the superconducting coil and the sample. The low temperature is effectively conveyed to the sample by the gaseous helium in the tube. For this experiment, excitation light from the laser is brought to an optical table on top of the magnet via optical fibre. The beam is directed along the central tube via a beam splitter and down to the sample. The signal emitted from the sample is then collected through another optical fibre linked to a single spectrometer and CCD. The sample can be placed either in Faraday (fig. 4.11 (b)) or Voigt geometry (fig. 4.11 (c)).

4.5.2 Results

Applying a magnetic field to the sample allows for the extraction of useful information about exciton g-factor and diamagnetic shift. These quantities in turn will give us insight about the shape and size of the dots, so that the effects of the concentration of As over the properties of the dots are better understood. The g-factor, also called dimensionless magnetic moment is a quantity that links the total magnetic moment μ_S of a particle with its spin S and the Bohr magneton μ_B (equ. 4.1). It is

directly proportional to the Zeeman splitting that emission lines experience when a quantum dot is placed in a magnetic field.

$$\mu_S = \frac{g\mu_B}{\hbar} S \quad (4.1)$$

The diamagnetic shift represents the particle's response to an applied magnetic field. Since the magnetic field is known to shrink the excitonic wavefunction and to make it more confined, the emission line of the exciton shifts to higher energy [24, 25]. The spectra represented on figure 4.12 (a), of a neutral quantum dot line under different magnetic fields demonstrate modification of QD PL.

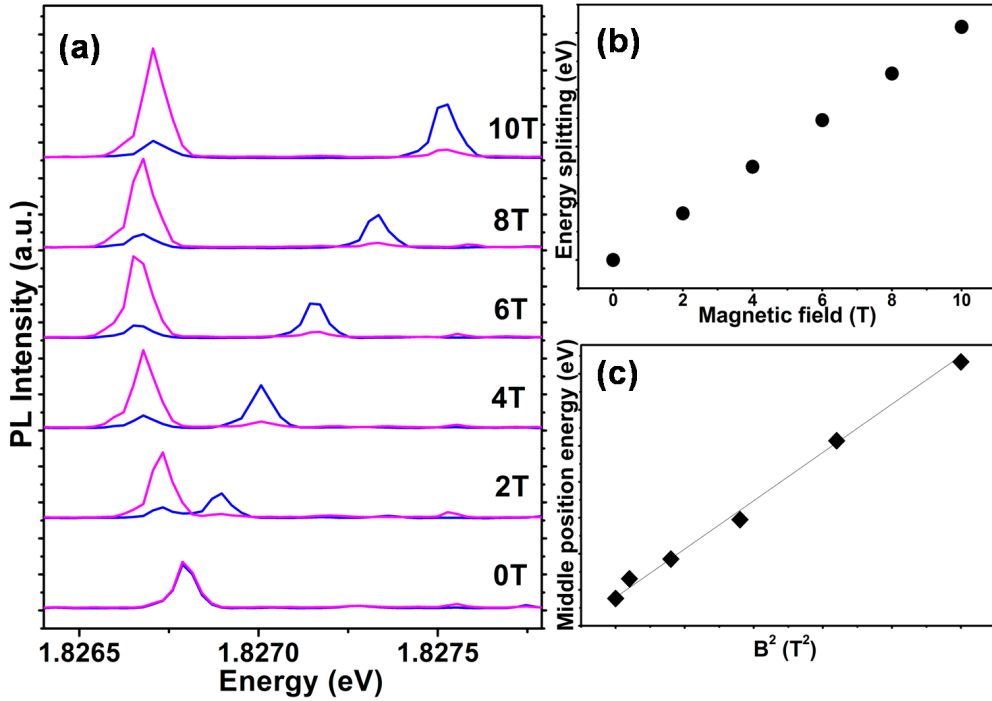


Figure 4.12: (a) Micro-photoluminescence of the InPAs sample containing 3 sccm of As. The luminescence is measured for various applied magnetic fields, applied in Faraday geometry. The detection of two linear orthogonal polarizations allows for clear observation of a splitting of the QD line. (b) Energy splitting plotted against magnetic field. (c) Middle position of the two energy lines plotted against the square of the magnetic field.

At zero field the QD exhibits a single PL line, which splits due to Zeeman effect under non-zero field. Six spectra are displayed, representing the same neutral dot emission at six different magnetic fields, from bottom to top 0, 2, 4, 6, 8 and 10 T. The amplitude of the splitting is represented figure 4.12 (b) as a function of

the magnetic field. It appears clearly that the splitting is linear with the magnetic field B , as it is expected. We can also see the diamagnetic shifts acting on the dot, blue-shifting the median position between the two emissions of the dot quadratically with B . This effect is observed on figure 4.12 (c) where the average between the two energy lines is plotted as a function of B^2 the square of the magnetic field. Equation 4.2 explains the behaviour of the energy of the two lines $E(B)$ with respect to magnetic field B using the diamagnetic shift κ , the energy of the dot at zero-field E_0 , the g-factor g and the Bohr magneton μ_B .

$$E(B) = E_0 + \kappa B^2 \pm \frac{1}{2}g\mu_B B \quad (4.2)$$

The diamagnetic shift measured on 19 dots on the sample with 3 sccm of AsH₃ do not show any trend of being dependent on the energy of the dot, though they seem to be situated mostly in the region between 3 $\mu\text{eV}/\text{T}^2$ and 4.5 $\mu\text{eV}/\text{T}^2$ (see figure 4.13).

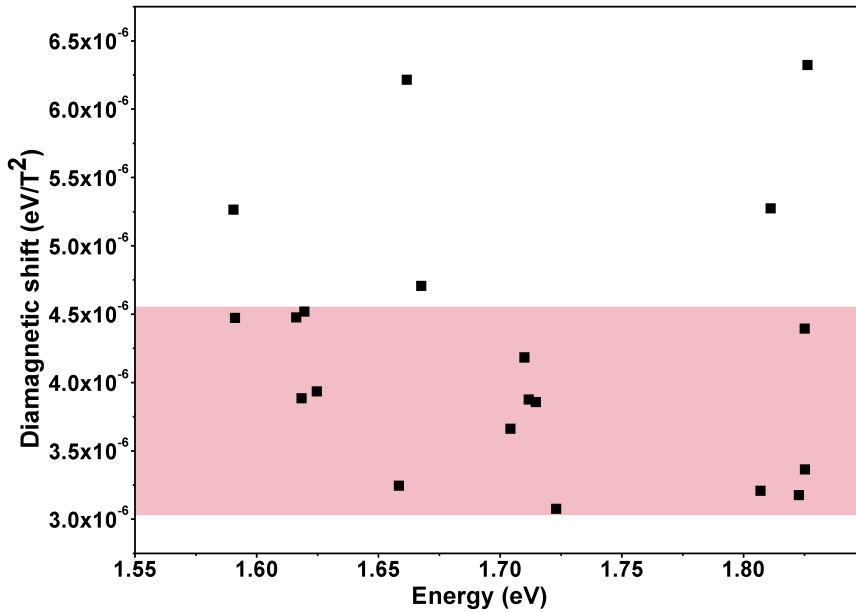


Figure 4.13: Diamagnetic shift of 19 dots from the sample with 3 sccm of AsH₃ plotted as a function of the energy emission of the dot. The magenta band represents the region containing the most data plots.

The size of the measured dots can be estimated through the following formula [25, 26]:

$$\kappa = \frac{e^2}{8\mu} r_X^2 \quad (4.3)$$

Where κ is the diamagnetic shift, μ the reduced exciton mass and r_X is the exciton Bohr radius, from which we can deduce an estimate of the dot size. If we take the reduced mass of the exciton to be $\mu \approx 1.0 \times 10^{-31}$ kg [27] we find a range of exciton radii going from 3.9 to 4.7 nm. From the fact that the estimated exciton radii (and thus quantum dot size) does not depend on emission energy, we can deduce that in the InPAs samples the wide range of emission energies is less due to an inhomogeneous size distribution of the dots than to a varying level of As concentration in the dots throughout the sample.

Further knowledge could be extracted from the magneto-optical measurements of the samples with other concentrations of As, as well as measurements in Voigt geometry. Those measurements would allow us to obtain the electron and hole g-factors and to see how they are modified with the change in As concentration. Knowing the behaviour of electron and hole g-factor and comparing it to g-factors for known structures like InP/GaInP and InAs/GaAs would provide useful insight about the way the charge carriers are confined into the InPAs quantum dots. More experiments have been carried out in a separate project, and reported by Del Pozo-Zamudio et al. ([12], in the process of submission). The insight about dot structure brought by this project is important because it could lead to a better growth control of the material, and the ability to grow dots with uniform size and As concentration for use in quantum communication [28] or wideband ensembles for OCT applications [13, 15].

4.6 Conclusion

In this chapter we have investigated a new type of quantum dot, grown using an optimized technique for InP but with arsenic deposited during the process. The various concentrations of As in the different samples allowed for characterization of the dependence of the dot characteristics with As. Among those characterizations, micro-photoluminescence demonstrated a dependence of the emission lines energies with As, with the minimum of emission being lower with higher concentration. The application of a magnetic field up to 10 T helped understand how the As concentration affects properties of the dots, through measurements of the exciton g-factor and diamagnetic shift. Particularly, the dots exhibit a wide range of emission energies not due to changes in size but more in As concentration. Finally, The fabrication of Schottky diodes and good charge control have been proven possible with this structure. The emission properties of these dots finally bring a way to

fill the gap in energy between the better studied InGaAs dots (1.05-1.4 eV region) and the InP dots (1.7-1.8 eV). Furthermore, the magnetic field and electric field experiments conducted on these samples were decisive in opening the way to the exploration of InPAs spin properties, in work that will be based on similar projects conducted on InP [10, 29, 30], some of which having already been concluded [12].

References

- [1] S. P. DenBaars, C. M. Reaves, V. Bressler-Hill, S. Varma, W. H. Weinberg, and P. M. Petroff, “Formation of coherently strained self-assembled InP quantum islands on InGaP/GaAs(001),” *Journal of Crystal Growth*, vol. 145, pp. 721–727, Dec. 1994.
- [2] N. Carlsson, W. Seifert, A. Petersson, P. Castrillo, M. E. Pistol, and L. Samuelson, “Study of the two-dimensional–three-dimensional growth mode transition in metalorganic vapor phase epitaxy of GaInP/InP quantum-sized structures,” *Applied Physics Letters*, vol. 65, no. 24, pp. 3093–3095, 1994.
- [3] D. Hessman, J. Persson, M. E. Pistol, C. Pryor, and L. Samuelson, “Electron accumulation in single InP quantum dots observed by photoluminescence,” *Physical Review B*, vol. 64, pp. 233308+, Nov. 2001.
- [4] P. G. Blome, M. Wenderoth, M. Hübner, R. G. Ulbrich, J. Porsche, and F. Scholz, “Temperature-dependent linewidth of single InP/Ga_xIn_{1-x}P quantum dots: Interaction with surrounding charge configurations,” *Physical Review B*, vol. 61, pp. 8382–8387, Mar. 2000.
- [5] C. J. Elliott, E. A. Chekhovich, M. S. Skolnick, A. I. Tartakovskii, and A. B. Krysa, “Optimization of low density InP/GaInP quantum dots for single-dot studies,” *Journal of Physics: Conference Series*, vol. 245, pp. 012093+, Sept. 2010.
- [6] M. H. M. van Weert, N. Akopian, U. Perinetti, M. P. van Kouwen, R. E. Algra, M. A. Verheijen, E. P. A. M. Bakkers, L. P. Kouwenhoven, and V. Zwiller, “Selective Excitation and Detection of Spin States in a Single Nanowire Quantum Dot,” *Nano Lett.*, vol. 9, pp. 1989–1993, Apr. 2009.
- [7] M. H. M. van Weert, M. den Heijer, M. P. van Kouwen, R. E. Algra, E. P. A. M. Bakkers, L. P. Kouwenhoven, and V. Zwiller, “Surround-gated vertical

- nanowire quantum dots,” *Applied Physics Letters*, vol. 96, no. 23, pp. 233112+, 2010.
- [8] M. E. Reimer, M. P. van Kouwen, M. Barkelid, M. Hocevar, Maarten, R. E. Algra, E. P. A. M. Bakkers, M. T. Bjork, H. Schmid, H. Riel, L. P. Kouwenhoven, and V. Zwiller, “Single photon emission and detection at the nanoscale utilizing semiconductor nanowires,” Sept. 2010.
- [9] A. Michon, R. Hostein, G. Patriarche, N. Gogneau, G. Beaudoin, A. Beveratos, I. R. Philip, S. Laurent, S. Sauvage, P. Boucaud, and I. Sagnes, “Metal organic vapor phase epitaxy of InAsP/InP(001) quantum dots for 1.55 μm applications: Growth, structural, and optical properties,” *Journal of Applied Physics*, vol. 104, no. 4, pp. 043504+, 2008.
- [10] O. D. D. Couto, J. Puebla, E. A. Chekhovich, I. J. Luxmoore, C. J. Elliott, N. Babazadeh, M. S. Skolnick, A. I. Tartakovskii, and A. B. Krysa, “Charge control in InP/(Ga,In)P single quantum dots embedded in Schottky diodes,” *Physical Review B*, vol. 84, pp. 125301+, Sept. 2011.
- [11] V. A. Shchukin and D. Bimberg, “Spontaneous ordering of nanostructures on crystal surfaces,” *Reviews of Modern Physics*, vol. 71, pp. 1125+, July 1999.
- [12] O. Del Pozo-Zamudio, J. Puebla, E. Chekhovich, R. Toro, A. Krysa, R. Beanland, A. M. Sanchez, M. S. Skolnick, and A. I. Tartakovskii, “Growth and magneto-optical characterization of InPAs/GaInP Quantum Dots,” *Unpublished*, 2013.
- [13] D. Huang, E. Swanson, C. Lin, J. Schuman, W. Stinson, W. Chang, M. Hee, T. Flotte, K. Gregory, C. Puliafito, and J. Fujimoto, “Optical coherence tomography,” *Science*, vol. 254, p. 1178, 1991.
- [14] A. Fercher, W. Drexler, C. Hitzenberger, and L. T., “Optical coherence tomography - principles and applications,” *Rep. Prog. Phys.*, vol. 66, p. 239, 2003.
- [15] S. Miyake, W. Lee, T. Ujihara, and T. Y., “The wideband light emission around 800 nm from ternary InAsP quantum dots with an intentionally broadened size and composition distribution,” *IPRM Conference Proceedings*, p. 208, 2006.
- [16] S. Fuchi, S. Miyake, S. Kawamura, W. Lee, T. Ujihara, and Y. Takeda, “Optical coherence tomography,” *Journal of Crystal Growth*, vol. 310, p. 2239, 2008.

- [17] A. J. Ramsay, S. J. Boyle, R. S. Kolodka, J. B. B. Oliveira, J. Skiba-Szymanska, H. Y. Liu, M. Hopkinson, A. M. Fox, and M. S. Skolnick, “Fast Optical Preparation, Control, and Readout of a Single Quantum Dot Spin,” *Physical Review Letters*, vol. 100, pp. 197401+, May 2008.
- [18] T. M. Godden, J. H. Quilter, A. J. Ramsay, Y. Wu, P. Brereton, S. J. Boyle, I. J. Luxmoore, J. Puebla-Nunez, A. M. Fox, and M. S. Skolnick, “Coherent Optical Control of the Spin of a Single Hole in an InAs/GaAs Quantum Dot,” *Physical Review Letters*, vol. 108, pp. 017402+, Jan. 2012.
- [19] P. W. Fry, I. E. Itskevich, D. J. Mowbray, M. S. Skolnick, J. J. Finley, J. A. Barker, E. P. O’Reilly, L. R. Wilson, I. A. Larkin, P. A. Maksym, M. Hopkinson, M. Al-Khafaji, J. P. R. David, A. G. Cullis, G. Hill, and J. C. Clark, “Inverted electron-hole alignment in InAs-GaAs self-assembled quantum dots,” *Physical Review Letters*, vol. 84, pp. 733+, Jan. 2000.
- [20] P. W. Fry, I. E. Itskevich, S. R. Parnell, J. J. Finley, L. R. Wilson, K. L. Schumacher, D. J. Mowbray, M. S. Skolnick, M. Al-Khafaji, A. G. Cullis, M. Hopkinson, J. C. Clark, and G. Hill, “Photocurrent spectroscopy of InAs/GaAs self-assembled quantum dots,” *Physical Review B*, vol. 62, pp. 16784+, Dec. 2000.
- [21] N. A. J. M. Kleemans, J. van Bree, A. O. Govorov, J. G. Keizer, G. J. Hamhuis, R. Notzel, Silov, and P. M. Koenraad, “Many-body exciton states in self-assembled quantum dots coupled to a Fermi sea,” *Nat Phys*, vol. 6, pp. 534–538, July 2010.
- [22] R. Oulton, J. J. Finley, A. D. Ashmore, I. S. Gregory, D. J. Mowbray, M. S. Skolnick, M. J. Steer, S.-L. Liew, M. A. Migliorato, and A. J. Cullis, “Manipulation of the homogeneous linewidth of an individual In(Ga)As quantum dot,” *Physical Review B*, vol. 66, pp. 045313+, July 2002.
- [23] R. J. Warburton, C. Schafflein, D. Haft, F. Bickel, A. Lorke, K. Karrai, J. M. Garcia, W. Schoenfeld, and P. M. Petroff, “Optical emission from a charge-tunable quantum ring,” *Nature*, vol. 405, pp. 926–929, June 2000.
- [24] G. Coli, K. K. Bajaj, J. L. Reno, and E. D. Jones, “Excitonic diamagnetic shifts and magnetic field dependent linewidths in AlGaAs alloys,” *Material Research Society Symposium Proceedings*, vol. 692, pp. 343+, 2002.
- [25] S. N. Walck and T. L. Reinecke, “Exciton diamagnetic shift in semiconductor nanostructures,” *Physical Review B*, vol. 57, pp. 9088+, Apr. 1998.

- [26] M. Erdmann, C. Ropers, M. Wenderoth, R. G. Ulbrich, S. Malzer, and G. H. Döhler, “Diamagnetic shift of disorder-localized excitons in narrow GaAsAl-GaAs quantum wells,” *Physical Review B*, vol. 74, pp. 125412+, Sept. 2006.
- [27] N. Schildermans, M. Hayne, V. V. Moshchalkov, A. Rastelli, and O. G. Schmidt, “Nonparabolic band effects in GaAs/Al_xGa_{1-x}As quantum dots and ultrathin quantum wells,” *Phys. Rev. B*, vol. 72, p. 115312, Sep 2005.
- [28] H. Kosaka, A. Kiselev, F. Baron, K. Kim, and E. Yablonovitch, “Electron g-factor engineering in III-V semiconductors for quantum communications,” *Electronics Letters*, vol. 37, p. 464, 2001.
- [29] E. A. Chekhovich, A. B. Krysa, M. S. Skolnick, and A. I. Tartakovskii, “Direct Measurement of the Hole-Nuclear Spin Interaction in Single InP/GaInP Quantum Dots Using Photoluminescence Spectroscopy,” *Physical Review Letters*, vol. 106, pp. 027402+, Jan. 2011.
- [30] J. Skiba-Szymanska, E. A. Chekhovich, A. E. Nikolaenko, A. I. Tartakovskii, M. N. Makhonin, I. Drouzas, M. S. Skolnick, and A. B. Krysa, “Overhauser effect in individual InP/Ga_xIn_{1-x}P dots,” *Phys. Rev. B*, vol. 77, p. 165338, Apr 2008.

Chapter 5

Conclusions

During the time of this PhD, many projects have been conducted. Some of them yielded no results and have not even been mentioned in this thesis, some produced impressive results that have been published in high profile journals [1, 2], but the link between these projects is difficult to understand at first sight.

Right now the silicon semiconductor technology that defines our modern world has reached a turning point, where the so much necessary power of processing depends on miniaturization, which is no longer possible using bulk silicon materials since quantum effects begin to be non-negligible. On the other hand the theoretical and more recently experimental progress made in the field of quantum mechanics [3–7] have lead us to envision new kinds of technologies, like quantum teleportation, quantum cryptography or quantum computation [8–12]. The quantum effects from which these technologies originate are made possible in semiconductors by new complex epitaxy techniques that allow for the growth of low-dimensional structures like quantum wells or quantum dots [13, 14]. Semiconductor materials offer us a wide range of properties and compound combinations. They are one of the main contenders in the ever growing race for the title of successor to silicon technology, but for that to happen we must understand their electronic properties at the atomic level. The exploration of many different material compounds and structures using a wide panel of experimental techniques is necessary to have a global view of the most promising ones, and the work presented in this thesis achieves a step toward this goal, with the optical investigation of three novel quantum dot structures.

The first two chapters offered results based on the same sample, comprising III-V nanostructures monolithically grown on silicon. Our current technology being silicon-based and III-V compounds having better optical properties, the integration

of the latter with the former is the next logical step for technological evolution. Indeed the field of hybrid IV/III-V semiconductor materials have seen an increasing amount of interest in the last decade, even though the epitaxial challenge is difficult to overcome. In chapter 2 we have proven that it was possible to grow a good quality InGaAs quantum dots system on top of a silicon substrate without resorting to wafer bonding or intermediate germanium layers. The dots, grown atop a complex system of InAlAs/GaAs strain filter layers showed excellent photoluminescence emission. What is more, the ability to emit single photons which is essential to any application in quantum optics has been demonstrated both with continuous and pulsed laser. The measured $g^{(2)}(\tau)$ at zero time delay is as low as 16%. The most exciting result though about this sample is certainly the successful fabrication and characterization of photonic crystal cavities. The cavities exhibited average Q-factors of 9000, with a maximum measured of 13000, emphasizing the good quality of III-V-on-Si epitaxial growth. Light-matter interaction within the cavities was also investigated, and weak coupling (effective Purcell enhancement of 2) as well as strong coupling (vacuum Rabi splitting of 212 μeV) regimes are demonstrated, opening the way to cavity quantum electrodynamics on silicon.

On top of the exciting results displayed in chapter 2, the silicon sample featured an unexpected yet interesting formation of quantum dots, originating from interface fluctuations of GaAs/AlGaAs layers used to remove dislocations. Studied in chapter 3, these dots were submitted to a simple experiment to confirm their origin, where multiple slabs of the same sample were etched at various depths to compare their emissions. After confirming that the emission lines originated from GaAs/AlGaAs short-period superlattice, polarization selective photoluminescence measurements gave us insight about the fine structure of the dots. Neutral excitons and bi-excitons were identified, presenting a substantial binding energy of 5 meV and a fine structure splitting ranging from 40 μeV to 100 μeV . Finally autocorrelation measurement under continuous-wave excitation demonstrated anti-bunching of more than 65%. This will have proven that the growth of good quality interface fluctuation dots is possible on a silicon substrate, and is made particularly interesting by its emission energy in the 1.75-1.8 eV region, a visible region of the spectrum widely considered for free-space communication applications [15].

The project related in chapter 4 deals with a new approach to grow InP quantum dots, by introducing various levels of arsenic during the metal-organic chemical vapour deposition process. The main idea behind this approach was to fill the emis-

sion energy gap between InP and the more classical InGaAs quantum dot systems, and it was concluded in the experiments that indeed good intensity emission lines spread from 1.8 eV and down to 1.4 eV as samples with higher As concentration were measured. Magneto-optic characterization allowed us to extract exciton g-factor and diamagnetic shift from 20 dots, a study that constituted the starting point for another ongoing project. The last part of this project is the study of excitonic complexes under electric field, made possible by the fabrication of Schottky diode structures. The application of negative biases modifies the resident charges in the dots, allowing for the observation on-demand of neutral and negatively charged excitons from the same quantum dot. Now future work can be undertaken using these Schottky structures like polarizability, characterization of the wave-function or photocurrent [16].

References

- [1] I. J. Luxmoore, R. Toro, O. Del Pozo-Zamudio, N. A. Wasley, E. A. Chekhovich, A. M. Sanchez, R. Beanland, A. M. Fox, M. S. Skolnick, H. Y. Liu, and A. I. Tartakovskii, “III-V quantum light source and cavity-QED on Silicon,” *Sci. Rep.*, vol. 3, p. 1239, 2013.
- [2] R. Toro, O. Del Pozo-Zamudio, M. N. Makhonin, J. Dixon, A. M. Sanchez, R. Beanland, H.-Y. Liu, M. S. Skolnick, and A. I. Tartakovskii, “Visible light single photon emitters monolithically grown on silicon,” *Unpublished*, 2013.
- [3] C. Cohen-Tannoudji, B. Diu, and F. Laloë, *Mécanique quantique*. Enseignement des sciences, Hermann, 1973.
- [4] J. E. Sharping, K. F. Lee, M. A. Foster, A. C. Turner, B. S. Schmidt, M. Lipson, A. L. Gaeta, and P. Kumar, “Generation of correlated photons in nanoscale silicon waveguides,” *Opt. Express*, vol. 14, pp. 12388–12393, Dec 2006.
- [5] R. M. Stevenson, R. J. Young, P. Atkinson, K. Cooper, D. A. Ritchie, and A. J. Shields, “A semiconductor source of triggered entangled photon pairs,” *Nature*, vol. 439, pp. 179–182, Jan. 2006.
- [6] A. J. Ramsay, “A review of the coherent optical control of the exciton and spin states of semiconductor quantum dots,” *Semiconductor Science and Technology*, vol. 25, pp. 103001+, Oct. 2010.
- [7] D. Bonneau, E. Engin, K. Ohira, N. Suzuki, H. Yoshida, N. Lizuka, M. Ezaki, C. M. Natarajan, M. G. Tanner, R. H. Hadfield, S. N. Dorenbos, V. Zwiller, J. L. O’Brien, and M. G. Thompson, “Quantum interference and manipulation of entanglement in silicon wire waveguide quantum circuits,” *New J. of Phys.*, vol. 14, p. 045003, 2012.
- [8] D. Deutsch, “Quantum theory, the church-turing principle and the universal quantum computer,” *Proceedings of the Royal Society of London. A. Mathematical and Physical Sciences*, vol. 400, no. 1818, pp. 97–117, 1985.

- [9] T. Hey, “Quantum computation: an introduction.” https://www.researchgate.net/publication/3363605_Quantum_computing_an_introduction?ev=srch_pub, Sept. 1999.
- [10] J. L. O’Brien, A. Furusawa, and J. Vuckovic, “Photonic quantum technologies,” *Nat Photon*, vol. 3, pp. 687–695, Dec. 2009.
- [11] C. H. Bennett and S. J. Wiesner, “Communication via one- and two-particle operators on Einstein-Podolsky-Rosen states,” *Physical Review Letters*, vol. 69, pp. 2881–2884, Nov. 1992.
- [12] X.-S. Ma, T. Herbst, T. Scheidl, D. Wang, S. Kropatschek, W. Naylor, B. Wittmann, A. Mech, J. Kofler, E. Anisimova, V. Makarov, T. Jennewein, R. Ursin, and A. Zeilinger, “Quantum teleportation over 143 kilometres using active feed-forward,” *Nature*, vol. 489, pp. 269–273, Sept. 2012.
- [13] P. D. Dapkus, “A critical comparison of MOCVD and MBE for heterojunction devices,” *Journal of Crystal Growth*, vol. 68, pp. 345–355, Sept. 1984.
- [14] P. M. Petroff, A. Lorke, and A. Imamoglu, “Epitaxially self-assembled quantum dots,” *Physicstoday*, vol. 54, pp. 46+, May 2001.
- [15] K. D. Langer and J. Grubor, “Recent Developments in Optical Wireless Communications using Infrared and Visible Light,” in *9th International Conference on Transparent Optical Networks, 2007. ICTON '07.*, vol. 3, pp. 146–151, IEEE, July 2007.
- [16] O. D. D. Couto, J. Puebla, E. A. Chekhovich, I. J. Luxmoore, C. J. Elliott, N. Babazadeh, M. S. Skolnick, A. I. Tartakovskii, and A. B. Krysa, “Charge control in InP/(Ga,In)P single quantum dots embedded in Schottky diodes,” *Physical Review B*, vol. 84, pp. 125301+, Sept. 2011.